Development of Biomimetic Soft Robotic Fish

by

Wenjing Zhao

A Dissertation Submitted in Partial Fulfillment
of the Requirements for the Degree of
Doctor of Philosophy

The University of Electro-Communications
Tokyo, Japan

December 2014

Development of Biomimetic Soft Robotic Fish

APPROVED BY SUPERVISORY COMMITTEE:

CHAIRPERSON: Professor Aiguo Ming

MEMBER: Professor Makoto Shimojo

MEMBER: Professor Hiroshi Maekawa

MEMBER: Professor Hisayuki Aoyama

MEMBER: Professor Kazuo Tanaka

生物模倣ソフト魚ロボットの研究開発

趙　文静

概要

自然界において、その環境は日々変化している。自然淘汰と適者生存の競争法則により、優れた生物が自然の中で生き残り、その種が持続していく。その事実が裏付けられるように、生物には多くの有益な特徴が存在する。近年、多くの研究機関が自然界の生物の特徴に着目し、生物の形態や機能などを解明し、模倣・応用しようという取り組みが活発に行われている。その中で、ロボット工学に生物の構造や機能を取り入れた生物模倣（バイオミメティック）ロボットの研究開発が最近活発になってきている。

本研究では、生物模倣魚ロボットを取り上げる。今まで生物模倣魚ロボットに関する研究開発が多く行われているが、運動性能、効率の向上などがまだ重要な課題となっている。特に、生物のように柔軟性を有効に活用する生物模倣ソフト魚ロボットについて、試行錯誤による研究開発がほとんどで、設計と制御に関する明確な手法がまだ確立されていないのが現状である。そこで、本論文ではロボットの柔らかい構造体と周囲の流体の相互作用を考慮した数値シミュレーションに基づいた設計と制御を行い、高性能な生物模倣ソフト魚ロボットの実現を研究目的とする。

本論文では、まず高性能な生物模倣ソフト魚ロボットを開発するための基本的な設計手法を考え、それを実現するためのシミュレーションシステムの構築を行う。次に、有限要素法を用いて魚の形状、柔らかい構造、駆動などを模倣できるソフト魚ロボットのモデリングを行い、二つの方法を用いてロボットの推進運動と推進力の関係を解析する。一つ目は流体を付加質量としたモーダル解析と過渡応答解析で、魚の推進メカニズムと性能に直接関係する推進モードと推進運動の大きさを解析する。二つ目は流体と構造の連成解

析で、上記の流体を付加質量とした解析方法で無視している粘性、渦などの影響を考慮し、より精確にロボットの推進運動と推進力を解析することできる。この連成解析に基づいてロボットの設計と制御を行うと、生物模倣ソフト魚ロボットの性能の更なる向上が可能である。これらのモデリング方法と解析方法を生物模倣ソフト魚ロボットの設計と制御への適用性を調べるために、シミュレーション結果と実際のロボットによる実験結果を比較しながら、検証と改善を行う。最後に、有効性が確認できたシミュレーションシステムを用いて、生物模倣型ソフト魚ロボットの最適設計を行い、実際にロボットの試作と性能評価をし、ロボットの性能の向上ができることを実証する。

本論文は以下の 6 章より構成される。

第 1 章は緒論である。生物模倣ソフト魚ロボットの研究背景と先行研究について解説し、その現状と課題をまとめ、本研究の目的を述べている。

第 2 章では高性能生物模倣ソフト魚ロボットを開発するための設計方法、手順とシミュレーションシステムについて述べる。従来の研究開発と異なって、柔らかい構造と流体の相互作用を活用することを前提としている。そのため、魚のような柔らかい構造、柔らかいアクチュエータによる分布駆動および流体などをモデリングする必要がある。また、柔らかい構造と流体の相互作用を考慮した解析により、魚の推進運動を実現させ、そして性能向上のための構造と制御入力の最適化を行う必要がある。これらの要求を満たすために、本研究では有限要素法によるモデリング、流体を付加質量としてのモーダル解析および過渡応答解析により必要な推進運動の実現、そして流体と構造の連成解析により流体力の更なる活用ができるシミュレーションシステムを構築した。シミュレーションに基づいたロボットの設計と制御の最適化を行うことによって、高性能な生物模倣ソフト魚ロボットの開発が効率良く行うことができる。

第 3 章では第 2 章の方法を用いて、具体的な生物模倣ソフト魚ロボットについて、モデリングと解析を行う。このロボットでは、ソフトアクチュエータとして圧電繊維複合材料を用いている。まず、圧電繊維複合材料の入力電圧と発生応力の関係式を導き、この発生応力をロボットの柔らかい構造体に与

えることでロボットの運動を解析できるようにした。簡単な片持ちはりのモデルについて、数値シミュレーションと実験により本駆動モデルの有効性を確認した。次に、ロボットのモデルについて周囲流体を付加質量としてのモーダル解析を行い、流体中におけるロボットのモード形状と周波数を求めた。これらのモードの運動と魚の推進運動と比較して、推進運動を実現するためのモードを特定した。また、先に求めた駆動モデルを用いて、圧電繊維複合材料への入力電圧の周波数と推進運動の大きさの関係を調べた。さらに、流体と構造の連成解析により、ロボットの頭部が固定された状態における入力電圧の周波数と推進力および推進運動の大きさの関係を調べた。

第 4 章では第 3 章で解析した結果の有効性を調べるために、実際のロボットを用いて流体中のロボットのモード形状と推進運動の大きさ、ロボットの頭部が固定された状態における推進力および推進運動の大きさを計測した。その実験結果は第 3 章での解析結果に近かいことが分かった。これによって、本研究で用いたモデリングと解析の方法の有効性が実証された。

第 5 章では上記の生物模倣ソフト魚ロボットのモデリングと解析の方法を用いて、新しい高性能のロボットを開発する。まずロボットの構造パラメータをある範囲の中で変化させ、解析によりロボットの推進運動の大きさを求め、大きな推進運動を実現できるロボットの構造パラメータを選定した。この結果に基づき、新しいロボットを設計し、試作した。試作したロボットを用いた評価実験の結果、高速度、高効率のロボットを開発することができた。

第 6 章は本研究で得られた成果をまとめ、今後の課題と展望について述べている。

Development of Biomimetic Soft Robotic Fish

Wenjing Zhao

Abstract

In nature, the environment varies from day to day. Through natural selection and competition law of survival of the fittest, the winning creatures survive and their species are able to retain and persist in nature. Based on this fact, creatures existent in nature have their unique features and advantages adapt to the surrounding environment. In recent years, many researches focused on the features of the creatures in nature have been done actively to clarify their morphology and functions and apply the morphology and functions to various fields. Among these researches, the development of the biomimetic robots based on mimicking the creature's structures and functions has become an active field in robotics recently.

In the research, the development of biomimetic robotic fish is focused. So far, there are many researches on biomimetic robotic fish, but improvement on motion performances and efficiency is still an important issue for robot development. Specially, on the biomimetic soft robotic fish utilizing the flexibility of fishes, the developments have been done by the trial and error approach. That is, the design and control method of soft robotic fish has not been established currently. Therefore, it motives us to investigate the design and control of soft robotic fish by numerical simulation that takes into account the interaction between flexible structure and surrounding fluid to develop the biomimetic soft robotic fish with high performance.

In order to develop the biomimetic soft robotic fish with high performance, the basic design method and corresponding numerical simulation system are firstly proposed and constructed in this dissertation. Then, based on finite element method (FEM), modelling of soft robotic fish by mimicking the soft structure and driving mechanism of fishes is carried out. The propulsion motion and propulsive force of the soft robotic fish are in-

vestigated through two kinds of numerical analyses. One is the modal and transient analysis considering the surrounding fluid as acoustic fluid. The propulsion mode and amplitude of the propulsion motion of soft robotic fish corresponding directly to the propulsion mechanism and motion performance of the robotic fish can be investigated. The other is the fluid-structure interaction (FSI) analysis. The interaction between soft robot structure and surrounding fluid including the dissipation due to fluid viscosity and influence of wake performance around the soft robotic fish are taken into account. From FSI analysis, the hydrodynamic performances of the soft robotic fish can be obtained for investigating its propulsion motion. It is possible to further improve the performance of the soft robotic fish through its design and control based on FSI analysis. Besides, based on coupling analysis by using acoustic fluid, the turning motion control of the soft robotic fish is investigated by its propulsion modes in the fluid. In order to investigate the feasibility of modelling method and numerical simulation analysis on design and control of the biomimetic soft robotic fish, the performance evaluation is carried out by comparison between the simulation and experiment on an actual prototype. Finally, the optimization and improvement are performed for developing the biomimetic soft robotic fish with higher performance based on verified coupling analysis considering the fluid as acoustic fluid, and corresponding performance evaluation on new robot prototype is presented. The performance improvement of the soft robotic fish is confirmed through the new robot prototype.

The dissertation consists of six chapters and the main contents are shown as follows.

Chapter 1 is an introduction. The background and relative previous work about biomimetic soft robotic fish are briefly reviewed. It summarizes the current research status and problems of biomimetic soft robotic fish, and describes the purposes of this research.

Chapter 2 presents the design method, procedures and numerical simulation system in the present research for developing the biomimetic soft robotic fish with high performance. Different from previous development method, our purpose is how to design and control the soft robotic fish by utilizing interaction between the flexible structure

and surrounding fluid effectively based on numerical simulations. Therefore, it is necessary to model a fish-like soft robot structure including soft actuators and an enclosed fluid. Besides, by the numerical analysis considering the interaction between flexible structure and fluid, the fish-like propulsion motion should be realized and established, and then the robot structure and control inputs are needed to be optimized for performance improvement. In order to meet these requirements of designing and developing the optimal soft robotic fish, the design method based on modelling, simulation analysis and improvement is presented and the numerical simulation system for soft robotic fish is built. In the simulation system, modelling of soft robotic fish, modal and transient analysis considering the enclosed fluid as acoustic fluid are firstly described based on FEM to realize the fish-like propulsion motion with large amplitude for the soft robotic fish. Then, the FSI analysis is performed to describe and establish the hydrodynamic performances of the soft robotic fish. Based on this numerical simulation system, it is possible to develop the biomimetic soft robotic fish with high performance effectively by optimization of design and control of the soft robotic fish.

Chapter 3 describes the modelling and numerical analysis of biomimetic soft robotic fish by using the method presented in Chapter 2. The soft robotic fish uses the piezoelectric fiber composite (PFC) as soft actuator. Firstly, the relationships between the input voltage and generated stress of the PFC are derived. The generated stress can be applied on soft structure to investigate the motion performance of the soft robotic fish. To support the driving model of the PFC, the corresponding experiments on simple beam model are carried out. By comparing the simulation results with experimental results, the effectiveness of the driving model is verified. Then, the modal analysis in which the fluid is considered as acoustic fluid is performed. The structural mode frequencies and mode shapes of the soft robotic fish in the fluid are calculated. By comparing these modes' motion with those of the real fishes, the fish-like propulsion mode is identified to realize the corresponding propulsion motion of the soft robotic fish. Furthermore, based on the verified driving model of soft actuator, the amplitude of the main propulsion motion of soft robotic fish is calculated. Through FSI analysis, the relationships of

driving frequencies of input signal with propulsive force and displacement of propulsion motion, and vortex distribution in the wake around the soft robotic fish are investigated for the case of fixing robot head. Besides, the motion control of soft robot is investigated to realize turning motion in the fluid. Through controlling the input voltage amplitude on soft actuators of the robot, turning right and turning left motion are identified in the swimming when the input voltage amplitudes on two actuators are in asymmetric distribution.

Chapter 4 is experiment evaluation. In order to validate the results of numerical simulation analysis described in Chapter 3, the mode shapes, amplitude of propulsion motion, propulsive force and vortex distribution around soft robotic fish for the case of fixing robot head, and turning motion are measured by using actual robot prototype. The present simulation results are congruent with experiments. By the results, the effectiveness of the modelling method and numerical analysis used in the research is verified and they are useful to predict the propulsion characteristics of the soft robotic fish in the fluid for performance improvement.

Chapter 5 develops a new soft robotic fish with high performance based on above modelling method and numerical analysis by optimization. Firstly, the structural parameters of the robot are allowed to vary within a range and the amplitude of the propulsion motion for the soft robot is calculated for different parameters by the numerical analysis. Then the structural parameters of the robot capable of propulsion motion with larger-amplitude are chosen for improvement. Based on this result, new soft robot is designed and evaluated by experiments. From the experimental results of the new soft robot, it is confirmed that the higher swimming speed, better fish-like swimming performance and larger turning velocity are realized. It can be said that the new soft robotic fish has been developed successfully for improvement.

Chapter 6 summarizes the conclusions and future works of this research.

Contents

List of Figures

List of Tables

Chapter 1. Introduction

1.1 Background and Motivations

1.1.1 Swimming Modes of Fishes

In nature, the fish evolves various motion performances to adapt to the environments. The interest of many biologists and researchers of hydrodynamics is primarily in periodic steady (or sustained) swimming locomotion. In 1984, Webb classified the swimming motion into body and/or caudal fin (BCF) propulsion and median and/or paired fin (MPF) propulsion through utilizing the different part of fish body [1], [2]. Figure 1.1 shows the motion performances of BCF and MPF propulsion [2]. According to these propulsion characteristics, the robotic fish can be designed to make oscillating, undulating or flapping motion. The oscillating form has not the wave propagation motion on robot and usually refers to caudal fin propulsion, while the undulation involves the wave propagation on whole fish body and generally indicates the body propulsion. The flapping motion is attributed to the MPF propulsion, such as pectoral fin propulsion of cow-nosed ray. The BCF propulsion is focus on acceleration, while the MPF is on manoeuvring.

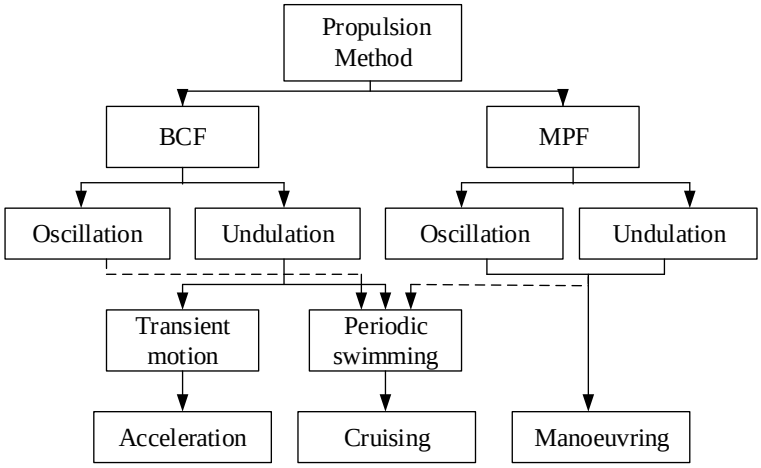

Fig. 1.1 Motion performances of BCF and MPF propulsion.

The undulation motion of BCF propulsion is the swinging motion of caudal fin coordinated with the fish body. It can be classified into anguilliform, subcarangiform, carangiform and thunniform based on proportion of fish body in swing motion, shown in Fig. 1.2 [1], [3]-[5]. The anguilliform also called as undulating model, such as eel and lamprey. The whole fish body from the head to tail makes the large-amplitude undulation. It can use very small thrust to make the forward motion for unit distance. However, it's driving mechanism and power source is needed much space to realize the fish body propulsion. The similar motion is observed in the subcarangiform, but the amplitude of the undulation is limited anteriorly and increases only in the posterior half of the body. The subcarangiform makes for higher swimming speed and has the better balance ability in speed, acceleration and manoeuvring, such as trout fish. The inertia force of fluid is nearly 7 times of pressure drag for propulsion in its swimming motion [6]. Fish in the caragiform group have the faster swimming speed, but their turning and accelerating abilities are compromised due to the relative rigidity of their body. The vast majority of motion is restricted to the last third of body length. The thrust is provided by a rather stiff caudal fin. The thunniform is the most efficient propulsion mode in the aquatic environment and the hotspot in the fields of biomimetic robotic fish. Only stiff caudal fin is utilized for propulsion. The thrust is generated by the lift-based method. The high cruising speed with long periods is maintained on this mode for large aspect ratio's caudal fin. The fishes, such as tuna and mackerel, are involved in this propulsion mode. The

design of this kind of the swimmers is optimised for high-speed swimming and is not suitable for actions such as turning manoeuvres and rapid acceleration from stationary.

For the oscillation motion of the BCF propulsion, there is only one type, that is, ostraciiform. In this propulsion, there is no any motion occurs on fish body, and only the hard caudal fin is oscillating for propulsion. The swimming velocity of this propulsion type is relatively low. Although this oscillation propulsion mode is similar to the propulsion of tuna (thunniform type), but the efficiency of the ostraciiform type is lower than the thunniform type.

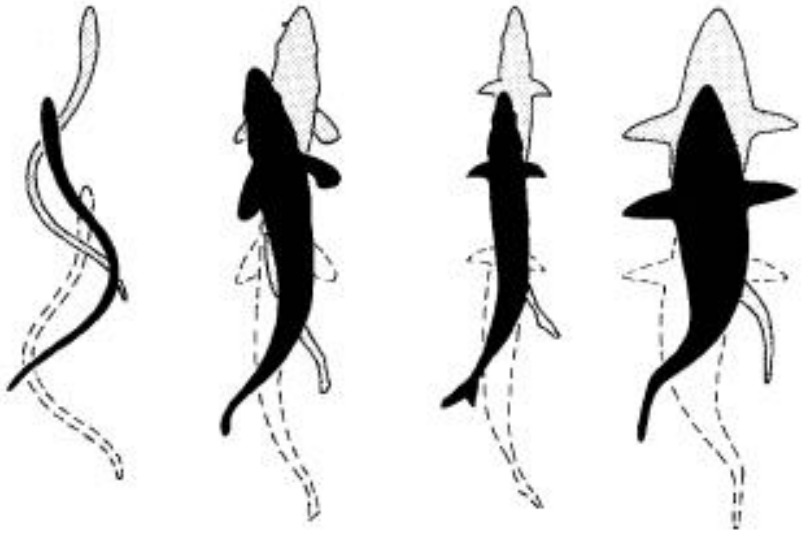

(a) Anguilliform (b) Subcarangiform (c) Carangiform (d) Thunniform

Fig. 1.2 BCF propulsion [1], [5].

The MPF propulsion is mainly using the fins expect for caudal fin to make the propulsion, such as pectoral fin, dorsal fin, pelvic fin, anal fin, and so on. Many fishes use these fins for stabilization and steering. The comparison of propulsion characteristics between BCF and MPF on efficiency, speed and mobility is described in Table 1.1. An estimated only 15% of the fishes use MPF propulsion [7]. The BCF propulsion is more popular for fishes due to the relatively higher efficiency. The subcarangiform as one of the typical BCF propulsion makes for higher swimming speed and better balance ability in speed, acceleration and manoeuvring. Therefore, in the present research, the BCF

propulsion with subcarangiform mode is mainly focused for developing the biomimetic soft robotic fish. The propulsion motion is dominated by inertial force of fluid [6].

Table 1.1 Comparison between BCF and MPF Propulsion

Name	Propulsion	Efficiency	Speed	Mobility
BCF	Anguilliform	lower	slower	better
	Subcarangiform	higher	higher	better
	Carangiform	higher	faster	good
	Thunniform	highest	fastest	good
MPF	Swing or undulation	lowest	slowest	best

From the view of temporal domain, the fish swimming can be classified into two types: steady or sustained swimming and unsteady or transient swimming. In the steady swimming, the fish makes swimming propulsion motion for a long distance at a constant speed. As for the unsteady swimming, it is characterised by fast start, sharp turn and burst behaviours in the swimming.

Traditionally, the steady fish swimming has been the research focus in the fields of biological, mathematics and robotics. Swimming motion at constant speed along the straight path is the special swimming pattern for fishes in the practice. For the unsteady swimming motion, it plays an important part in fish swimming characterised by high accelerations. Many researches have concentrated on the kinematics of fishes based on BCF or MPF propulsion due to fish swimming's complexity and particularity. By mimicking the fish swimming motion, such as fish-like propulsion pattern and hydrodynamics, the propulsion characteristics of fish are investigated for development in related field. It is known that underwater vehicles or underwater robots are developed for high stability and payload capability based on steady-state hydrodynamics. However, their steady-state performances are unable to match the mobility and manoeuvring capability of real fish. Thus, to obtain the propulsion characteristics and hydrodynamics of

the robotic fish, the propulsion theories of real fishes are necessary to be investigated for advanced control mechanism design on robot.

1.1.2 Propulsion Theories of Fishes

In nature, there are thousands of species of aquatic organisms. They have various morphologies and motions, can be classified into three types: firstly, cilia propulsion, many protozoa and coelenterates use their cilia on body surface to make the motion; secondly, the jet propulsion, for example, the jellyfish and squid get the recoil force by jetting the fluid in the opposite direction of motion to make the propulsion; thirdly, the undulation propulsion, aquatic organisms swing their body to achieve the propulsive force for swimming motion. A large number of aquatic organisms use this undulation approach to make the propulsion. In this research, the concerned fish propulsion is the undulation propulsion. The fish swings its body or caudal fin, pectoral fin, and so on, to make the swimming propulsion motion. This undulating propulsion is mainly focused to design and develop the soft robotic fish.

The fish's undulation propulsion is different from the propulsion mechanism of the conventional propeller. In fish swimming, Reynolds number is a dimensionless number describing the relative importance of force from fluid viscosity and fluid inertia. It is generally described as (1-1). According to different value of Reynolds number, the fluid flows are divided into different patterns. When Re < 1, the fluid viscous force dominates, and if Re is larger than 1000, the fluid inertial force is dominated in fluid flow [8].

$$R_e = \frac{\rho UL}{\mu} \tag{1-1}$$

where U is forward swimming speed of the fish; L is fish length; ρ is fluid density; η is fluid dynamic viscosity.

The kinematics of fish swimming involves in different propulsion mechanisms, such as meandering propulsion with traveling wave. These kinematics result from the complicated coupling dynamics between forces from muscles and from surrounding fluid. In

the swimming motion of fishes, the muscles deform the fish body, which applies force to the surrounding fluid. As a return, the fluid also applies force on fish body and changes the body shape, which changes the muscle force of fish body.

In order to model the deformation of fish body accurately, the forces mentioned above must be taken into account simultaneously. Few models attempt to solve this coupling problem due to its complexity [9]. Instead, according to the different motion scales of fish swimming, most theories define fish body as a given shape to predict the fluid forces. The basic propulsion model of fishes can be classified into resistive model and reactive model.

Firstly, resistive model.

A simple model proposed by Taylor is defined as the resistive model [10]. The thrust is estimated from the sum of drag forces on fish body with a traveling wave whose speed is larger than the forward swimming velocity of the fish. The fish body is divided into many segments along the body length. The drag force for each segment can be calculated by the following equation,

$$D = 0.5 C_d \rho u^2 s \tag{1-2}$$

where C_d is drag coefficient; ρ is fluid density; s is surface area of segment; u is swimming velocity including contributions from forward motion and lateral undulation of fish.

This resistive model is built based on a quasistatic method using steady flow theory to predict the fluid force in the swimming motion of the fish. In this model, the inertial force of fluid is neglected so that its applicability is restricted to low Reynolds number, and it assumes that anterior segments of the fish do not affect fluid flow moving past the body, so that this model may not hold for undulation motion of the real fishes. Based on different kinds of swimming modes, the anguilliform swimming where viscous forces play a significant role belongs to this resistive model. The problems of the resistive models are discussed on details by Webb [11]. Although this resistive model has some limitation for estimating resistive forces, it is important in thrust generation of fishes

whose drag force play the dominated part in the interaction with surrounding fluid [12] and may make the effort on reduction of propulsive efficiency [11].

Secondly, reactive model.

Later models deal with more realistic fish-type motions, assuming an inviscid fluid, that is, the fluid viscosity is assumed to be negligible. A two-dimensional waving plate theory is developed originally by Wu [13]. Based on the slender body theory stemming from aerodynamics, the elongated-body theory is formed and it is suitable for subcarangiform and carangiform modes of the real fish. The favourite mathematical model of fish swimming is elongated-body theory developed by Lighthill [14]-[16]. In this model, the force from fluid flow induced by lateral acceleration and deceleration of the undulating fish body is estimated based on acceleration reaction in which the surrounding fluid is viewed as the added virtual mass on fish body [17], [18]. Thus, this model is termed reactive model generally. This model estimates force and power by changes in energy. Due to ignored fluid viscosity, the average thrust power of fish swimming can be calculated by following equations [14], [19]. The average thrust force can be approximated by thrust power divided by forward swimming speed.

$$P_T = mwUW - 0.5mw^2U \tag{1-3}$$

$$m = \left(\frac{d}{2}\right)^2 \pi\rho \tag{1-4}$$

$$w = W - W\frac{U}{V} \tag{1-5}$$

$$W = \frac{\pi f A}{1.414} \tag{1-6}$$

where P_T is thrust power; m is added virtual mass per unit length; w is velocity of water at the trailing edge; W is rms value of the lateral velocity of the trailing edge; U is forward swimming speed; V is velocity of the body propulsive wave; ρ is density of water;

d is span of the caudal fin at the trailing edge; *f* is oscillating frequency of the caudal fin; *A* is oscillating amplitude of the caudal fin.

The hydromechanical efficiency is fish swimming for propulsion, that is, the propulsive efficiency of the fish is calculated as the ratio of the thrust power to the total power, shown as follows. According to this equation, the propulsive efficiency is never lower than 0.5.

$$\eta = 1 - \frac{1}{2}\left(1 - \frac{U}{V}\right) \tag{1-7}$$

The reactive model described above makes the assumption that undulating amplitude is small, so that the angles fish body makes with the swimming direction are close to zero. When angle becomes large, more energy is lost into the wake around the fish body. A large-amplitude elongated-body theory developed by Lighthill considers this effect and caters for fish motion of arbitrary amplitude [1], [16]. This theory is better suited to carangiform type of fish swimming, where lateral motion of the caudal fin is large.

The elongated-body theory assumes the inertial force completely dominates viscous force in the fish swimming. Thus, this theory is not suitable for anguilliform swimming where viscous forces play a significant role. Besides, it cannot be applied to thunniform mode due to the shape of the caudal and pectoral fin violating the fundamental assumption of slenderness. Nevertheless, elongated body theory has been used regular in fish swimming studies, both directly to make predictions of force, and indirectly to inform analyses of parameters such as propulsive efficiency [11], [20]-[23].

1.1.3 Development of Biomimetic Robotic Fish

Human has had a dream on robots for many years, hoping the people can be replaced by the robot to do some desired work or tasks. In 1954, the first robot with point to point control developed by George Devol was born in Unite States [24]. From then, the robot has come into human life and people's dream comes true. The robot begins to play more

and more important roles in many fields. Due to the complicated working environment and tasks, the robot needs to have the better mobility and motion performance in the special and unknown environment. The robot with simple moving mechanism of wheels and crawler has not been able to meet the demand of carious and complicated environment or work. This kind of robot has poor adaptability and flexibility, and can cause enormous energy deficiency in its propulsion.

Today many researchers are looking in the cupboards of their local diners and under rocks for biological inspiration to create a new generation of flying, crawling, and swimming automatons known as biomimetic robots. Biomimetic robot is a kind of robots, which mimics the external shape, body structure, motion principle and behaviour of living creature in nature, and is able to undertake the work has characteristics of living creature [25]. They make a lot of irreplaceable contributions in human life with the development of interdisciplinary sciences, including the science of electronic information and biological technology [26]-[29].

As one of the best active fields in the development of science and technology, biomimetic robots, are achievements of the interdisciplinary science, robot technology, micro-fabrication technology and biological science. Essentially, the biomimetic robot has a complicated system. It utilizes many inorganic components (such as mechanical, electrical, hydraulic) and organic body to build the robot system. The scientists from the world have concentrated on development of biomimetic robots by mimicking the creatures, refers to underwater biomimetic robots, underground biomimetic robots and biomimetic flapping robots.

Fishes, as the first vertebrates in the nature, they have abundant species and different living environments. In order to grab prey, avoid predators, propagation and migration, fish has a long experience on natural selection and evolution to become the creature with extraordinary underwater motion performances. It not only has the characteristics of low-power and high swimming speed and efficiency, but also has good flexibility and manoeuvrability in some fast and sharp swimming motion. In modern time, the exploration of seabed enters a new stage. In hopes of mimicking the swimming propulsion and

manoeuvrability of the fish for meeting the demand of exploration and underwater work and, the fishes become one of the focuses to be mimicked, and numerous researchers are dedicated to the fields of biomimetic underwater robots, especially on the development of biomimetic robotic fish by mimicking the real fishes [1], [29]-[37].

The biomimetic robotic fish is an underwater propulsion device utilizing the mechanic and electronic components or intelligent materials by mimicking the fish propulsion. Compared with the propeller propulsion device, the biomimetic robotic fish has some following advantages.

First, high mobility. At high propulsion velocity, the propeller device has the larger turning radius, but the biomimetic robotic fish can overcome this shortcoming and enhance its ability of start, acceleration and turning. It has higher mobility than propeller device.

Second, better hydrodynamic performance. The biomimetic robotic fish has smaller fluid resistance than propeller device in the propulsion due to its fish-like streamline shape. The vortex can be obtained and developed for propulsion in the wake of the biomimetic robotic fish.

Third, small noise. The biomimetic robotic fish has smaller noise than propeller device, difficult to be detected and identified by sonar.

Fourth, the propulsion system is integrated with the control system. Conventional propeller device uses propeller for propulsion and rudder for control. The propulsion system and control system are complicated and they are independent. However, to simplify the mechanism, the biomimetic robotic fish integrates the propulsion system with control ability. This increases its effective volume and payload capacity.

Fifth, high efficiency. The biomimetic robots with fishlike swimming can save enormous energy and improve the work efficiency in its swimming motion.

Due to these advantages of biomimetic robotic fish in the propulsion, such as high mobility, good hydrodynamic performances and small noise, its propulsion and control method can be applied to make some special or dangerous underwater tasks effectively cannot be done by manual labour.

Numerous researchers concentrate on propulsion mechanism by biomimetic approach to develop the fishlike robots for good motion performances. The researches on biomimetic robotic fish mainly include two stages: basic theory study, and development of robotic fish with high speed, efficiency and good mobility. With the advancement of robot technologies, materials and driving system, development of biomimetic robotic fish came into human life after 1990s, such as Robotuna of MIT, robotic fish with rigid tail of MSU, Nanyang Awana (NAF-I), snake-like robot (AmphiBot) of EPFL, snake-like robot (HELIX-I) of TIT, SSSA lamprey-like robot, FILOSE robot from Tallinn University, robotic fish in London Aquarium from the University of Essex, robotic eel of Methran Mojarrad group, and so on [1], [29]-[37]. The biomimetic robotic fish, expressed as its high efficiency, good mobility and small disturbance, will be widely available for the application of rescue, exploration and observation of the seabed, underwater investigation and other special underwater tasks [26]-[30].

In order to fulfil some complicated works or tasks in the unknown environment accurately and reliably, the biomimetic robotic fish must have good flexibility, high safe actor and high adaptability in the principle and behaviours of moving, information processing, control and calculation inference, and so on. And it is very important to make the biomimetic robotic fish as soft as fishes. However, it has been proven difficult to reproduce the fish-like motion by using the conventional rigid mechanisms, causing relatively complex and unreliable underwater propulsion structure with low efficiency and mobility [38], [39]. To utilizing the fish-like propulsion, the new actuation strategy based on soft structure is needed. And soft robotic fish that combines soft behaviour of real fishes with robotics are turning up and spreading out in our life. The soft robotic fish, intended as the use of soft component with soft materials in robotics for robot development, is a relatively new research field, aiming to overcome the disadvantages of conventional rigid robotic fish. Using soft material to apply forces on the working environment, as expected in a soft robotic fish capable of drifting, acceleration, balance, steering and perform other special underwater tasks, poses new problems on design of propulsion mechanism among different components. The development of soft robotic

fish as a young field is dependent on the available and fastest computing technologies. The possible collaborations among biologists, soft robotic engineers, and advanced computer science have not begun absolutely [38]. Theories and technologies have not yet been defined in a general method and activities of robot development are still exploring new ways for a new generation of fish robots [38]. Thus, it motivates us to challenge the design and control problem of soft robotic fish through biomimetic approach for developing the soft robotic fish with high performance.

1.1.4 Current Research Status of Biomimetic Soft Robotic Fish

With the rapid development of biomimetics and robotics technology, the MIT developed the first biomimetic robotic tuna (Robotuna) in the world in 1994 [40]**.** From then, the robotic fish has become the popular topic with the combination of biomimetics and mechanics, and many fish robots are turning up gradually. For example, as shown in Fig. 1.3 [41] [42], RoboPike and vorticity control unmanned undersea vehicle (VCUUV) from MIT are the improved version of Robotuna. RoboPike whose length is 810mm can swim well but it is not autonomous. The VCUUV is fully autonomous and very stable in the straight and forward motion.

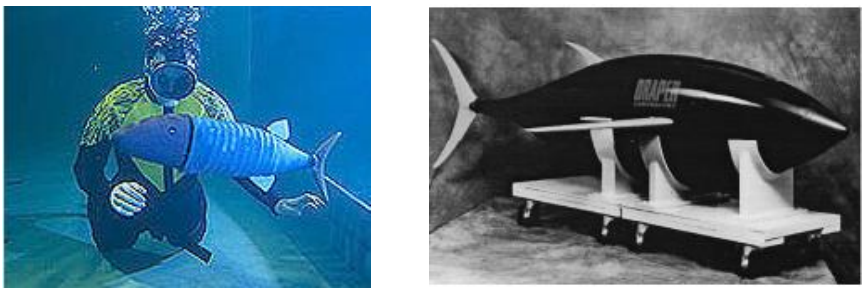

(a) RoboPike [41] **(b) VCUUV [42]**

Fig. 1.3 RoboPike and VCUUV robot from MIT.

Mitsubishi Animatronics robotic fish is the first pet fish robot with wireless control in the world, whose length is 80cm, shown in Fig. 1.4 [43]. It is inspired by the carp koi a symbol of

force and chance in Japan. The sensors being used to control the oxygen concentration in water is equipped into its mouth.

Fig. 1.4 Mitsubishi Animatronics robotic fish [43].

A robotic blackbass with pectoral fin propulsion is designed by Kato Laboratory from Tokai University [44], [45]. The robotic fish UPF-2001 with motor mechanism in Fig. 1.5 is presented by National Maritime Research Institute (NMRI) and the velocity can reach up to 0.97m/s [46].

Fig. 1.5 Robotic fish-UPF-2001 from NMRI [46].

The biomimetic robotic fish in London aquarium described in Fig. 1.6 from Essex University is used for detection of pollutants [34], [47]. It is an autonomous robotic fish and can realize various motion behaviours by the computer, such as forward, turns, acceleration. The snake-like robot AmphiBot with motor mechanism shown in Fig. 1.7 is developed by EPFL [33]. The snake-like motion is realized on this robot. Besides, Autonomous Systems Lab of the University of ETH proposed an underwater robot with fin-based undulating propulsion based on the principle of camshaft, called as CUTTLEFIN [48]; Tallinn University developed a FILOSE robot from designing a compliant tail for imitating the kinematics of a real fish; Nanyang Technologi-

cal University presents the biomimetic robotic fish using caudal fin and pectoral fin propulsion with motor mechanism, named NAF-1 and RoMan-II, respectively [31], [49]. Among above mentioned these fish robots, the propulsion methodologies are mainly by conventional motor mechanism. The motor mechanism is simple but lack of flexibility with high energy cost. The robots usually have large size and heavy weight with rigid materials and complex control system [3], [38]. The propulsion is not smooth as the real fishes, reducing the swimming efficiency and flexibility of the robotic fish [50], [51]. The fish-like propulsion performance with good flexibility is not realized from these robots.

Fig. 1.6 Biomimetic robotic fish used in detection of pollutants from Essex University [34].

Fig. 1.7 Snake-like robot AmphiBot developed by EPFL [33].

In recent years, a new trend occurs on the biomimetic robotic fish. Various biomimetic soft robotic fish based on soft materials and compliant parts have been developed and shown in Table 1.2. Some new materials and technologies begin to be used in the design of soft robotic fish for improvement.

Table 1.2 Research Status on Development of Soft Robotic Fish

	Research Team	Robotic fish
America	MIT	An eight-foot long autonomous robotic tuna with artificial muscle-based actuation
		Soft-bodied robotic fish with planar motion
		Soft-bodied robotic fish with 3D motion
		Fish-like pectoral fin with conducting polymer based actuation
	University of New Mexico (Methran Mojarrad Team)	Robotic fish using polyelectrolyte ion-exchange membrane (IEM) for anguilliform propulsion
	Northeastern University (NU)	Undulatory robotic lamprey using SMA
	University of Central Florida	Micro robotic fish with shape memory alloy (SMA) technology
	Texas A&M University	Underwater biomimetic vehicle using SMA technology
	Michigan State University (MSU)	Robotic fish with servo motor using a rigid and flexible tail fin
		Robotic fish with an artificail caudal fin using IPMC
	University of California (UC)	Mathematical model of fish propulsion
Japan	Nagoya University	Micro propeller with body propulsion using SMA
		Robot mimicking pectoral fin propulsion based on IPMC actuator
		Micro robot with pectoral fin propulsion using piezoelectric ceramic
	University of Tokyo	Robotic fish with caudal fin propulsion using electrostatic film
	Kagawa University	Micro robotic fish with tail fin propulsion using ionic conducting polymer film (ICPF)
		Tortoise-like flexible microrobot using ICPF
		Swimming micro robot using IPMC actuator
	Okayama University	Soft bodied manta robot
Italy	SSSA	Lamprey robot with muscle-like actuators
Spain	Universidad Polit ́ecnica de Madrid	Robotic fish using SMAs

Canada	University of Victoria	A simplified SMA-actuated tuna
German	Swiss Federal Laboratories for Materials Testing and Research	Fish-like airship that uses DEA sheets to produce a large-scale motion
Korea	Korea Insitute of Science and Technology	Undulatory tadpole robot (TadRob) using ionic polymer metal composite (IPMC)
Singapore	Nanyang Technological University	Undulating three-body segment system by using SMA
China	Robotics Institute of Beihang University	Robotic fish with flapping wing (ROBO-MANTA III)
	Harbin Inst. of Technol.	Micor biomimetic manta ray robot using SMA
	Harbin Engineering University	Centimeter-scale robotic fish using IMPC
Columbus	The Ohio State University	Swimming vehicle by a flexible fin
New Zealand	The University of Auckland	Biomimetic robotic fish using trilayer polypyrrole polymer actuator
	Feso's Bionic Learning Network	Swimming robotic fish named Airacuda

The Charles Stark Draper Laboratory from MIT suggested artificial muscle-based actuation strategies for fish-like vehicles (FLVs), based on experience with the Vorticity Control Unmanned Undersea Vehicle (VCUUV), an eight-foot long autonomous robotic tuna is developed [52]. And the Andrew D. Marchese group from MIT proposed an autonomous soft robotic fish shown in Fig. 1.8 based on fluidic elastomer actuators, focus on its rapid escape responses [53], [54]. Its length is about 33.9cm. It uses a soft continuum body and innovative fluidic actuation system for soft body. The continuum body has an embedded flexible spine and embedded anatomically proportioned muscle like actuators. During escape responses, the soft-bodied robot has the similar input-output relationships with those of real fishes. The linear velocity of the soft robot is about 0.15m/s and it can be both self-contained and capable of rapid planar body motion. After that, they further developed an autonomous soft-bodied robotic fish that is hydraulically actuated and capable of sustained swimming in three dimensions, shown in Fig. 1.9 [55]. This fish-like soft body has been extended to deform under hydraulic replacing the pneumatic power. Circulation of water provides control over caudal fin propulsion and yaw motion of the soft robotic fish. It is enabling a wide-range of con-

tinuous body deformations. Moreover, the dynamic diving capabilities of the soft robot are described though pectoral fin as dive planes. These capabilities enable fish-like motion in three dimensions. In addition, the fish-like pectoral fin based on conducting polymer is developed from MIT. Through conducting polymer actuators, the necessary structural flexibility can be attainable for fish-like robot.

Fig. 1.8 Soft robotic fish developed by MIT [53].

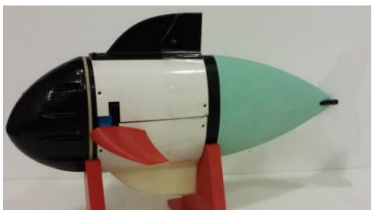

Fig. 1.9 Soft robotic fish with 3-D swimming developed by MIT [55].

Methran Mojarrad group in the University of New Mexico used the polyelectrolyte ion-exchange membrane (IEM) as artificial muscle to design the soft robotic fish with anguilliform propulsion in 1996 [56], [57]. Northeastern University (NU) developed an undulatory robotic lamprey using SMA and the latest prototype was shown in Fig. 1.10 [58]-[60]. It not only can swim forward by body propulsion but can control swimming depth. The generated undulatory motion similar to that of fishes in small robotic system was realizable.

Fig. 1.10 Undulatory robotic lamprey using SMA [60].

The University of Central Florida and Texas A & M University also used SMA to design the micro robotic fish and underwater biomimetic vehicle [61]. The SMA can realize force and moment control of the fin for propulsion. The Michigan State University (MSU) developed a robotic fish with the flexible tail shaft controlled precisely by a servo motor, shown in Fig. 1.11 [62]. If a flexible fin attached to the tail shaft, the robot can achieve faster turning with a smaller radius than the case of a rigid fin. The Smart Microsystems Laboratory (SML) at Michigan State University designed an autonomous robotic fish [63], [64]. Figure 1.12 shows the prototype of robotic fish. The robotic fish propelled by an artificial caudal fin using IPMC are designed for autonomous operation. The robot body is about 20 cm in length without the tail, about 180cm^3 in volume and about 290g in total weight. It can make the swimming motion with a speed of about 0.02m/s. The modules of sensing, wireless communication, localization and navigation are all considered in the robot development. It is capable of interfacing with a number of aquatic sensors.

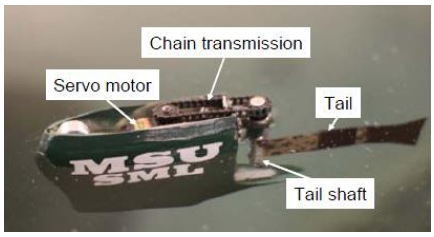

Fig. 1.11 Robotic fish developed by MSU [62].

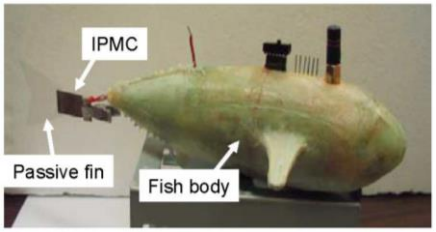

Fig. 1.12 Robotic fish using SMA [64].

In Japan, Toshio Fukuda from Nagoya University developed the underwater micro robot with body propulsion using SMA [65] and micro robotic fish with pectoral fin propulsion using piezoelectric ceramic [66]. For the body propulsion of micro robot in

the water, Toshio Fukuda proposed a synthesized sum of excited modes from SMA, like the mode expansion and synthesis, to design the anguilliform propulsion for robotic fish. Besides, the Nagoya University, Kobe University and AIST have a corporation on design an underwater robot with IPMC actuator to mimic rajiform swimming such as pectoral fin motion. Fins are designed using 16 IPMCs, shown in Fig. 1.13 [67]. A simple traveling wave control input is employed to generate moment on the fin.

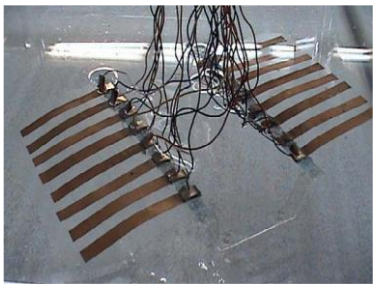

Fig. 1.13 Fins used in experiment for underwater robot [67].

The University of Tokyo presented the biologically inspired robotic fish using electrostatic film, named Seidengyo [68]. The graph of robot Seidengyo I and II are shown in Fig. 1.14 and Fig. 1.15, respectively [68]. The electrostatic film motor is made of two pieces of flexible printed circuit film and can be utilized as the new artificial muscle. Its power transmission system permits reciprocating power to be converted to periodic oscillations and distributed to the caudal fin. The Seidengyo I is designed with a lunate flexible caudal fin and its body consists of the stator and slider films. The entire fish body can be considered to be an electrostatic film motor. The weight of Seidengyo I is only 5g and the average cruising speed can reach up to approximately 0.018m/s. The Seidengyo II is the improved version of the Seidengyo I. It uses a waterproof coat, a versatile microcomputer and a self-made high-voltage amplifier to solve some deficits in Seidengyo I, such as lack of manoeuvrability, incompatibility with water and expensiveness of the controller, and enhance the propulsion performance and adaptability of the robotic fish. It makes itself swim at the speed of about 0.04m/s, larger than the 0.018m/s of Seidengyo I.

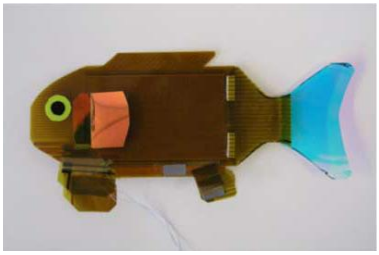

Fig. 1.14 Robotic fish of the Seidengyo I [68].

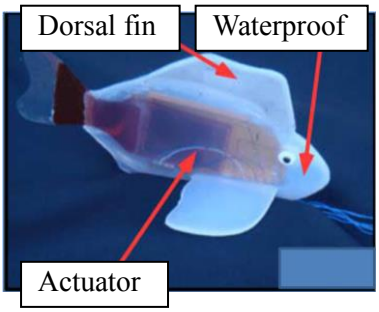

Fig. 1.15 Robotic fish of the Seidengyo II [68].

Shuxiang Guo's group from Kagawa University presented a fishlike micro robot using ICPF actuator to make the tail fin propulsion [69]. The total structure of the micro robot is shown in Fig. 1.16 [69]. It has two tails with a fin driven, a body posture adjuster and a buoyancy adjuster. The micro robotic fish is 45mm in length, 10mm in width and 4mm in thickness. Later, they presented a novel tortoise-like flexible micro robot with four legs actuated by ICPF [70] and underwater swimming micro robot using IPMC actuator shown in Fig. 1.17 [71].

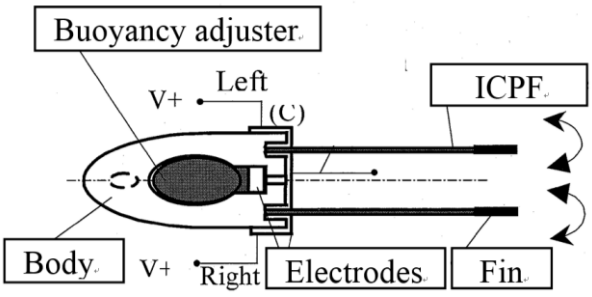

Fig. 1.16 Structure of micro robotic fish developed by Kagawa University [69].

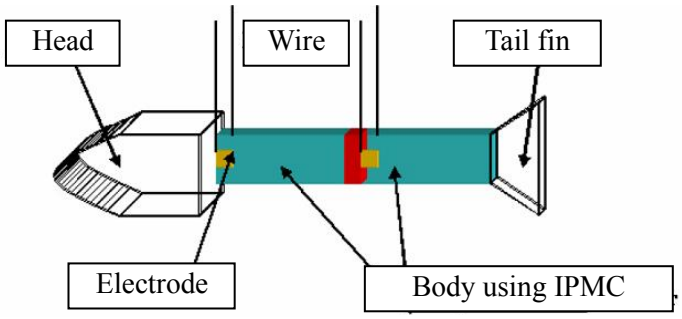

Fig. 1.17 Structure of micro robotic fish using IPMC [71].

The Okayama University designed a soft-bodied manta swimming robot using an optimal bending pneumatic rubber actuator [72]. The prototype is shown in Fig. 1.18. The developed manta swimming robot is made only of rubber and it swims in water smoothly and flexibly similar to a living fish. It is not suitable for remote navigation and self-control.

Fig. 1.18 Prototype of manta swimming robot [72]

The SSSA Lamprey robot used neuroscientific models of goal-driven locomotion to design the soft robot body for river exploration. The Universidad Politecnica de Madrid developed a swimming fish-like robot by using SMA actuators, shown in Fig. 1.19 [73]. The six SMA-based actuators are adopted. These actuators are suitable for bending the continuous backbone of the fish, which in turn causes a change in the curvature of the body. The length of robot body is 300mm.The robot can make the steady motion with 0.1BL/s (body length per second). From this research, it is confirmed that the smart actuators and flexible structures can be a promising field for making alternative bio-inspired robots.

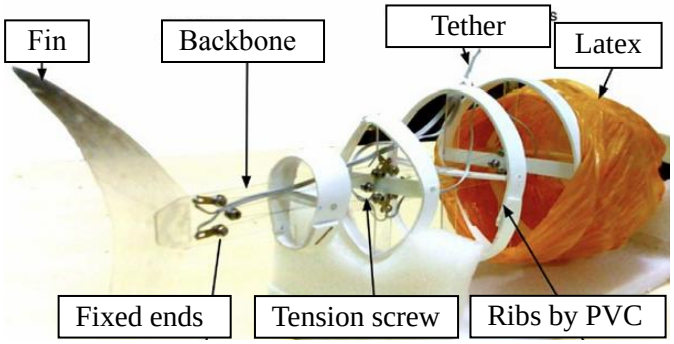

Fig. 1.19 Robotic fish using SMAs [73].

The University of Victoria made a simplified SMA-actuated tuna and its SMA actuated tail design was described in Fig. 1.20 [74]. It was found that the actuators had better cooling and thus could maintain higher tail beat frequencies. The Swiss Federal Laboratories for Materials Testing and Research developed a fish-like airship that uses dielectric elastomer (DE) actuator sheets to produce a large-scale carangiform motion [75], but to date, there has been no attempt to realize this in an aquatic environment. The final version of prototype of fish-like airship using DE actuators is described in Fig. 1.21.

Fig. 1.20 Tail of robot using SMA [74].

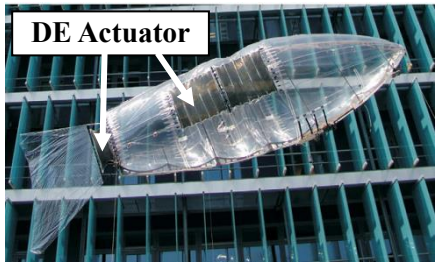

Fig. 1.21 Tail of robot using SMA [75].

The Korea Institute of Science and Technology developed a wireless undulatory tadpole robot (TadRob) using ionic polymer metal composite (IPMC) actuator [76]. The velocity of TadRob can be controlled by changing frequency of input voltage and the steering angle can be increased by increasing the duty ratio. In Singapore, the Nanyang Technological University (NTU) developed a metamorphic underwater vehicle (MUV) that propels by changing shape through the inflation and deflation of water-filled balloons [77]. The mechanical system designed on MUV proves to be very reliable and flexible in producing desired body shapes. Through the corporation with University of Science and Technology of China (USTC), they also designed an undulating finned body system using SMA as actuators. The undulating waveform of the anguilliform mode is chosen to develop this system. The designed body is made of flexible polyurethane, which is actuated and controlled by the SMA wires. The prototype of three-body segments by mimicking the eel-like undulating wave motion is shown in Fig. 1.22 [78].

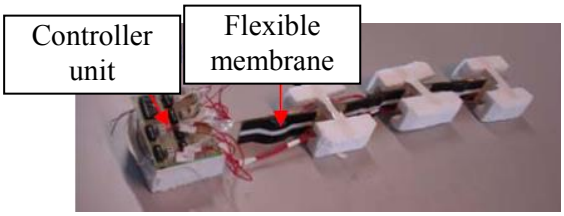

Fig. 1.22 Prototype of eel-like undulating body by using SMA [78].

In China, the Robotic Institute of Beihang University designed the manta robotic fish ROBO-MANTA III with MPF propulsion, shown in Fig. 1.23 [79]. This robot focuses on the design of soft fish body and soft propulsion mechanism. A micro biomimetic manta ray robotic fish actuated by SMA wire in Fig. 1.24 was developed by the Harbin Institute of Technology [80]. The robot fish has a flat-form body and a pair of triangular flexible pectoral fins. The total length of the prototype is about 243mm and the weight is 354g. The relatively good stability and stealthily are realized in the swimming motion of the robotic fish. However, its maximum swimming speed is not fast, just 57mm/s, the performance of the micro manta ray should be improved. The Harbin Engineering University also developed a centimetre-scale robotic fish using IPMC actuator, shown in

Fig. 1.25 [81]. Two pieces of Polyvinylchloride (PVC) film and an IPMC construct a caudal fin. The remote control function is realized at the base of an infrared sensor. Its swimming pattern of cruise-straight, cruise-in-turning, burst and coast are realized respectively.

Fig. 1.23 ROBO-MANTA III [79].

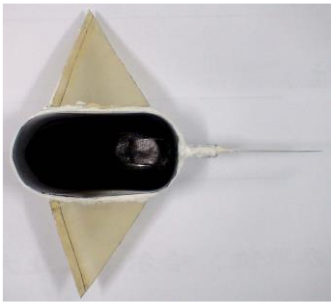

Fig. 1.24 Micro robotic manta ray developed by Harbin Institute of Technology [80].

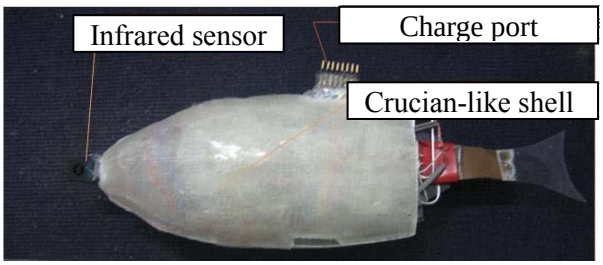

Fig. 1.25 Robotic fish using IPMC developed by Harbin Engineering University [81].

The Ohio State University in Columbus designed a swimming vehicle propels itself through the oscillations of a flexible fin mounted in the stern, shown in Fig.1.26 [82]. It is actuated by two curved-beam bending piezoelectric actuators. Each actuator consists of layer of stainless steel, piezoceramic layer (PZT-5A), two layers of LaRC-SI heat-

activated adhesive and layer of aluminium foil. The swimming vehicle prototype achieves fish-like manoeuvring and an approximate velocity of 0.25m/s.

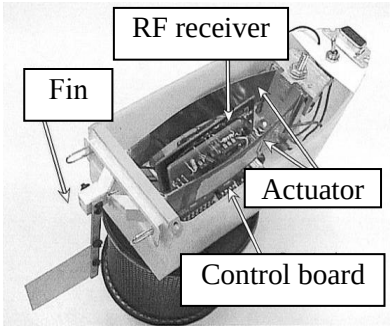

Fig. 1.26 Prototype of swimming vehicle [82].

The University of Auckland in New Zealand developed a trilayer polypyrrole (PPy) polymer actuated biomimetic robotic fish, described in Fig.1.27 [83]. The trilayer polymer actuators have PPy films attached on both sides of inner passive films. The inner passive films are polyvinylidine fluoride (PVDF), an electronically insulating porous film. The fish embeds a microcontroller, a Lithium battery and circuitry for navigation and control. Waterproof packaging is designed for protecting the electronics inside. The fish cruises by its actuated tail fin. The length of the body is only 9cm. However, the speed of the swimming is low. This robotic fish can operate 10-12 hours lifetime with an average speed of 1-2mm/s.

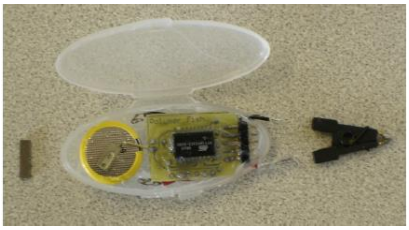

Fig. 1.27 Robotic fish developed by The University of Auckland [83].

Besides, the Festo's Bionic Learning Network designed a swimming robotic fish named Airacuda shown in Fig. 1.27 [84]. It uses pneumatic muscles made of rubber reinforced with aramid fibre. There are two muscles that are alternately pressurised to bend the tail and drive the robot forward existent on the soft robotic fish.

Fig. 1.28 Robotic fish named Airacuda [84].

Among these fishlike soft robots, the propulsion methodologies of the robotic fishes are varies. Many robots use flexible actuators with smart materials for robot actuation. The flexible actuators using SMA, electrostatic film, PZT film, IPMC, or piezoelectric fibre composite (PFC) are soft and flexible. The flexible actuators have high power/weight ratio and simple mechanical structure. The soft robotic fish using flexible actuator can obtain relatively better propulsion characteristics and motion performances similar to those of fishes. However, above mentioned previous work of soft robotic fish using flexible actuators just considers that whether these flexible actuators can be applied into the robots for actuation or not to realize the simple swimming motion in the fluid. Through the corresponding prototypes and experiments of the designed robotic fish using flexible actuators, they just verified the feasibility of the application of flexible actuators on robot structure for actuation, and their researches only present the possibility of utilizing the flexible actuators in achieving the simple swimming motion. The propulsion characteristic and motion performance of the soft robotic fish are not mainly focused in these researches, not to mention the performance improvement of the soft robotic fish and the interaction between the flexible robot structure and surrounding fluid in its propulsion. In order to meet the requirement of complicated working environment and overcome the shortcomings from the previous work, the propulsion performance and characteristics of the soft robotic fish using flexible actuators are necessary to be investigated and improved to realize the fishlike propulsion and high manoeuvrability. To improve the propulsion performance of the soft robotic fish in the fluid, its hydrodynamic characteristics are needed to be investigated by taking into ac-

count the interaction between the flexible robot structure and surrounding fluid to overcome the drawbacks from previous work.

By comparison of motion characteristics of the typical flexible actuators, described in Table 1.3, the PFC actuator has the larger output, fast response and multi-functions. Thus, in the present research, the flexible actuator using piezoelectric fiber composite is adopted for developing the soft robotic fish. The propulsion mechanism based on PFC actuator can be constructed to a simple and compact structure with high energy conversion efficiency and large displacement response through the high input voltage.

Table 1.3 Performance Comparison among Typical Flexible Actuators

Item	Response	Durability	Environment	Output
IPMC	Fast	Good	Water is essential	Low
SMA	Slow	Good	Cooling & Temperature control	large
Electrostatic Film	Slow	Good	High voltage	Large
PFC	Fast	Good	High voltage	Large

1.2 Research Objectives

In the research, development of the biomimetic soft robotic fish with high motion performance is main objective.

When designing soft robotic fish, a surrounding fluid must be considered. The presence of fluid increases the system mass, stiffness and damping, and changes the mechanical dynamic characteristics of the contained robot structure. FSI, firstly developed in the 1980s, is the interaction of some movable or deformable structure with an internal or surrounding fluid flow [85]. Therefore, to fully investigate the structural dynamic responses and hydrodynamic performances of the soft robotic fish, the interaction

between the fluid and robot structure must be taken into account and the coupling mechanisms for FSI analysis must be modelled accurately.

However, the coupling problem is very difficult to be solved due to the large deformation of flexible robot structure and complicated coupling dynamics with surrounding fluid. This is the main reason why the design and control method of soft robotic fish has not been established while many trial developments have been done up to now. It motivates us to investigate the design and control problems of the soft robotic fish by analytical simulation with coupling between the flexible structure and surrounding fluid. The aim of this study is not only to develop a biomimetic soft robotic fish with high performance, but also to establish the design and control method of the soft robotic fish based on numerical simulation considering the interaction between flexible robot structure and surrounding fluid for future improvement. Through numerical coupling simulation of biomimetic soft robotic fish, the propulsion characteristics will be investigated to improve its propulsion performance such as large propulsive force and achieve the relatively optimal soft robotic fish with high performance.

In the dissertation, to achieve the biomimetic soft robotic fish with high performance, the following content are developed.

Firstly, the basic design method and corresponding numerical simulation system are proposed and constructed. Through the proposed design method and numerical simulation, it is possible to develop the biomimetic soft robotic fish with high performance effectively by optimization of design and control of the soft robotic fish.

Secondly, modelling of soft robotic fish by mimicking the soft structure and driving mechanism of fishes is carried out based on FEM. The propulsion motion and propulsive force of the soft robotic fish are investigated through two kinds of numerical analyses. One is the modal and transient analysis considering the surrounding fluid as acoustic fluid. The propulsion mode and amplitude of the propulsion motion of soft robotic fish are investigated, which are directly related to the propulsion mechanism and motion performance of the fishes. The other is the fluid-structure interaction (FSI) anal-

ysis. The interaction between the soft robot structure and surrounding fluid is taken into account. From FSI analysis, the hydrodynamic performances of the soft robotic fish can be obtained for studying its propulsion motion. It is possible to further improve the performance of the soft robotic fish through studying its design and control based on FSI analysis.

Thirdly, the performance evaluation is carried out by comparison between the simulation and experiment on actual prototype to validate the feasibility of the modelling method and numerical simulation analysis on design and control of the biomimetic soft robotic fish.

Finally, the optimization and improvement are performed for developing the biomimetic soft robotic fish with high performance based on verified coupling analysis. The corresponding performance evaluation on robot prototype is presented to confirm the performance improvement of the optimized soft robotic fish.

1.3 Technical Advantages and Contributions

The main technical advantages and contributions within the scope of this dissertation are shown as follows.

Firstly, to consider the interaction with surrounding fluid for FSI solution, the desired coupling simulation platform and modelling method has been established specifically for the soft robotic fish coupled with fluid through utilizing the verified numerical algorithms.

Secondly, fish-like propulsion motion of the soft robotic fish in the fluid is identified and realized by verified coupling simulation analysis. The successful application of structural motion control by controlling the deformation modes about frequencies and mode shapes of robot structure in the fluid is realized on soft robotic fish. It is suitable to identify the fish-like propulsion motion of the soft robotic fish in the fluid and use

different propulsion modes to design different propulsion mechanism in the fluid for improvement.

Thirdly, the hydrodynamic force and displacement of soft robotic fish can be evaluated effectively by established FSI analysis. The present numerical results about propulsive force and displacement of the soft robot are congruent with experiments on robot prototype. The FSI analysis is useful to describe the hydrodynamic performance of the soft robotic fish and evaluate its propulsion characteristics in the fluid for improvement.

Fourth, new optimal soft robotic fish with higher swimming velocity and better fish-like swimming performance is developed successfully based on established coupling method. Fish-like body bending propulsion motion is successfully achieved on robot prototype. It lays a foundation for establishing the design and control method of the soft robotic fish, and provides a way for further optimization and improvement on motion performance of the soft robotic fish.

Fifth, this study not only presents the possibility and feasibility of utilizing the flexible actuators in achieving fish-like swimming motion using flexible actuator, but also enhances propulsion performance of soft robotic fish in the fluid by investigating its propulsion characteristic taking into account the interaction between flexible robot structure and surrounding fluid in the propulsion. These overcome the shortcomings from previous work in which the propulsion characteristics such as propulsion mode and interaction with surrounding fluid are not focused.

Sixth, different from many researches only focusing on hydrodynamics of robot body (that is, no oscillating or undulating motion occurs on robot), the hydrodynamic performance caused by robot oscillating motion is investigated in the study. In the numerical analysis, the robotic fish's flexible deflection, large-amplitude propulsion motion, and vortex distribution in the wake of the soft robotic fish are all considered for performance improvement. It plays powerful role in development of soft robotic fish effectively, enhances the design flexibility of the soft robotic fish, and provides multiple angles to develop the soft robotic fish with high performance in depth.

1.4 Outline of the Dissertation

The content of the dissertation is outlined as follows.

Chapter 1 is an introduction. The background and relative previous work about biomimetic soft robotic fish are briefly reviewed. It summarizes the current research status and problems of biomimetic soft robotic fish, and describes the purposes of this research.

Chapter 2 presents the design method, procedures and numerical simulation system in the present research for developing the biomimetic soft robotic fish with high performance. Different from previous development method, our purpose is how to design and control the soft robotic fish by utilizing interaction between the flexible structure and surrounding fluid effectively based on numerical simulations. Therefore, it is necessary to model a fish-like soft robot structure including soft actuators and an enclosed fluid. Besides, by the numerical analysis considering the interaction between flexible structure and fluid, the fish-like propulsion motion should be realized and established, and then the robot structure and control inputs are needed to be optimized for performance improvement. In order to meet these requirements of designing and developing the optimal soft robotic fish, the design method based on modelling, simulation analysis and improvement is presented and the numerical simulation system for soft robotic fish is built. In the simulation system, modelling of soft robotic fish, modal and transient analysis considering the enclosed fluid as acoustic fluid are firstly described based on FEM to realize the fish-like propulsion motion with large amplitude for the soft robotic fish. Then, the FSI analysis is performed to describe and establish the hydrodynamic performances of the soft robotic fish. Based on this numerical simulation system, it is possible to develop the biomimetic soft robotic fish with high performance effectively by optimization of design and control of the soft robotic fish.

Chapter 3 describes the modelling and numerical analysis of biomimetic soft robotic fish by using the method presented in Chapter 2. The soft robotic fish uses the piezoelectric fiber composite (PFC) as soft actuator. Firstly, the relationships between the input

voltage and generated stress of the PFC are derived. The generated stress can be applied on soft structure to investigate the motion performance of the soft robotic fish. To support the driving model of the PFC, the corresponding experiments on simple beam model are carried out. By comparing the simulation results with experimental results, the effectiveness of the driving model is verified. Then, the modal analysis in which the fluid is considered as acoustic fluid is performed. The structural mode frequencies and mode shapes of the soft robotic fish in the fluid are calculated. By comparing these modes' motion with those of the real fishes, the fish-like propulsion mode is identified to realize the corresponding propulsion motion of the soft robotic fish. Furthermore, based on the verified driving model of soft actuator, the amplitude of the main propulsion motion of soft robotic fish is calculated. Through FSI analysis, the relationships of driving frequencies of input signal with propulsive force and displacement of propulsion motion, and vortex distribution in the wake around the soft robotic fish are investigated for the case of fixing robot head. Besides, the motion control of soft robot is investigated to realize turning motion in the fluid. Through controlling the input voltage amplitude on soft actuators of the robot, turning right and turning left motion are identified in the swimming when the input voltage amplitudes on two actuators are in asymmetric distribution.

Chapter 4 is experiment evaluation. In order to validate the results of numerical simulation analysis described in Chapter 3, the mode shapes, amplitude of propulsion motion, propulsive force and vortex distribution around soft robotic fish for the case of fixing robot head, and turning motion are measured by using actual robot prototype. The present simulation results are congruent with experiments. By the results, the effectiveness of the modelling method and numerical analysis used in the research is verified and they are useful to predict the propulsion characteristics of the soft robotic fish in the fluid for performance improvement.

Chapter 5 develops a new soft robotic fish with high performance based on above modelling method and numerical analysis by optimization. Firstly, the structural parameters of the robot are allowed to vary within a range and the amplitude of the propulsion

motion for the soft robot is calculated for different parameters by the numerical analysis. Then the structural parameters of the robot capable of propulsion motion with larger-amplitude are chosen for improvement. Based on this result, new soft robot is designed and evaluated by experiments. From the experimental results of the new soft robot, it is confirmed that the higher swimming speed, better fish-like swimming performance and larger turning velocity are realized. It can be said that the new soft robotic fish has been developed successfully for improvement.

Chapter 6 summarizes the conclusions and future works of this research.

References for Chapter 1

[1] M. Sfakiotakis, David M. Lane and J. Bruce C. Davies, “Review of fish swimming modes for aquatic locomotion,” IEEE Journal of Oceananic Engineering, Vol. 24, No. 2, pp. 237-252, 1999.

[2] P. W. Webb, “Form and Function in Fish Swimming,” Scientific American, Vol. 251, No. 1, pp. 58-68, 1984.

[3] C. M. breder, “The locomotion of fishes,” Zoologica, Vol. 4, pp. 159-297, 1926.

[4] C. C. Lindsey, “Form, function, and locomotory habits in fish,” Fish Physiency, W.S. Hoar and D. J. Randall. Eds, NewYork: Academic, pp. 1-100, 1978.

[5] X. Tan, Y. Zhong and Y. Yang, “Study and analysis of current situation towards swimming microrobot in liquid,” Robot, Vol. 23, No. 5, pp. 467-470, 2001.

[6] A. Azuma, Encyclopaedia of Creature’s Motion, Asakura Publishing, 1997.

[7] J. J. Videler, Fish Swimming, Chapman & Hall, London, 1993.

[8] T. E. Faber, Fluid dynamics for physicists, Cambridge Univ. Press, Cambridge, UK, 1995.

[9] R. Cortez, L. Fauci, N. Cowen and R. Dillon, “Simulation of swimming organisms: coupling internal mechanics with enternal fluid dynamics,” Comp. Sci. Eng. Vol. 6, pp. 38-45, 2004.

[10] G. I. Taylor, “Analysis of the swimming of long and narrow animal,” Proc. Of the Roy. Soc. Lond. A, Vol. 214, pp. 158-183, 1952.

[11] P. W. Webb, “Hydrodynamics and energetics of fish propulsion,” Bull. Fish. Res. Bd. Can, Vol. 190, pp. 1-159, 1975.

[12] E. D. Tytell, “The hydrodynamics of eel swimming II. Effect of swimming speed,” Journal of Exp. Biol., Vol. 207, pp. 3265-3279, 2004.

[13] T. Y. Wu, “Swimming of a waving plate,” Journal of Fluid Mech., Vol. 10, pp. 321-344, 1961.

[14] M. J. Lighthill, “Note on the swimming of slender fish,” Journal of Fluid Mech., Vol. 9, pp. 305-317, 1960.

[15] M. J. Lighthill, “Aquatic animal propulsion of high hydromechanical efficiency,” Journal of Fluid Mech., Vol. 44, pp. 265-301, 1970.

[16] M. J. Lighthill, “Large-amplitude elongated-body theory of fish locomotion,” Proc. Of the R. Soc. Lond. (B), Vol. 179, pp. 125-138, 1971.

[17] G. K. Batchelor, An introduction to fluid mechanics, Cambridge Univ. Press, Cambridge, UK, 1973.

[18] T. L. Daniel, “Unsteady aspects of aquatic locomotion,” Amer. Zool. Vol. 24, pp. 121-134, 1984.

[19] P. W. Webb, “Is the high cost of body caudal fin undulatory swimming due to increased friction drag or inertial recoil,” Journal of Exp. Biol., Vol. 162, pp. 157-166, 1992.

[20] F. Hess and J. J. Videler, “Fast continuous swimming of saithe (Pollachius virens): a dynamic analysis of bending moments and muscle power,” Journal of Exp. Biol., Vol. 109, pp. 229-251, 1984.

[21] T. L. Daniel and P. W. Webb, Physics, design and locomotor performance, Liviana Press, Springer Verlag, New York, pp. 343-369, 1987.

[22] U. K. Muller, E. J. Stamhuis and J. J. Videler, “Riding the waves: the role of the body wave in undulatory fish swimming,” Integr. Comp. Biol., Vol. 42, pp. 981-987, 2002.

[23] E. D. Tytell and G. V. Lauder, “The hydrodynamics of eel swimming. I. wake structure,” Journal of Exp. Biol., Vol. 207, pp. 1825-1841, 2004.

[24] S. R. Ded and S. Deb, Robotics Technology and Flexible Automation, Tata McGraw Hill Education, 2010.

[25] G. Ma, “The research of the biomimetic robots,” Vol. 23, No. 5, pp. 463-466, 2001.

[26] E. Kim and Y. Youm, “Design and dynamic analysis of fish robot: PoTuna,” Proc. Of the IEEE International Conference on Robotics and Automation, pp. 4887-4892, 2004.

[27] J. M. Anderson, “The vorticity control unmanned undersea vehicle,” Proc. Of the International Symposium on Seawater Drag Reduction, pp. 479-483, 1998.

[28] X. Deng and S. Avadhanula, “Biomimetic micro underwater vehicle with oscillating fin propulsion: system design and force measurement,” Proc. Of the IEEE International Conference on Robotics and Automation, pp. 3312-3317, 2005.

[29] J. M. Kumph, “Maneuvering of a robotic pike,” M. S. Thesis, Massachusetts Institute of Technology, USA, 2000.

[30] M. S. Triantafyllou, A. H. Techet and F. S. Hover, “Review of experiment work in biomimetic foils,” Journal of Oceanic Engineering, Vol. 29, No. 3, pp. 585-593, 2004.

[31] K. H. Low, C. W. Chong and C. Zhou, “Performance study of a fish robot propelled by a flexible caudal fin,” Proc. Of the IEEE International Conference on Robotics and Automation, pp. 90-95, 2010.

[32] X. Tan, M. Carpenter, J. Thon and F. Alequin-Ramos, “Analytical modeling and experimental studies of robotic fish turning,” Proc. Of the IEEE International Conference on Robotics and Automation, pp. 102-108, 2010.

[33] Alessandro Crespi, Andr´e Badertscher, Andr´e Guignard, et al., “AmphiBot I: an amphibious snake-like robot,” Robotics and Autonomous Systems, Vol. 50, pp. 163-175, 2005.

[34] H. Hu, “Biologically inspired design of autonomous robotic fish at Essex,” Proc. Of the IEEE SMC UK-RI Chapter Conference on Advances in Cybernetic Systems, pp. 1-8, 2006.

[35] M. Mojarrad and M. Shahinpoor, “Biomimetic robotic propulsion using polymeric artificial muscles,” Proc. Of the IEEE International Conference on Robotics and Automation, pp. 2152-2157, 1997.

[36] J. M. Anderson and P. A. Kerrebrock, “The vorticity control unmanned undersea vehicle (VCUUV)—an autonomous vehicle employing fish swimming propulsion and maneuvering,” Proc. Of the l0th Int. Symposium on Unmanned Untethered Submersible Technology, pp. 189-195, 1997.

[37] S. Hirose and E. F. Fukushima, “Snakes and strings: new robotic components for rescue operations,” International Journal of Robotics Research, Vol. 23, pp. 341-349, 2004.

[38] D. Trivedi, C. D. Rahn, W. M. Kier and I. D. Walker, “Soft robotics: biological inspiration, state of the art, and future research,” Applied Bionics and Biomechanics, Vol. 5, No. 3, pp.99-117, 2008.

[39] H. Liu, Y. Tang, Q. Zhu and G. Xie, “Present research situations and future prospects on biomimetic robot fish,” International Journal of Smart Sensing and Intelligent Systems, Vol. 7, No. 2, pp. 458-480, 2014.

[40] K. Streitlien, G. S. Triantafyllou and M. S. Triantafyllou, “Efficient foil propulsion through vortex control”, AIAA Journal, Vol. 34, No. 11, pp. 2315-2319, 1996.

[41] Http://www.robotic-fish.net. RoboPike, MIT.

[42] J. M. Anderson and N. K. Chhabra, “Maneuvering and stability performance of a robotic tuna”, Integ. And Comp. Biol., Vol. 42, pp. 118-126, 2002.

[43] P. Menzel and F. D. Aluisio, “Robo sapiens: evolution of a new species,” Art & Licensing Int., Inc., pp. 80-81, 2002.

[44] N. Kato and T. Inaba, “Hovering performance of fish robot with apparatus of pectoral fin motion,” Proc. Of the 10th Int. Symposium on Unmanned Untethered Submersible Technology, pp. 177-188, 1997.

[45] N. Kato and M. Furushima, “Pectoral fin model for manoeuvre of underwater vehicles,” Proc. Of the IEEE AUV Symposium, pp. 49-56, 1996.

[46] Http://www.nmri.go.jp/eng/khirata/fish/experiment/upf2001/index_e.html. Prototype Fish Robot, UPF-2001.

[47] Schools of robofish to sniff out pollution in the Thames. Daily Mail Reporter. March, 2009.

[48] B. Peter, R. Ratnaweera, W. Fischer, C. Pradalier and R. Y. Siegwart, “Design and evaluation of a fin-based underwater propulsion system,” Proc. Of the IEEE International Conference on Robotics and Automation, pp.3751-3756, 2010.

[49] C. Zhou, K. H. Low, “Better endurance and load capacity: an improved design of manta ray robot (RoMan-II),” Journal of Bionic Engineering, No. 7, pp.137-144, 2010.

[50] K. H. Low and A. Willy, “Biomimetic motion planning of an undulating robotic fish fin,” Journal of Vibration and Control, Vol. 12, No. 12, pp. 1337-1395, 2006.

[51] R. B. Williams and D. J. Inman, “An overview of composite actuators with piezoceramic fibers,” Proc. Of the 20th International Modal Analysis Conference, pp. 421-427, 2002.

[52] P. A. Kerrebrock, J. M. Anderson and J. R. Parry, “Application requirements of artificial muscles for swimming robots,” Proc. Of the SPIE4329, Smart Structures and Materials: Electroactive Polymer Actuators and Devices, pp. 364-374, 2001.

[53] A. D. Marchese, C. D. Onal and D. Rus, “Autonomous soft robotic fish capable of escape maneuvers using fluidic elastomer actuators,” Soft Robotics, Vol. 1, No. 1, pp. 75-87, 2014.

[54] A. D. Marchese, C. D. Onal and D. Rus, “Towards a self-contained soft robotic fish: on-board pressure generation and embedded electro-permanent magnet valves,” International Symposium on Experimental Robotics (ISER), Quebec City, 2012.

[55] R. K. Katzschmann, A. D. Marchese, D. Rus, “Hydraulic Autonomous Soft Fish for 3D Swimming,” International Symposium on Experimental Robotics (ISER), 2014. (Submission).

[56] M. Mojarrad and M. Shahinpoor, “Noiseless propulsion for swimming robotic structures using polyelectrolyte ion-exchange membrane,” Proc. Of the SPIE North American Conference on Smart Structures and Materials, pp.183-192, 1996.

[57] M. Mojarrad and M. Shahinpoor, “Biomimetic robotic propulsion using polymeric artificial muscles,” Proc. Of the IEEE International Conference on Robotics and Automation, pp. 2152-2157, 1997.

[58] J. Ayers, J. Davis and A. Rudolph, Neurotechnology for Biomemetic Robots, Cambridge, MA: MIT Press, 2002.

[59] J. Jalbert, S. Kashin, J. Ayers, “A biologically based undulatory lamprey-like auv,” Proc. Of the Autonomous Vehicles in Mine Countermeasures Symposium, pp. 39-52, 1995.

[60] C. Wilbur, W. Vorus, Y. Cao and S. Currie, “A lamprey-based undulatory Vehicle,” In: “Neurotechnology for Biomimetic Robots”, J. Ayers, J.L. Davis, A. Rudolph, eds., MIT Press, pp. 285-296, 2002.

[61] O. Rediniotis, D. Lagoudas, L. Garner, et al., “Development of a shape memory alloy actuated underwater biomimetic vehicle,” Smart Materials and Structures, Vol. 9, No. 5, pp. 673-683, 1999.

[62] X. Tan, M. Carpenter, J. Thon and F. Alequin-Ramos, "Analytical modeling and experimental studies of robotic fish turning," Proc. Of the IEEE International Conference on Robotics and Automation, pp.102-108, 2010.

[63] X. Tan, D. Kim, N. Usher, D. Laboy, J. Jackson, A. Kapetanovic, J. Rapai, B. Sabadus and X. Zhou, "An autonomous robotic fish for mobile sensing," Proc. Of the IEEE/RSJ International Conference on Intelligent Robots and Systems, pp. 5424-5429, 2006.

[64] Z. Chen, S. Shatara and X. Tan, "Modeling of biomimetic robotic fish propelled by an ionic polymer-metal composite caudal fin," IEEE/ASME Transactions on Mechatronics, pp. 1-12, 2009.

[65] T. Fukuda, H. Hosokai and I. Kikuchi, "Distributed type of actuators of shape memory alloy and its application to underwater mobile robotic mechanisms," Proc. Of the IEEE International Conference on Robotics and Automation, pp. 1316-1321, 1990.

[66] T. Fukuda, A. Kawamoto, F. Arai, et al., "Mechanism and swimming experiment of micro mobile robot in water," Proc. Of the IEEE Interactional Conference on Robotics and Automation, pp. 814-819, 1994.

[67] K. Takagi, M. Yamamura, Z. Luo, etc., "Development of a rajiform swimming robot using ionic polymer artificial muscles," Proc. Of the IEEE/RSJ International Conference on Intelligent Robots and Systems, pp.1861-1866, 2006.

[68] Z. Zhang, N. Yamashita and M. Gondo, "Electrostatically actuated robotic fish: design and control for high-mobility open-loop swimming," IEEE Transactions on Robotics, Vol. 24, No. 1, pp. 118-129, 2008.

[69] S. Guo, T. Fukuda and K. Asaka, "A new type of fish-like underwater microrobot," IEEE/ASME Transactions on Mechatronics, Vol. 8, No. 1, pp. 1-6, 2003.

[70] L. Nie, D. Li and S. Guo, "Design and analysis on the dynamics of ICPF actuated tortoise-like flexible micro-robot," Proc. Of the SPIE Sixth Interactional Symposium on Instrumentation and Control Technology: Signal Analysis, Measurement Theory, PHOTE-Electric Technology, and Artificial Intelligence, pp. 6357571-6357576, 2006.

[71] S. Guo, Y. Ge, L. Li and S. Liu, "Underwater swimming micro robot using IPMC actuator," Proc. Of the IEEE International Conference on Mechatronics and Automation, pp. 249-254, 2006.

[72] K. Suzumori, S. Endo, T. Kanda, N. Kato, et al., "A bending pneumatic rubber actuator realizing soft-bodied manta swimming robot," Proc. Of the IEEE International Conference on Robotics and Automation, pp. 4975-4980, 2007.

[73] C. Rossi, J. Colorado, W. Coral and A. Barrientos, "Bending continuous structures with SMAs: a novel robotic fish design," Bioinspiration & Biomimetics, Vol. 6, pp. 1-15, 2011.

[74] A. Suleman and C. Crawford, "Design and testing of a biomimetic tuna using shape memory alloy induced propulsion," Comput. Structs, Vol. 86, No.3-5, pp. 491-499, 2008.

[75] C. Jordi, S. Michel and E. Fink, "Fish-like propulsion of an airship with planar membrane dielectric elastometer actuators," Bioinspiration Biomimetics, Vol. 5, No. 2, 2010.

[76] J. Jung, B. Kim, Y. Tak and J. Park, "Undulatory tadpole robot (TadRob) using ionic polymer metal composite (IPMC) actuator," Proc. Of the IEEE/RSJ International Conference on Intelligent Robots and Systems, pp. 2133-2138, 2003.

[77] I. Chen, H. Li and A. Cathala, "Design and simulation of amoebot-a metamorphic underwater vehicle," Proc. Of the IEEE International Conference on Robotics and Automation, pp. 90-95, 1999.

[78] K. H. Low, Jie Yang, A. P. Pattathil and Y. Zhang, "Initial prototype design and investigation of an undulating body by SMA", Proc. Of the IEEE International Conference on Automation Science and Engineering, pp.472-477, 2006.

[79] Http://robot.buaa.edu.cn/achievement.htm. ROBO-MANTA III.

[80] Z. Wang, Y. Wang, J. Li and G. Hang, "A micro biomimetic manta ray robot fish actuated by SMA," Proc. Of the IEEE International Conference on Robotics and Biomimetics, pp. 1809-1813, 2009.

[81] X. Ye, Y. Su, S. Guo, L. Wang, "Design and realization of a remote control centimetre," Proc. Of the IEEE/ASME. pp. 1-6, 2008.

[82] M. G. Borgen, G. N. Washington and G. L. Kinzel, “Design and evolution of a piezoelectrically actuated miniature swimming vehicle,” IEEE/ASME Transactions on Mechatronics, Vol. 8, No.1, pp. 66-76, 2003.

[83] H. Wang, S. S. Tjahyono, B. MacDonald, P. A. Kilmartin, J. Travas-Srjdic and R. Kiefer, “Robotic fish based on a polymer actuator,” CiteSeer, 2007.

[84] Festo. Airacuda, The Remote Controlled, Pneumatically Driven Fish, Available from: Http://www.festo.com/cms/en_corp/9761.htm.

[85] H. J. Bungartz and M. Schäfer, “Fluid-structure Interaction: Modelling, Simulation, Optimization,” Springer-Verlag, 2006.

Chapter 2. Methodology

This chapter presents the design method, procedures and numerical simulation system in the present research for developing the biomimetic soft robotic fish with high performance. Different from previous development methods, it takes into account the interaction between flexible structure and surrounding fluid by numerical simulations. Therefore, it is necessary to model a driving structure by soft actuators, a fish-like soft robot structure and surrounding fluid domain. Besides, based on numerical analysis considering the interaction between flexible structure and fluid, the fish-like propulsion motion should be realized and established, and then the robot structure is needed to be optimized for performance improvement. In order to meet these requirements of developing the optimal soft robotic fish, the design method based on modelling, simulation analysis and improvement is presented and the corresponding numerical simulation system for soft robotic fish is built. In the simulation system, based on FEM, the modelling of soft robotic fish, modal and transient analysis considering the surrounding fluid as acoustic fluid are presented to investigate and achieve the fish-like propulsion motion with large amplitude of the soft robotic fish. Then, in order to describe and establish the hydrodynamic performances of soft robotic fish in the fluid, the numerical simulation of FSI analysis is performed for performance improvement. Based on these numerical simulations, the biomimetic soft robotic fish with high performance can be developed effectively by optimization of design and control of the soft robotic fish.

2.1 Design Approach of Soft Robotic Fish

With the development of biomimetics and robotics in underwater robots, soft robotic fish as a different branch of robotics turns up in the research field. The soft robotic fish is intended that the components of the robotic fish are soft and flexible, and using the soft material in robot, so that the robot can carry soft payloads without causing damage due to little resistance and move in a small space with good flexibility and mobility. Besides, using large strain deformation of soft components on robot, it can make soft robotic fish that interact with people or working environment without causing injury in unknown environment. The safe actor of the robots is largely improved. To achieve these advantages of the soft robotic fish, development of the soft robotic fish is needed to be carried out. In the development, the bio-inspired technology is the only winner. The investigation of the morphology of the soft material in the nature such as skeletons and muscular from the creatures can get the new insight for robot design. One of the first multi-gait soft robots from the fishes is the robotic starfish developed by the Harvard University [1]. The soft lithography is used to design the robot for sophisticated motion. This prototype validates the soft robot can generate the complicate motions and has good adaptability to interact with its unstructured environments based on simple structure.

Soft robotic fish as a relatively young research field in the underwater robots avoids the rigid components and overcomes the difficulties of the traditional rigid robotic fish in the unknown or high dangerous environments. It can be used to fulfil the work that involves contacting with humans, plants or delicate objects with small injury in the complex underwater environment. Flexibility and mobility are the biggest advantages of the soft robotic fish compared with the rigid one. It is expected that a soft robotic fish can do the special tasks with smaller cost in the underwater exploration and rescue compared with an equivalent rigid robot. Thus, the new problems at the lever of the different components as well as the whole system lever are posed compared with the conventional theories and technologies of rigid robots. Theories and technologies of the

soft robotic fish have not yet been defined in a general form and studies are still exploring new ways for robot development. The special design and control on the accuracy and stability for bio-inspired compliance and physical robustness are needed to come true our desired demand. As a continuum, the exact measurement on shape, point position, controllability, path planning and position sensing of the soft robotic fish is complicated and difficult by comparing with those of rigid robot. There is a challenge of sensing and control for soft robot with high mobility. Therefore, the design method of the soft robotic fish is important and needed to pay more attention on it.

So far, the biomimetic approach has been used to design the soft robotic fish for operation in the unknown or complicated environments. Through mimicking the real fish, the concerned functions of the soft robotic fish can be classified into two types: moving like a fish and looking like a fish, described in Fig. 2.1.

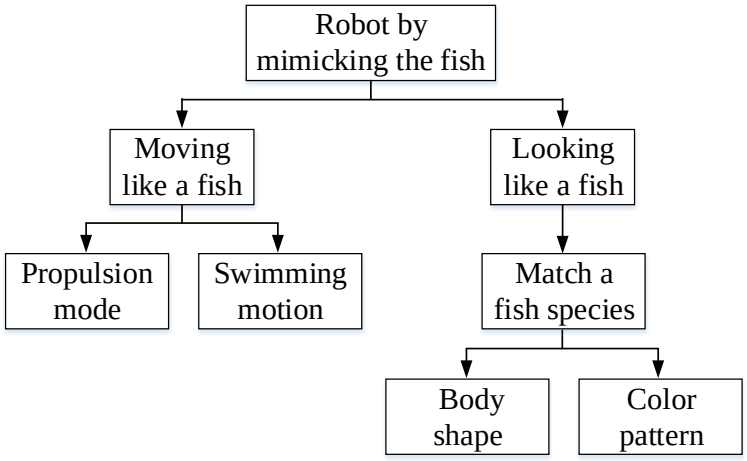

Fig. 2.1 Decomposition of functions for soft robot mimicking the fish.

The type of moving like a fish focuses on the swimming propulsion modes and motions similar to those of real fishes. In the fish-like swimming motion, the swimming performance such as swimming velocity, swimming number, energy consumption, flexibility, adaptability, payload, and son on, are adopted to evaluate the motion performance of the robotic fish. For the type of looking like a fish, it concerns a fish species by matching its body shape and colour pattern. The colour pattern is composed

of pigment-based and structural colour patches. It can signify the quality of a fish or its motivation, and can be used to communicate among species [2]. In the study, the function of moving like a fish is mainly focused by biomimetic approach.

In the design of soft robotic fish by mimicking the real fish, some blocks presented in Fig. 2.2, such as frame members, body structure and materials, actuation mechanism, control system and buoyancy modulation, need to be considered in the robot design. Based on the decided biomimetic fish type and the corresponding swimming mode, the robot body structure is designed. It is important to the robot's strength, stability, safety, payload, durability, and so on. The reasonable materials also need to be adopted in robot body design. The properties of the material determine its suitability for a design. It has close relationship with the robot's strength, rigidity (softness), efficiency, durability, etc. The material cost and availability are also the important factors needed to be focused in the design. Generally, there are many different materials can be used to develop the soft robotic fish, but the reasonable and suitable materials are preferred. As for the actuation of the robotic fish, the appropriate actuation mechanism, such as by motors or flexible actuators with DC/AC source, should be adopted for desired robot performance. Based on the actuation mechanism of the soft robotic fish, the corresponding control systems are designed and constructed for its propulsion, including the communication system and driving system. The wireless or tethered options will be described in the communication control system in which the interaction with people is also considered. The driving devices of the actuation mechanism by using actuator or motor are presented in the driving system of the soft robotic fish. In order to realize the dive motion of the soft robot, the buoyancy modulation is necessary to be investigated. The performance about orientation and depth of the dive motion for the soft robot should be evaluated.

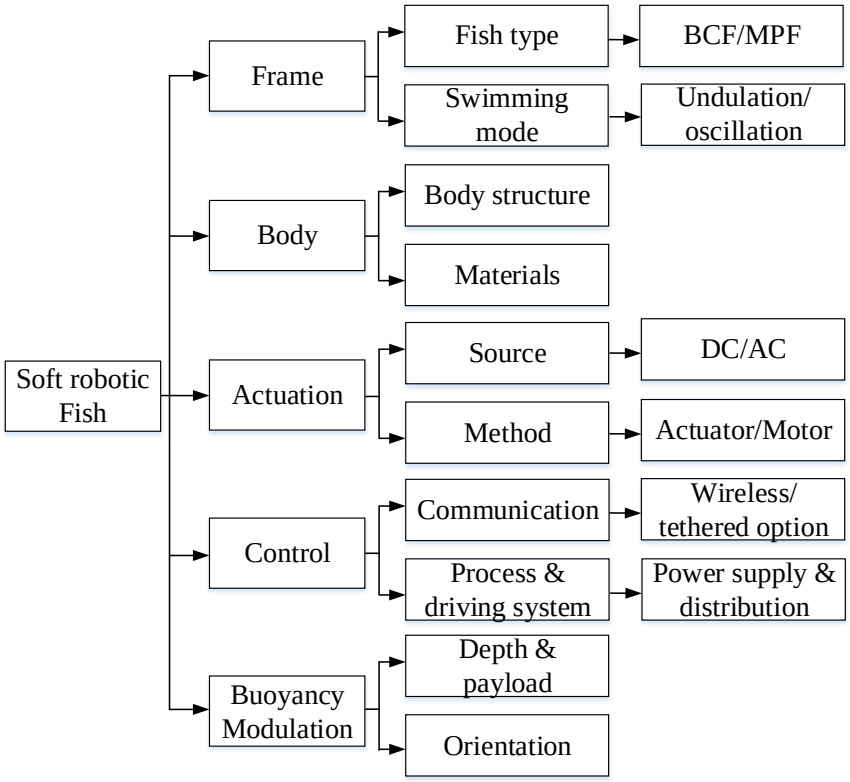

Fig. 2.2 System architecture of design of soft robotic fish.

Fig. 2.3 presents the components of the design system of the soft robotic fish in the study. In this study, the fish type with BCF propulsion is adopted as the biomimetic object, and the swimming mode with subcarangiform type is adopted to design the soft robotic fish. The swimming propulsion mode of the soft robotic fish is mainly focused to realize that the soft robot can move like a real fish. In order to achieve the smooth propulsion and good flexibility, the flexible PFC actuator with larger stain and faster response is adopted to design the actuation structure of the soft robotic fish. The corresponding driving system is also built to meet the requirements of the flexible PFC actuator, including the control input design of basic signals. Based on the characteristics of the flexible PFC actuator, the carbon fiber is adopted as the main material of the robot body to obtain the desired deformation motion of the soft robotic fish. To obtain the dynamical response of the soft robotic fish in the fluid, the fluid effect and interaction between robot structure and fluid are considered in the structural dynamic analysis for performance improvement, which is differ from the general design method in which the

body structure is only concerned and fluid effect is not considered. Through concerning these components in the design, it is committed to realize the basic forward and turning motion of the soft robotic fish by BCF propulsion. The buoyancy modulation about dive motion of the soft robotic fish is not considered in the study.

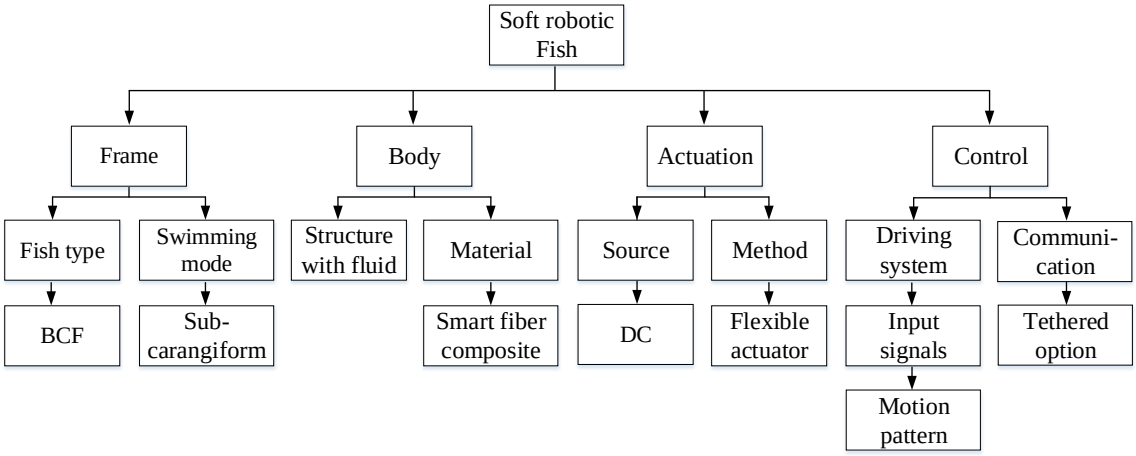

Fig. 2.3 Components of design system of soft robotic fish in the study.

In the present research, development of the soft robotic fish with high performance through the biomimetic method is the main purpose. In many previous work of robot development, design of soft robotic fish is confined to robot structure and ignores the interaction with surrounding fluid to investigate its propulsion performances. And the control technologies of the soft robotic fish are only suitable for special functionality or propulsion motion. Besides, the development of soft robotic fish involves the method of trial and error. Thus, many problems generate, for example, the hydrodynamic model of the soft robotic fish has not been established and defined in a general form; it is difficult in mobility design, performance improvement and the path planning and position sensing due to the single design and control technologies; high cost on robot development and improvement from trial and error. The studies are still exploring the new ways for robot design and development. In order to solve these problems, the design method different from that of previous work is presented. It takes into account the interaction between flexible structure and surrounding fluid based on numerical simulations. There-

fore, it is necessary to model a driving structure by soft actuators, a fish-like soft robot structure and a surrounding fluid domain. Besides, by the numerical analysis considering the interaction between flexible structure and fluid, the fish-like propulsion motion should be realized and established, and then the robot structure and control inputs are needed to be optimized for performance improvement. In order to meet these requirements of developing the optimal soft robotic fish, modelling of soft robotic fish with surrounding fluid, modal and transient analysis considering the surrounding fluid as acoustic fluid are firstly presented in the numerical simulation system based on FEM to investigate and realize the fish-like propulsion motion with large amplitude. Then, the FSI analysis is performed for describing and establishing the hydrodynamic performances of the soft robotic fish. Based on numerical analysis, it is possible to develop the biomimetic soft robotic fish with high performance effectively by optimization of design and control of the soft robotic fish.

In the design procedure of soft robotic fish, the optimal robot model is firstly proposed through the numerical simulation analysis. Then the manufacture and experiment evaluation of the designed robot through the optimal model are carried out. Figure 2.4 shows the design procedure of the soft robotic fish in the present research.

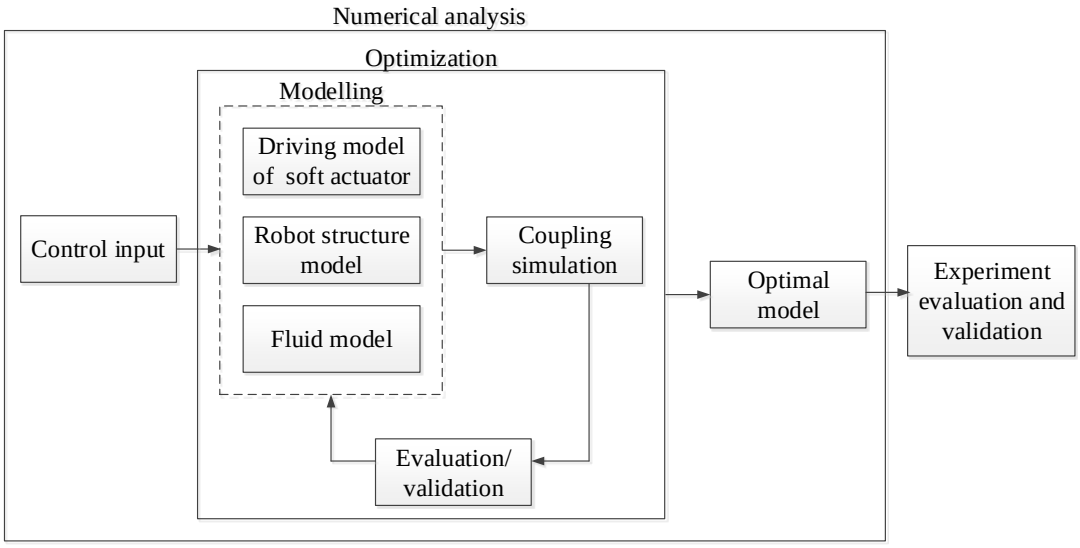

Fig. 2.4 Design procedure of soft robotic fish.

According to the research purpose of developing the soft robotic fish with high performance by biomimetic method, the propulsion approach of the soft robotic fish is needed to be decided firstly based on different propulsion modes of the real fishes. In the research, the real fish with subcarangiform propulsion mode is focused and viewed as biomimetic object to develop the soft robotic fish moving like a fish. In this propulsion mode, the propulsion motion is dominated by inertial force of fluid [3]. Then, the driving model by soft actuator is presented for desired propulsion motion, in which the input signal is also considered for robot actuation. Through the determined propulsion approach and driving model, the modelling of the soft robotic fish including the robot structure model and surrounding fluid model is built, and the corresponding material properties of the robot structure model and fluid model are defined. Based on this robot model, the numerical coupling simulation is performed to realize and establish the fish-like propulsion motion of soft robotic fish, and then the robot structure are optimized by established coupling simulation for performance improvement until achievement of the optimal model with desired performances. Through the optimization using coupling simulations, it can obtain a relatively optimal model for our desired purposes effectively. When the optimal model is achieved, the corresponding experiment evaluation and validation will be done by using actual robot prototype. The detailed scheme of the numerical simulation system is described in next section.

2.2 Numerical Simulation System for Soft Robotic Fish

In order to develop the optimal soft robotic fish with subcarangiform propulsion, the numerical simulation analysis is carried out in the present research for robot development. Different from the conventional analytical method, it considers the interaction between flexible structure and fluid.

When designing a soft robotic fish, a surrounding fluid must be considered. The fluid increases the system mass, stiffness and damping, changes the mechanical dynamic

characteristics of the contained soft robot structure. FSI is the interaction of some movable or deformable structure with an internal or surrounding fluid flow [4]. It becomes particularly important if the fluid is incompressible and the deformation of the structure can't be neglected. To fully investigate the dynamic responses of the soft robotic fish in the fluid, the interaction between fluid and soft robot structure must be taken into account, and the coupling mechanisms should be modelled accurately for numerical coupling analysis. Therefore, the driving structure by using soft actuator, a fish-like soft structure and an enclosed fluid cavity are modeled and presented in the numerical simulation analysis of the soft robotic fish.

By the numerical coupling simulation considering the interaction between flexible structure and surrounding fluid, the fish-like propulsion motion performance can be described and evaluated for further robot design. To obtain the optimal robot structure with high performance by optimization, based on FEM, modeling of soft robotic fish by mimicking the soft structure and propulsion mode of real fish, modal and transient analysis considering the fluid as acoustic fluid are firstly presented to investigate and identify the fish-like propulsion motion with large amplitude of the soft robotic fish. Then, the simulation of FSI analysis is performed to describe and establish the hydrodynamic performances of the soft robotic fish in the fluid for final behavior design.

In the numerical coupling analysis, a broad class of FSI problems involves a fluid without significant flow and the main concern in the fluid is the pressure wave propagation. The structure-acoustic coupling analysis considering the acoustic pressure can be used to solve the FSI problems and identify the structural behaviors and its mode for the soft robot structures in the fluid [5]-[7]. It provides a basis of flow formation and boundary conditions of coupling analysis for soft robotic fish. Thus, the modal and transient analysis based on this coupling method is perform through ANSYS software for realizing and establishing the propulsion motion about deformation modes and corresponding amplitude of the soft robotic fish in the present numerical simulation system.

CFD is a branch of fluid mechanics that solves the problems of fluid flows through the numerical methods. More and more researchers use the CFD technology to perform the calculations involving in the simulating interaction between gas/liquid and solid structure for FSI analysis [8]-[10]. It can be used to describe and establish the hydrodynamic performances of the flexible structure in the fluid. In the present research, the CFD numerical method is adopted in fluid computational domain to consider the interaction and evaluate the hydrodynamic performances of the soft robotic fish in the FSI analysis through ANSYS software. The traditional computational structural dynamics (CSD) technology is used for robot structure domain to predict the structural dynamic responses of soft robotic fish in the coupling analysis [11].

Based on above two different kinds of numerical simulations using different coupling method, the propulsion motion and hydrodynamic force of the soft robotic fish are investigated for performance improvement. Figure 2.5 describes the detailed system architecture of the numerical simulation analysis of the soft robotic fish in the research.

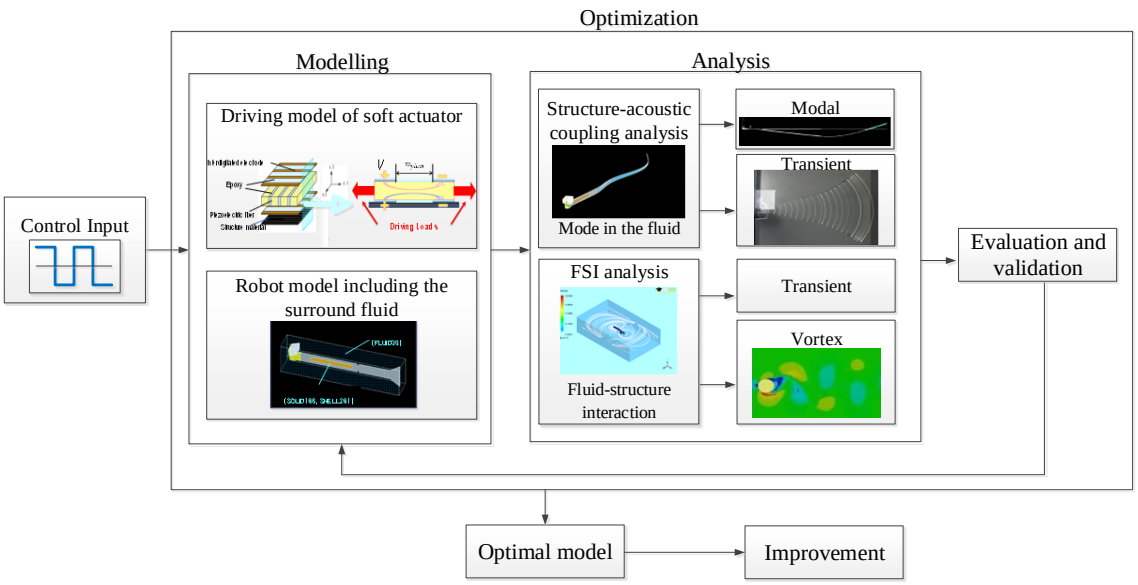

Fig. 2.5 System architecture of numerical simulation analysis of soft robotic fish.

When the propulsion approach of the soft robotic fish is decided, that is, subcarangi-form propulsion in the present research, the numerical simulation analysis is used to evaluate the motion performances of the designed soft robot and propose the optimal

model for final behaviour design through optimization. In the numerical simulation analysis, based on FEM method, modelling of the soft robotic fish including the driving structure of soft actuator and fluid cavity is firstly described. The general CSD simulation is adopted to build the driving model of soft actuator and evaluate its reasonability for soft robot actuation. After establishing the feasibility of the driving model, the numerical model of soft robotic fish including the surrounding fluid is presented. Then, based on this numerical robot model and input driving load, the coupling analysis using structure-acoustic coupling method and FSI method is developed. The structure-acoustic coupling analysis, in which the fluid is started to be taken into account as acoustic fluid, includes the modal and transient simulation. The soft robotic fish's propulsion mode and amplitude directly related to the propulsion mechanism and motion performance of the real fishes are investigated in the structure-acoustic coupling analysis. The modal simulation is carried out to identify the fish-like propulsion modes about frequencies and mode shapes of the soft robotic fish in the fluid. And corresponding amplitude of the established propulsion motion for the soft robotic fish is calculated through the transient simulation. In order to describe and establish the hydrodynamic performances of the soft robotic fish in the fluid for final behaviour design, such as fluid pressure or streamline distribution, the FSI analysis is performed based on CFD method for performance evaluation. The interaction between soft robot structure and fluid flow is taken into account, includes the dissipation due to fluid viscosity and influence of wake performance around the soft robotic fish. From the FSI analysis, the hydrodynamic performances of the soft robotic fish can be obtained for investigation of propulsion motion for further performance improvement. Based on these numerical simulation analyses, the relatively optimal numerical model can be proposed by optimization. It can develop the biomimetic soft robotic fish with high performance effectively by these numerical simulation analyses for improvement.

2.2.1 Structure-Acoustic Coupling Method

Many FSI problems involve a fluid field without significant flow and main concern in the fluid is the pressure wave propagation. The structure-acoustic coupling analysis considering the acoustic pressure can be adopted to solve these FSI problems and establish the structural mode and deformation behaviour of the structures in the fluid. The FEM and boundary element method (BEM) are the solution approaches for the structure-acoustic coupling analysis. A review from Atalla presented these two approaches and described the difference between them [12]. In the thesis, the FEM approach is performed to solve the structure-acoustic coupling analysis and predict the structural mode and motion amplitude of the soft robotic fish in the fluid. S. M. Ai, et al. investigated the vibration response of underwater cylindrical shells through the coupled structural acoustic analysis [6]. D. J. Nefske, et al. investigated the dynamic responses of the automobile compartment based on the structure-acoustic coupling using FEM [5], [13]. H. Djojodihardjo applied the acoustic-structure interaction technology with FEM method into spacecraft structures [7]. These researches provide a basis of boundary conditions in the coupling analysis using structure-acoustic method for soft robotic fish.

In structure-acoustic coupling method, a flexible robot structure is in contact with an enclosed acoustic fluid. The differential equation of motion for a continuum body is used to describe the solid structure. The structural finite element formulation of the governing equations describes the motion equations for the structural domain. For the fluid domain, the acoustic wave equation shown as (2-1) is used for describing the surrounding fluid that meets the basic conditions: inviscid, no mean flow of the fluid and relatively small acoustic pressures. And the mean density and pressure are uniform throughout the fluid.

$$\frac{1}{c^2}\frac{\partial^2 P_f(t)}{\partial t^2} - \nabla^2 P_f(t) = 0 \qquad \textbf{(2-1)}$$

where $P_f(t)$ is acoustic pressure, c is sound speed in fluid medium.

The interaction between the fluid and structure at the interface causes the acoustic fluid pressure to exert a force applied to the structure and the structural motion produces effective load acting on the fluid described in terms of structural acceleration. The governing equations of the robot structure and surrounding fluid are coupled at the boundary between them. The coupling boundary conditions at the interface between robot structure and fluid domain meet the continuity of displacement and fluid pressure between the domains. And the fluid momentum equations yield the relationships between the normal pressure gradient of fluid and the normal acceleration of structure at the interface, described as follows, where $P_f(t)$ is acoustic pressure, $U_f(t)$ is displacement vector of the structure at the interface, ρ is fluid density.

$$\nabla P_f(t) + \rho \frac{\partial^2 U_f(t)}{\partial t^2} = 0 \tag{2-2}$$

The fluid and solid structure move together in the normal direction of the interface boundary. Through the coupling boundary condition and coupling algorism between solid structure and surrounding fluid, the soft robotic fish's coupling problem using structure-acoustic coupling method can be described by an unsymmetrical system in finite element matric equation shown as (2-3) [14]. In the coupling system, the coupling matric is built on the interface between fluid and solid structure. Both structural and fluid loads are transferred at the fluid-structure interface. The nodes on the fluid-structure interface have both displacement and pressure DOF. If F_s equals zero, (2-3) will become the equation of coupled modal analysis for the robot.

$$\begin{bmatrix} M_S & 0 \\ \rho R^T & M_F \end{bmatrix} \begin{Bmatrix} \ddot{U} \\ \ddot{P} \end{Bmatrix} + \begin{bmatrix} K_S & -R \\ 0 & K_F \end{bmatrix} \begin{Bmatrix} U \\ P \end{Bmatrix} = \begin{Bmatrix} F_S \\ F_F \end{Bmatrix} \tag{2-3}$$

where M and K are structural element mass and stiffness matrix, respectively; F is body force; U is displacement; P is fluid acoustic pressure; ρ is fluid density; subscript S and F are expressed as structure and fluid domain, respectively. R is coupling matrix that represents the effective surface area associated with each node on the fluid-structure interface. It transfers the fluid pressure on interface to a force applied to the structure. And

through the coupling matrix, the load produced by structure is acting on the fluid in the coupling analysis.

2.2.2 Fluid-Structure Interaction Method

Due to the uncompleted understanding of swimming mechanism of the real fish [15] and the limited studies to develop the bionic flexible structure and functions with large deformation, the hydrodynamic performances of the robotic fish a bit differ from the real fish and have not been revealed completely. The swimming kinematical parameters of the robotic fish cannot be controlled well to achieve good mobility and high efficiency. There is no published report on systematic study for the detailed swimming kinematical performances of the hydrodynamics on robotic fish [16]. Although a linearized inviscid flow theory using by Wu [17], a large-amplitude elongated-body theory proposed by Lighthill [18], a slender-body theory applied by Newman [19], a three-dimensional (3-D) waving plate theory developed by Cheng [20], a vortex-lattice method used by Kagemoto [21] can be used to investigate the hydrodynamic performances of the fish, these conventional theories are only established on a basis of potential flow, linearized body boundary conditions and an assumed shape for the wake. They neither get the solution of nonlinear flow-body interaction nor allow the coupling wake dynamics to develop [22].

With the rapid development of the numerical studies, especially the CFD, many researchers apply this numerical method to predict the hydrodynamic behaviours of the FSI system. In order to capture the influence of deformed robotic fish on hydrodynamic performances, the robot deformation has to be passed back as a load into the fluid dynamics solution. Thus, two-way transfer including the results of structural analysis and fluid dynamic analysis occurs between the fluid and structure domain. The fluid loads in the structure analysis and structural deformation in the fluid dynamics analysis are all considered in the FSI system based on CFD method. It is largely applied into the fields of engineering and biomedicine to solve the FSI problems of flexible structures and

predict their hydrodynamic characteristics. W. Dettmer et al. [23] investigated the model of the interaction of fluid flow with flexible beam and pipe structures based on Navier-Stokes equations. S. Gong et al. [24] investigated the FSI of rotor blade in the last stage of steam turbine by the coupling approach. D. Tang [25], [26] and Joseph R. Leach et al. [27] used FSI models to explore the mechanical system for atherosclerosis development. S. Geller et al. [28] developed an explicit 3-D FSI model with large structural deflection through the commercial solver. H. Schmucker et al. [29] made a coupling analysis of a propeller turbine using the FSI method. The FSI model and coupling characteristics of flexible polymeric turbo machinery and wind turbine were also developed successfully [30], [31]. These researches provide a basis of flow formulation and boundary conditions of fully FSI analysis, but the application of the FSI analysis has not been widely developed in the field of soft robotic fish. Due to larger deformation of flexible structure and complicated coupling dynamics with surrounding fluid, it is hard to make the modelling work and solve the FSI problems of the soft robotic fish. Compared with the conventional rigid robotic fish, the soft robot has larger deflection and it is easy to generate large deformation in the interaction with the surrounding fluid. The deformation results from soft robot cannot be ignored and easily generates the problems of mesh motion in the analysis, which increases the difficulty on solution of nonlinear problems of soft robotic fish, especially on the convergence of data transfer and computational cost in the FSI calculation of soft robot. Some mesh problems about large deformation can be solved by the special method such as grid reconstruction, while the FSI analysis has not been generally applied in the highly nonlinear problems and large deformation problems of the soft robot. Also, the good mesh quality at the interface increases the difficulty for solving these mesh problems. There is a challenge on convergence solution in these FSI problems. Besides, the selection of reasonable and suitable time scale in computational domain at lower computational cost increases the difficulty for FSI solution of the soft robotic fish. In the FSI analysis, the time scale, playing the key role on data convergence, depends on fluid force, scale of wake structures and oscillating frequency of soft robotic fish. For different oscillating frequencies, the fluid forces and

wake structures are different. The improper time scale will cause non-convergence of calculation and FSI solution of the soft robotic fish cannot be obtained. There is a difficulty on selection of appreciate time scale in FSI problems of soft robotic fish.

In addition, the soft robotic fish considering the soft behaviours of the real fishes based on soft materials is a young research field in the underwater robots, going to overcome the basic assumptions of conventional rigid robot in the unknown or high dangerous environments. Compared with rigid robot, the theories and technologies of the soft robotic fish have not yet been defined in a general form. It is still exploring new ways for soft robot design and performance improvement. The exact control on path planning and position sensing of the soft robotic fish as a continuum is complicated by comparing with those of rigid robots. There is a challenge of design and control for soft robot with high mobility. It motivates us to investigate the design and control problems of soft robotic fish by analytical simulation with interaction between flexible robot structure and fluid.

Addressing the FSI method based on CFD technology, the deformation results from robot structure and fluid pressure loads from corresponding fluid domain are all considered. Therefore, in the thesis, FSI analysis based on CFD method is adopted to deal with the FSI problem of the soft robotic fish based on ANSYS software. Mechanical application is used for structure domain and CFX is for fluid domain. Figure 2.6 describes the basic scheme of the FSI analysis for the soft robotic fish using soft PFC actuator.

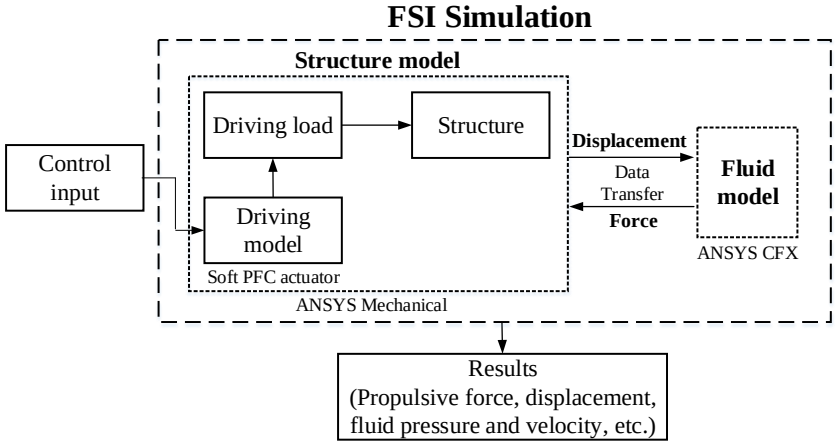

Fig. 2.6 Scheme of FSI analysis of soft robotic fish.

According to the driving model by PFC actuator, an external driving load can be derived and calculated. By the calculated results, the driving load is applied on the model of the robot structure for actuation in the ANSYS Mechanical. Then, in order to obtain the solution of the coupling analysis, the robot structure model with a time-varying driving load is solved firstly. After finishing the solution of structure model at current step, the results such as displacement and stress are exported, and all these results are converted to the input data for fluid model to make the solution of current step in the CFX application. The corresponding fluid pressure loads from fluid model are transferred into the structure model as external load to consider the fluid effect for solution. The interaction between robot structure model and fluid model happens and two-way data transfer is developed. Thus, the propulsion characteristics such as propulsive force and displacement of the soft robotic fish can be exported from the simulation results. In the FSI analysis, the governing equations of two domains can be written as (2-4). Between the robot structure and fluid domain, the coupling conditions at the interface meet continuous and conservation principle detailed described in Chapter 3.

$$\text{Structure: } \begin{cases} M\ddot{U} + KU = F_s \\ + \text{Boundary conditions and initial conditions} \end{cases}$$

$$\text{Fluid: } \begin{cases} \rho\left(\dfrac{\partial V}{\partial t} + V \cdot \nabla V\right) = -\nabla P + \mu \nabla^2 V + F_f \\ + \text{Boundary conditions and initial conditions} \end{cases} \tag{2-4}$$

where M and K are structural element mass and stiffness matrix, respectively; F is body force; U is displacement; V is fluid velocity; P is fluid pressure; ρ is fluid density; μ is dynamic viscosity; subscript s and f are expressed as structure and fluid domain, respectively.

Based on FSI analysis, the hydrodynamic performance of the soft robotic fish can be obtained and used to evaluate its propulsion characteristics in the fluid. The detailed procedure will be presented in Chapter 3.

2.2.3 Solution Method of FSI Analysis

In the FSI analysis, monolithic and partitioned method are different approaches for solution based on physical properties of the interaction between solid structure and fluid.

Monolithic method is a fully implicit method. There is a single system equation for the entire fluid and structural domain and a simultaneous solution is required in the whole problem domain. The interaction among the dependent equations is all taken into account in this method. It is seemed to be an ideal method to deal with the strong interaction involving in the nonlinear problems. This method can obtain good accuracy for a multidisciplinary problem. However, it needs more resources and professional technologies to develop its special algorithm and code for solving the different kinds of complicated coupling problems. The monolithic method is applied only in elementary examples in practice and its development is still in the initial stage. A simultaneous solution in the most FSI problems is difficult to obtain due to the complex geometry [10].

In contrast, the partitioned method defines the fluid filed and solid structure as two problem domains in the calculation. These two problem domains have their own mesh grid, numerical algorithm and solver, and can be made the solution separately. The interaction between these two fields are taken into account by the variables exchange at the interface. It is an explicit method for dynamic interaction between solid structure and fluid. The numerical algorithms of this method have been validated and applied to solve many complicated FSI problems in the engineering field [32]. But it is also a challenge for this method on accuracy and efficient FSI solution with minimal code modification. The good mesh quality and high precision solver are needed to considered for accurate FSI solution.

Figure 2.7 illustrates the solution procedures of the monolithic and partitioned method.

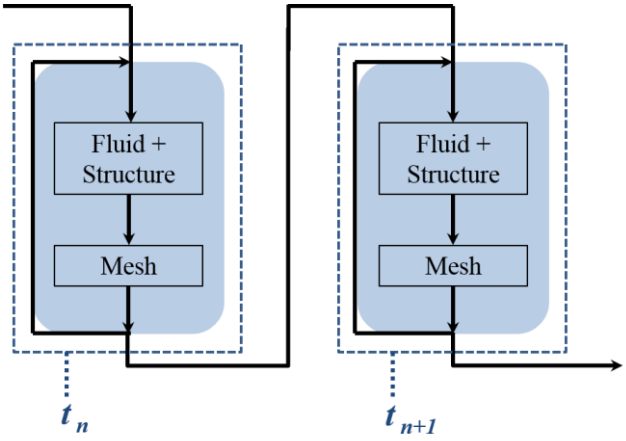

(a) Monolithic method

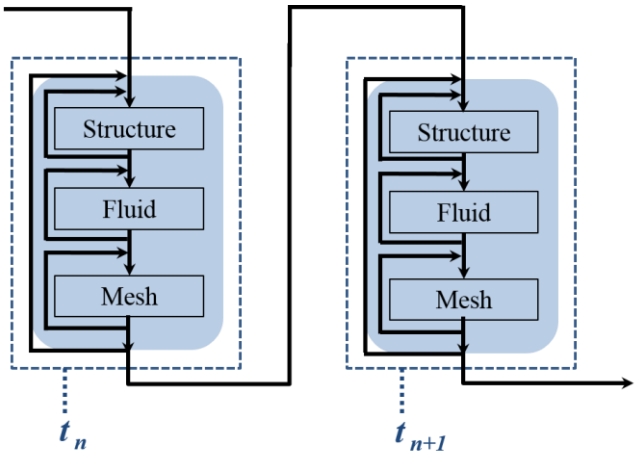

(b) Partitioned method

Fig. 2.7 Solution procedures of monolithic and partitioned method.

The main difference between monolithic and partitioned method is that the fluid and structural equations are solved one after another in the partitioned method, which is different with the monolithic method in which the equations of both domains are solved at the same time. Due to the verified numerical algorithms and successful FSI solution in partitioned method, the partitioned method is adopted to solve the FSI problems of the soft robotic fish in the present research. Due to the fluid flow caused by the motion of the soft robotic fish, the robot structural domain is firstly solved and then the surrounding fluid domain is solved.

In order to solve the FSI problems in our life, many commercial solvers turn up in market. FSI solution based on commercial software packages is a convenient method to get the solution of the FSI problems. The numerical algorithm in the commercial pack-

ages used for the fluid flow and solid structural analysis are validated and established well. The solving codes of the general problems exist in the form of separate modules and can be employed to solve the complicated problems easily. Therefore, the partitioned method based on commercial software code by ANSYS software will be used to obtain the FSI solution of the soft robotic fish in the presented research. Different solvers in CFX for the unsteady Navier-Stokes equations can be used for the simulation of transient flow field by CFD analysis. For the structure field, a number of commercial FEM codes are available for CSD analysis. Both calculations are coupled by exchanging parameters from the individual codes.

2.3 Summary

In this chapter, the design method, procedures and numerical simulation system for the soft robotic fish in the present research are presented for developing the biomimetic soft robotic fish with high performance. Different from the conventional development method, the interaction between soft robot structure and surrounding fluid are considered by numerical simulations. In order to meet the requirements of developing optimal soft robotic fish, the basic design process including modelling, simulation analysis and improvement are proposed and the numerical simulation system is introduced for soft robotic fish design. In the numerical simulation system, based on FEM, the modelling of the soft robotic fish containing the driving structure and surrounding fluid are firstly built. Through the modelling of the soft robotic fish, the coupling analysis by using structure-acoustic coupling method and CFD-based FSI method is developed for soft robot design. The structure-acoustic coupling analysis including the modal and transient simulation considers the surrounding fluid as acoustic fluid to investigate and realize the fish-like propulsion motion with large amplitude of the soft robotic fish. The numerical simulation of CFD-based FSI analysis is performed to describe and establish the hydrodynamic performances of the soft robotic fish in the fluid. Based on these numerical

simulations, it can develop the biomimetic soft robotic fish with high performance effectively by optimization of design and control of the soft robotic fish. The design approach and numerical simulation system lay the foundation for the organization and development of the dissertation.

References for Chapter 2

[1] R. Shepherd, F. Ilievski, W. Choi, S. Morin, A. Stokes, A. Mazzeo, X. Chen, M. Wang, and G. Whitesides, "Multigait soft robot," Proc. Of the National Academy of Sciences, Vol. 108, No. 51, pp. 20400-20403, 2011.

[2] A. C. Price, C. J. Weadick, J. Shim and F. Helen Rodd, "Pigments, patterns, and fish behaviour, " Zebrafish, Vol. 5, No. 4, pp. 297-307, 2008.

[3] A. Azuma, Encyclopaedia of Creature's Motion, Asakura Publishing, 1997.

[4] H. Bungartz and M. Schäfer, "Fluid-structure interaction: modelling, simulation, optimization," Springer-Verlag Berlin Heidelberg, 2006.

[5] S. H. Sung and D. J. Nefske, "A coupled structural acoustic finite element model for vehicle interior noise analysis," Transaction of the ASME, Journal of Vibration, Acoustics, Vol. 106, No. 2, pp. 314-318, 1984.

[6] S. Ai and L. Sun, "Fluid-structure coupled analysis of underwater cylindrical shells," Marine Science and Application, Vol. 7, No. 2, pp. 77-81, 2008.

[7] H. Djojodihardjo, "BEM-FEM acoustic-structure interaction for modeling and analysis of spacecraft structures subject to acoustic excitation," Proc. Of the International Conference on Recent Advances in Space Technologies, pp. 165-170, 2007.

[8] D. Tang, C. Yang, S. Kobayashi and D. N. Ku, "Effect of a lipid pool on stress/strain distributions in stenotic arteries: 3-D fluid–structure interactions (FSI) models," Biomech Eng., Vol. 126, No. 3, pp. 363-370, 2004.

[9] X. S and S. Li, "Coupled wind-induced vibration analysis of the membrane structure based on steady-state CFD," Applied Mechanics and Materials, Vol. 94-96, pp. 598-605, 2011.

[10] F. Benra and H. J. Dohmen, "Application of simulation methods considering the interaction between fluid and structure," Proc. Of the 7th IASME/WSEAS International Conference on Fluid Mechanics and Aerodynamics, pp. 116-121, 2009.

[11] G. P. Guruswamy, "Computational-fluid-dynamics and computational-structural-dynamics-based time-accurate aeroelasticity of helicopter rotor blades," Journal of Aircraft, Vol. 47, No. 3, pp. 858-863, 2010.

[12] N. Atalla and R. J. Bernhard, "Review of numerical solutions for low-frequency structural-acoustic problems," Applied Acoustics, Vol. 43, No. 3, pp. 271-294, 1994.

[13] D. J. Nefske, J. A. Wolf Jr and L. J. Howell, "Structural-acoustic finite element analysis of the automobile compartment: A review of current practice," Journal of Sound and Vibration, Vol. 80, No. 2, pp. 247-266, 1982.

[14] ANSYS Inc., ANSYS theory reference 12.1, ANSYS Inc., 2009.

[15] L. Jia and X. Yin, "Passive oscillations of two tandem flexible filaments in a flowing soap film," Physical Review Letters, Vol. 100, No. 22, pp. 1-4, 2008.

[16] D. Xia, J. Liu, W. Cheng and L. Han, "Numerical simulation of the hydrodynamics of fishlike robot swimming based on converged speed," Journal of Mechanical Engineering, Vol. 46, No. 1, pp. 48-54, 2010.

[17] T. Y. Wu, "Hydrodynamics of swimming propulsion. Part 1. Swimming of a two-dimensional flexible plate at variable forward speeds in an inviscid fluid," Journal of Fluid Mechanics, Vol. 46, No. 2, pp. 337-355, 1971.

[18] M. J. Lighthill, "Large amplitude elongated-body theory of fish locomotion," Proc. R. Soc. Lond. B, Vol. 179, No. 1055, pp. 125-138, 1971.

[19] J. N. Newman, "The force on a slender fish-like body," Journal of Fluid Mechanics, Vol. 58, No. 4, pp. 689-702, 1973.

[20] J. Cheng, L. Zhuang and B. Tong, "Analysis of swimming three-dimensional waving plates," Journal of Fluid Mechanics, Vol. 232, pp. 341-355, 1991.

[21] H. Kagemoto, M. J. Wolfgang, D. K. P. Yue and M. S. Triantafyllou, "Force and power estimation in fish-like locomotion using a vortex-lattice method," Journal of Fluids Engineering, Vol. 122, No. 2, pp. 239-253, 2000.

[22] H. Liu and K. Kawachi, "A numerical study of undulatory swimming," J. Comput. Phys., Vol. 155, No. 2, pp. 223-247, 1999.

[23] W. Dettmer and D. Peric, "A computational framework for fluid-structure interaction: finite element formulation and applications," Computer Methods in Applied Mechanics and Engineering, Vol. 195, pp. 5754-5779, 2006.

[24] S. Gong, L. Ren, H. Liu, L. Li and Z. Zou, "Fluid-solid interaction of rotor blade in last stage of steam turbine," Thermal Turbine, Vol. 36, No. 3, pp. 153-157, 2007.

[25] D. Tang, C. Yang, S. Kobayashi and D. N. Ku, "Effect of a lipid pool on stress/strain distributions in stenotic arteries: 3-D fluid–structure interactions (FSI) models," J. Biomech. Eng., Vol. 126, No. 3, pp. 363-370, 2004.

[26] D. Tang, C. Yang, S. Mondal, F. Liu, G. Canton, T. S. Hatsukami, and C. Yuan, "A negative correlation between human carotid atherosclerotic plaque progression and plaque wall stress: in vivo MRI-based 2D/3D FSI models," J. Biomech., Vol. 41, No. 4, pp. 727-736, 2008.

[27] J. R. Leach, V. L. Rayz, M. R. K. Mofrad and D. Saloner "An efficient two-stage approach for image-based FSI analysis of atherosclerotic arteries," Biomech. Model Mechanobiol, Vol. 9, No. 2, pp. 213-223, 2010.

[28] H. Bungartz, M. Mehl and M. Schäfer, "Fluid-structure interaction II: modelling, simulation, optimization," Springer-Verlag, 2010.

[29] H. Schmucker, F. Flemming and S. Coulson, "Two-way coupled fluid structure interaction simulation of a propeller turbine," The 25th IAHR Symposium on Hydraulic Machinery and Systems/ IOP Conf. Series: Earth and Environmental Science, Vol. 12, pp. 1-10, 2010.

[30] R. L. Campbell, "Fluid-structure interaction and inverse design simulations for flexible turbomachinery," Doctoral Dissertation of the Pennsylvania State University, 2010.

[31] M. Hsu and Y. Bazilevs, "Fluid-structure interaction modeling of wind turbines: simulating the full machine," Computational Mechanics, Vol. 50, No. 6, pp. 821-833, 2012.

[32] G. Hou, J. Wang and A. Layton, "Numerical method for fluid-structure interaction-a review," Commun. Comput. Phys., Vol. 12, No. 2, pp. 337-377, 2012.

Chapter 3. Numerical Analysis of Soft Robotic Fish

According to the design methodology and numerical simulation system of the soft robot in the present research mentioned in Chapter 2, the modelling and numerical analysis of biomimetic soft robotic fish are described in this chapter. The soft robotic fish uses the PFC as soft actuator in robot design, and the driving model of the PFC actuator is needed to be investigated for robot design. Thus, the driving model of the PFC actuator is firstly built. The relationships between input voltage and generated stress of the PFC actuator are derived. The generated stress can be applied on soft structure to investigate motion performance of the soft robotic fish. To support the driving model of the PFC, the corresponding experiments by using simple beam model are carried out. By comparing the simulation results with experimental results, the effectiveness of the driving model is verified. Then, the modal analysis considering the surrounding fluid as acoustic fluid is performed. The mode frequencies and mode shapes of the soft robotic fish in the fluid are calculated. By comparing these mode shapes with those of the real fishes, the robot propulsion mode is identified to realize the corresponding propulsion motion of the soft robotic fish in the fluid. Based on the verified driving model of PFC actuator, the amplitude of the main propulsion motion of soft robotic fish in the fluid is also calculated by transient analysis. Furthermore, the FSI analysis is carried out for describing the hydrodynamic performance of the soft robotic fish. Through FSI analysis, the relationships of driving frequencies of input signal with propulsive force and amplitude of the propulsion motion, and vortex distribution in the wake around the soft robotic fish are investigated for the case of fixing robot head. It provides the basic foundation for further performance improvement of soft robotic fish. Finally, the motion

control of the soft robotic fish is investigated to describe the turning motion of the soft robotic fish. Through controlling the input voltage amplitude on soft actuators of the robot, the motions of turning right and turning left are achieved in its swimming when the input voltage amplitude on two actuators are in asymmetric distribution.

3.1 Modelling of Driving by Piezoelectric Fiber Composite

3.1.1 Piezoelectric Fiber Composite

The development of active and smart materials has become a hot topic on host structures as an advanced approach to control or measure the structure behaviours recently. The smart materials, such as SMA, ICPF/IMPC, electrostatic film, PFC, and so on, have turned up in our personal lives to play their own roles on structure actuation applications.

PFC is a new kind of smart materials appropriate for structure actuation. It is a type of piezoelectric composite materials, has been investigated widely due to its good performances for actuators and sensors. The investigation of the PFC is mainly concentrated in United States. NASA focuses on the facture mechanism of the PFC [1], [2]. PFC is generally composed of piezoelectric fibers, polymer and interdigitated electrodes (IDEs), shown as in Fig. 3.1. It is the interdigitated electrode piezoelectric fiber composite (IDEPFC). The piezoelectric fiber is the active component and the polymer is the passive component. The IDES embedded in polymer film are placed on the top and bottom surface of the fibers. The IDEs technology is a main characteristic of the PFC. The utilization of the interdigitated electrodes makes the PFC structure obtain the higher force or displacement by capitalizing on the stronger longitudinal (d_{33} constant) piezoelectric effect, in which the largest mechanical response happens in the direction of the

corresponding electric field [3]. When the voltage is applied on PFC, the expended and contracted motion will occur in the direction of the fibers.

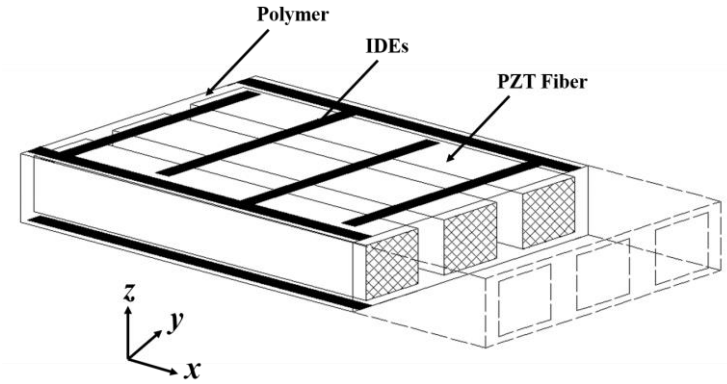

Fig. 3.1 Structure of PFC.

Compared with some typical active and smart materials, such as SMA, electrostrictive and magnetostrictive materials, PFC remains the most widely used smart material due to the high structural stiffness for voltage-dependent actuation and superior sensing capability. Also, it has the high bandwidth and can be interacted with the dynamic systems over a wide frequency range from zero to the megahertz range [4]. Furthermore, compared with the traditional piezoelectric ceramic actuators, the PFC has orthotropic properties and clear planar induced strain, and has good advantages on toughness and reliability. It can be used in the structure of curved surface [5]. Therefore, the PFC has been largely applied into the field of aerospace structures, automobiles, robotics and sport equipment to enhance their motion performances through the shape deformation control and vibration responses. They are typically utilized as the actuators in the vibration suppression systems of structures. For example, the inflatable satellite components [6], tail fins of the airplane [7], quieter and comfortable rides in the cars[8], tennis rackets and baseball bats for reducing vibrations[9], [10].

The development of PFC actuator overcomes the practical difficulties associated with using monolithic piezoceramic actuators in structural control problems [11], such as poor conformability, low strain energy density, non-directional strain actuation, and so on. The combination of the piezoceramic fiber composite and interdigitated electrode

technologies, forms IDEPFCs, increases the strain output, improves the flexibility and durability, and develops the directional actuation of PFC. The maximum free-strain output in the fiber direction is approximately three times greater than in the transverse direction [12]. The term “active fiber composite (AFC)” coined by Bent is used to take the place of IDEPFC [13], [14].

Although large improvement on actuation performance of the piezoceramic materials by development of the PFC and a great success on PFC application in above mentioned fields, the limitation on its performance is also exist due to design and manufacture problems. And it is vulnerable to accidental breakage during handling procedures. Most importantly, the round cross-section fiber of PFC tends to decrease the contact area with the adjacent copper electrodes, which causes an inefficient transfer of the electric field for the fibers.

In order to solve above mentioned limitation problems and improve the actuation performances of PFC, the macro fiber composite (MFC), one of the typical flexible PFCs, is developed by NASA Langley Research Centre to reduce the disadvantage of manufacturing and control application associated with previous PFC devices [3], [15], [16]. The appearance of the MFC is shown in Fig. 3.2.

It not only remains the advantages of the early generation PFC devices, such as high strain energy density, directional strain actuation, good flexibility and durability, but has some new features and improvements. Especially, the low-cost fabrication process of MFC makes it have uniform and repeatable electromechanical properties.

Fig. 3.2 Appearance of MFC.

MFC, greatly impressed by its large strain output response and high efficiency, is widely applied to control the deformation shape and vibration responses of the struc-

tures for high performance. The obvious effectiveness on reduction of the structural vibrations was verified through the finite element formulation by Bevan and Azzouz [17], [18]. Also, the suitability of the MFC on structural vibration application was investigated in the experiment by Sodano, Park and Inman [19]. The flexibility of the MFC convenient for double curved surface was verified from the research of Ruggerio et al. [20] and it was found that the MFC outperformed other actuators and had good sensitivity comparable to other monolithic piezoelectric sensors. It can be used for actuating, sensing and power generation with softness. Due to good flexibility, large force response, high level of strain deformation and anisotropic structure of the MFC, it can be applied into the large-deflection shape control problems such as morphing wing or fin technology.

MFC is a layered and planar structure. It employs the rectangular cross-section and unidirectional piezoceramic fibers (PZT-5A) embedded in a thermosetting polymer film. The use of the rectangular fibers makes the MFC structure get the maximum contact area between the piezocreamic and the adjacent electrodes, ensures the efficient transfer of the electric field into the fibers. Figure 3.3 shows the structure of MFC. It is a thin plate-like structure, consisting of piezoelectric fiber strengthened by interweaving comb pairs. The piezoceramic fiber is embedded in epoxy to make a rectangular plate which is sandwiched by two pieces of polyimide film on which the interdigitated electrodes are placed. All the fibers are rectangular in cross-section, uniformly spaced with the fibers perpendicular to the copper electrodes. The epoxy, polyimide and copper electrodes are isotropic. However, the piezoceramic fibers are transversely isotropic, the properties along the fiber are different with those in the transverse plane.

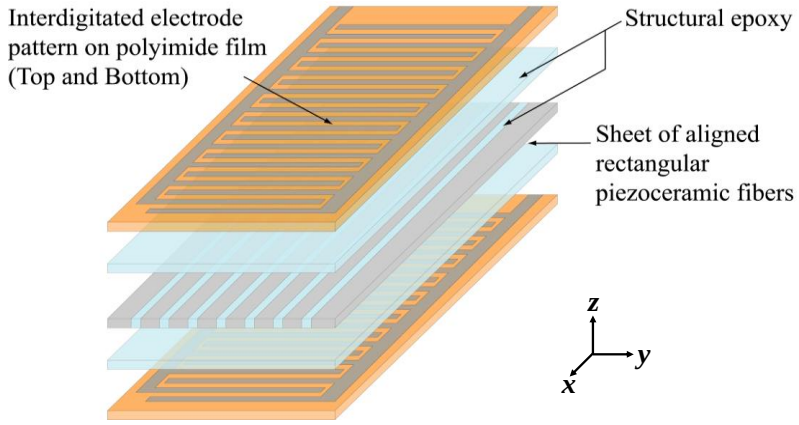

Fig. 3.3 Schematic diagram of the structure for MFC.

3.1.2 Driving Principle and Characteristics

MFC as an actuator has the effect of strain driving. The driving voltage is in the range from -500 to +1500. When the electric field is applied on a single piezoelectric actuator in the free state, the actuator has the piezoelectric strain, however, the stress is zero. The strain of the MFC is about 1800ppm in d_{33} type. Furthermore, the structure bending or distort deformation will be generated through piezoelectric strain if the piezoelectric actuator is placed on the elastic plate. If there is no voltage applied on MFC, it can work as a very sensitive strain gauge. The MFC is also an excellent device for harvesting energy from vibration.

Figure 3.4 describes the actuation structure of soft robotic fish based on MFC with an elastic plate for expansion and contraction motion when the voltage applied. For the biomorph structure, one MFC is expanding and the other is contracting. The biomorph beam structure has the larger displacement response than that of unimorph structure. The piezoelectric speaker is a product utilizing this biomorph actuation structure. Also, the positive piezoelectric effect will be generated on structure if the entire structure making the bending deformation by an external force. The utilization of this effect is mainly focused on accelerometer. Compared with the biomorph type, the unimorph structure is simple, but the relatively low vibration frequency and small force are generated for bending deformation. In order to meet the requirement in practical engineering design and application, the number of the MFC actuators can be decided freely to obtain

the suitable or desired actuation structures. These characteristics of the bending deformation are utilized to design the soft robotic fish with BCF propulsion in the research to mimic the swimming motion of the fishes. The biomorph actuation structure are used in robot design and carbon-fiber-reinforced polymer (CFRP) is adopted as the thin elastic plate in the present study.

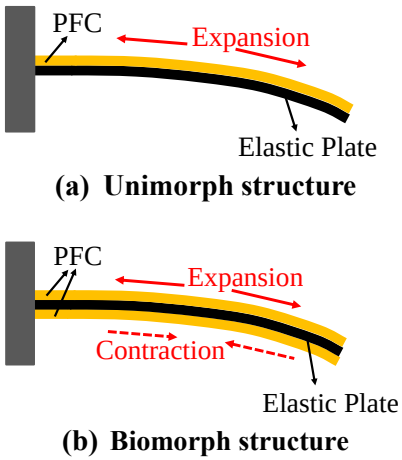

Fig. 3.4 Actuation structure of MFC.

If a voltage from -500V to +1500V is applied on MFC, the internal electric field happens and the crystals polarized cause the strain deformation. It can expand and contract in the direction of the fibers. When the MFC attached to an elastic plate completely, such as unimorph and biomorph structure, the power of expansion and contraction from the fibers is transmitted to the surface of the elastic plate. Thus, the corresponding bending or torsion deformation can be generated through the piezoelectric strain. The resonant response with large displacement will be obtained.

In the numerical model, the stress caused by piezoelectric strain is applied on the MFC to describe its driving characteristics and deformation responses. Figure 3.5 describes the loading method of stress on MFC to present the expansion and contraction motion of the piezoelectric fibers. The stress loads are applied perpendicularly to the four areas in the thickness direction of the MFC. When the MFC adhered to an elastic plate, the deformation response caused by driving stress load is described in Fig. 3.6.

The positive stress makes the contraction deformation and the negative stress is responsible for the expansion.

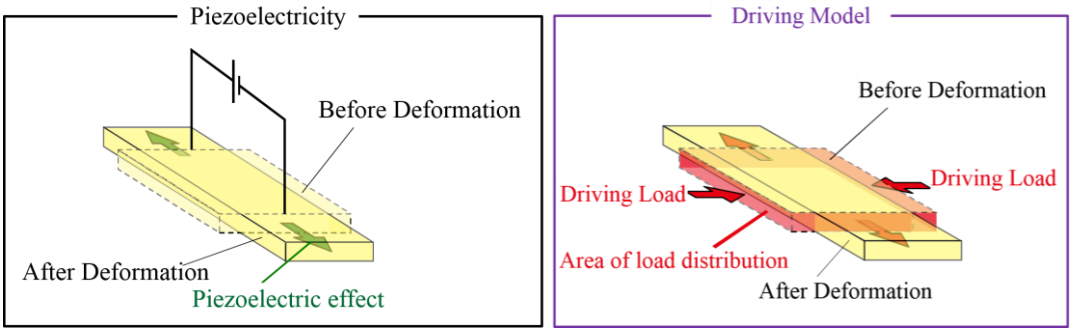

Fig. 3.5 Loading method of stress load on MFC.

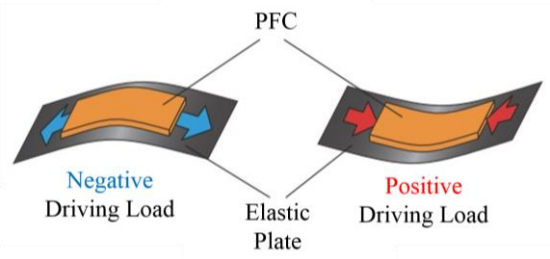

Fig. 3.6 Deformation response of actuation structure based on stress loads.

The properties of the MFC are described in Table 3.1 [21]. The tensile modulus in the rod direction and electrode direction are expressed as E_1 and E_2, respectively. G is shear modulus of the MFC. For the cantilever mode, the carbon plate had the same structural size with MFC actuator, except for the thickness. The thickness of CFRP is 0.2mm.

Table 3.1 Properties of MFC Actuator

Item	**Properties**	
	Symbol	***Specification***
Tensile modulus (GPa)	E_1	30.336
	E_2	15.9
Poisson's ratio	v_{12}	0.31
	v_{21}	0.16
Shear modulus (GPa)	G	5.515
Piezoelectric constants (pm/V) -Low electric field	d_{33}	400
	d_{31}	-170
Piezoelectric constants (pm/V) -High electric field	d_{33}	460
	d_{31}	-210
Thickness (mm)	H	0.3

3.1.3 Driving Model and Loads

MFC, served as a piezoelectric actuator, meets the basic piezoelectric equations. Based on the relationship between linear elasticity and piezoelectric constitutive equations, the standard piezoelectric equations of *d* and *e* type in metric are shown in (3-1) and (3-2) [22], [23], where the electric field intensity is views as the independent variable. The *d* type is piezoelectric strain metric and *e* type is piezoelectric stress metric.

$$\begin{bmatrix} D \\ \varepsilon \end{bmatrix} = \begin{bmatrix} \gamma^T & d \\ d & s^E \end{bmatrix} \begin{bmatrix} E_V \\ \sigma \end{bmatrix} \tag{3-1}$$

$$\begin{bmatrix} D \\ \sigma \end{bmatrix} = \begin{bmatrix} \gamma^S & e \\ -e & c^E \end{bmatrix} \begin{bmatrix} E_V \\ \varepsilon \end{bmatrix} \tag{3-2}$$

The D, E_V, σ and ε are electric displacement, electric field intensity, mechanical stress and total strain, respectively. γ^T and γ^S are dielectric constants of the stress and strain. d is piezoelectric strain constant and e is piezoelectric stress constant. s and c are compliance and stiffness coefficient matrix, respectively. The label T and S are expressed as the conditions of constant stress and strain, and label E is the condition of constant electric field intensity.

Based on the thermodynamic theory, the basic driving model of the MFC is shown in Fig. 3.7. When a voltage from -500V to +1500V is applied on MFC, the piezoelectric strain deformation will be generated in the fibers. And the equivalent stress loads caused by the strain can be obtained and shown in (3-3), where ε^E is piezoelectric strain under the condition of constant electric field intensity. Thus, the stress loads can replace of the extra voltage loads and act on MFC for structure expansion and contraction in the direction of the fibers. Through this driving stress load, the bending deformation of the MFC structure can be generated and it is benefit for the swimming motion design of soft fish robot.

$$\sigma = c^E \varepsilon^E = c^E d E_V \tag{3-3}$$

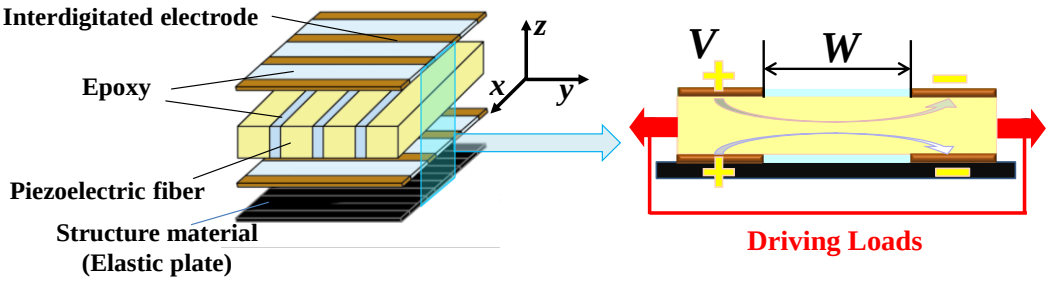

Fig. 3.7 Basic driving model of MFC.

In the research, the MFC actuator fixed on both side of a thin carbon plate (CFRP) shown in Fig. 3.8 is proposed to design the body structure of soft robotic fish for larger displacement. The direction of *x*-axis is expressed the distribution orientation of the piezoelectric fiber. The MFC with zero degree orientation type is adopted.

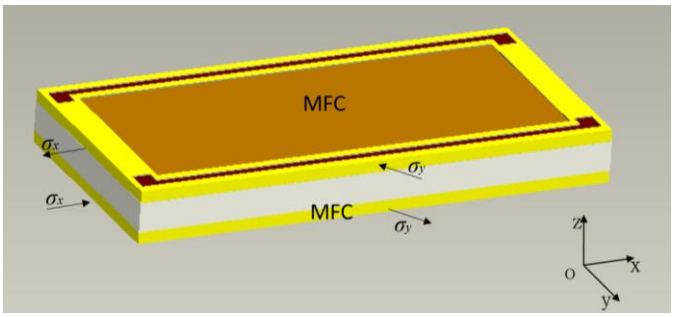

Fig. 3.8 Structure of MFC on carbon plate body.

Equation (3-4) describes the elastic constitutive equation of the piezoelectric material. In this equation, the stress distribution can be treated as plane stress problem. Due to the thickness of MFC is much less than the length and width, the stress in the direction of the thickness for MFC can be ignored and defined as zero, that is, the σ_z is zero in (3-4). The stress σ_x and σ_y, described in Fig. 3.8, can be obtained through the elastic constitutive equations from (3-5) and (3-6), where d_{33} and d_{31} are piezoelectric constants.

$$\begin{bmatrix} \sigma_x \\ \sigma_y \\ \sigma_z \\ \sigma_{xy} \\ \sigma_{yz} \\ \sigma_{xz} \end{bmatrix} = \begin{bmatrix} c_{11} & c_{12} & c_{13} & 0 & 0 & 0 \\ c_{21} & c_{22} & c_{23} & 0 & 0 & 0 \\ c_{31} & c_{32} & c_{33} & 0 & 0 & 0 \\ 0 & 0 & 0 & c_{44} & 0 & 0 \\ 0 & 0 & 0 & 0 & c_{55} & 0 \\ 0 & 0 & 0 & 0 & 0 & c_{66} \end{bmatrix} \begin{bmatrix} \varepsilon_x \\ \varepsilon_y \\ \varepsilon_z \\ 2\varepsilon_{xy} \\ 2\varepsilon_{yz} \\ 2\varepsilon_{xz} \end{bmatrix} \quad \textbf{(3-4)}$$

$$\sigma_x = \frac{c_{11}c_{33} - c_{13}c_{31}}{c_{33}} d_{33}E_V + \frac{c_{12}c_{33} - c_{13}c_{32}}{c_{33}} d_{31}E_V \quad \textbf{(3-5)}$$

$$\sigma_y = \frac{c_{21}c_{33} - c_{23}c_{31}}{c_{33}} d_{33}E_V + \frac{c_{22}c_{33} - c_{23}c_{32}}{c_{33}} d_{31}E_V \quad \textbf{(3-6)}$$

According to the characteristics of the PFC, the structure bending or torsion deformation can be achieved by fixing it on a thin elastic plate. And for the fishes with BCF propulsion, the bending deformation is suitable to obtain the corresponding oscillating or undulating swimming motion. Thus, in order to obtain the proper bending deformation and relatively large amplitude for the soft robotic fish, the distribution structure of MFC actuator for robot structure design is needed to investigate. There are three typical distribution structures for MFC actuator on a thin elastic plate, including symmetric, asymmetric and orthogonal distribution. Due to eccentric driving moment, the orthogonal distribution is not suitable for the design of soft robotic fish for desired bending deformation [24].

As for the symmetric distribution with same electric field and the asymmetric distribution with inverse electric field, only in-plane displacement is generated on structure. The asymmetric structure with same electric field makes the torsion deformation. The symmetric distribution with inverse electric field generates the desired structure bending deformation. Therefore, the symmetric distribution with inverse electric field is only suitable for the robot design and investigated to achieve the desired bending deformation in the research. In the current study, the structure with cantilever boundary condition is used to analyse the deformation characteristics of the MFC. Figure 3.9 displays the symmetric distribution structure of the MFC on an elastic plate with inverse electric field [22], [25]. The corresponding structure stress and moment distributions are also presented.

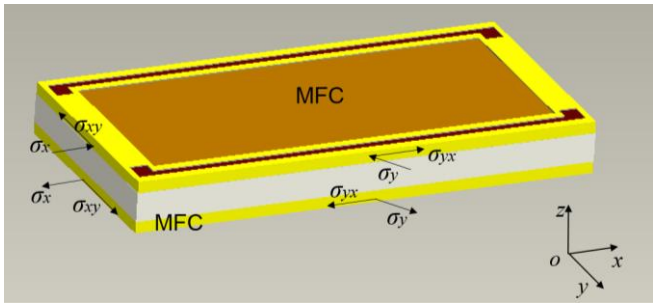

(a) Stress distribution

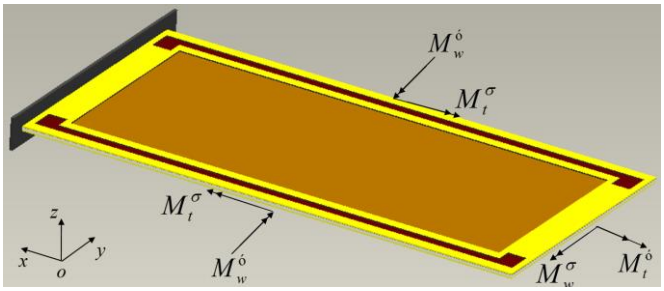

(b) Moment distribution

Fig. 3.9 Stress and moment of symmetrical distribution structure with inverse electric field.

The moment $M_t^{\acute{o}}$ at the free end of structure and lateral moment $M_w^{\acute{o}}$ on both front and back sides are made by the shear stress, shown in Fig. 3.9(b), where subscript *w* and *t* express bending effect and torsion effect, respectively. The moment M_w^{σ} at the free end is generated by the normal stress and the bending effect is obtained. The lateral moments M_t^{σ} on both sides are counteracted and the torsion deformation is only in local effect. The mainly bending deformation motion occurs in the direction of *z*-axis.

Using the compliance coefficient matrix *s* instead of stiffness matrix *c*, the relationship between normal stress and strain of the piezoelectric fiber composite from (3-5) and (3-6) can be expressed as follows [12]. The compliance coefficient matrix *s* can be described by the Poisson's ratio *v* and tensile modulus *E*.

$$\begin{bmatrix} \sigma_x \\ \sigma_y \end{bmatrix} = \begin{bmatrix} s_{xx} & s_{xy} \\ s_{yx} & s_{yy} \end{bmatrix}^{-1} \begin{bmatrix} \varepsilon_x \\ \varepsilon_y \end{bmatrix} \tag{3-7}$$

$$s = \begin{bmatrix} \frac{1}{E_x} & -\frac{v_{yx}}{E_y} \\ -\frac{v_{xy}}{E_x} & \frac{1}{E_y} \end{bmatrix} \tag{3-8}$$

$$\begin{bmatrix} \varepsilon_x \\ \varepsilon_y \end{bmatrix} = \begin{bmatrix} d_{33} \\ d_{31} \end{bmatrix} E_V \tag{3-9}$$

From above equations, the calculation equations of the normal stress can be obtained and shown in (3-10) when the voltage is applied on MFC. E_V is electric field intensity and can be calculated by (3-11), where V is voltage and W is distance between the electrodes on MFC.

$$\begin{bmatrix} \sigma_x \\ \sigma_y \end{bmatrix} = \frac{1}{1-\nu_{xy}\nu_{yx}} \begin{bmatrix} E_x & E_x\nu_{yx} \\ E_y\nu_{xy} & E_y \end{bmatrix} \begin{bmatrix} d_{33} \\ d_{31} \end{bmatrix} E_V \tag{3-10}$$

$$E_V = \frac{V}{W} \tag{3-11}$$

Therefore, the driving normal stress loads of the MFC can be determined based on the material properties of the MFC described in Table 3.1, and the structure can expand and contract in the direction of the fibers by these driving stress loads.

3.2 Experiment Evaluation of Driving Model

In order to verify and establish above mentioned driving model of piezoelectric fiber composite from input voltage to stress output, the corresponding numerical simulations and experiments by using simple cantilever beam model are carried out in this section. Transient dynamic analysis (time-history analysis) is a method to determine the dynamic deformation response of a structure under a time-varying load. In the present research, transient dynamics analysis is adopted to predict the displacement response of the beam model.

A simple cantilever beam structure is designed to verify the feasibility of the driving model of PFC actuator. Figure 3.10 and Fig. 3.11 show the geometric model and prototype of the cantilever beam model. It is composed of a MFC plate and a carbon plate (CFRP). The cantilever boundary condition is applied on the beam model, that is, one

end of the beam is fixed and the other end is free. The specifications of the beam model are described in Table 3.2.

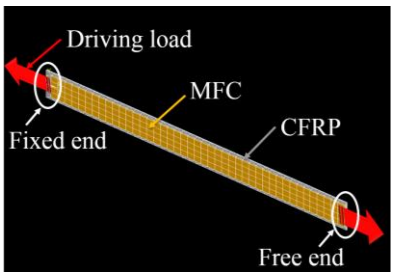

Fig. 3.10 Geometric model of beam structure.

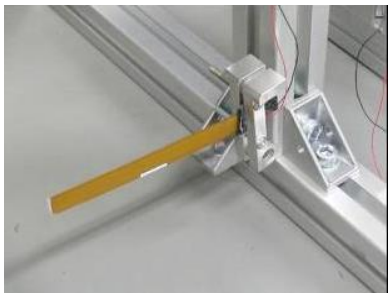

Fig. 3.11 Prototype of beam structure.

Table 3.2 Specifications of Beam Model

Item	**Material**	
	MFC	***CFRP***
Density (kg/m^3)	5440	1643
Tensile modulus (GPa)	30.3(15.9)	20.05
Poisson's ratio	0.31/0.16	0.3
Thickness (mm)	0.3	0.2
Length (mm)	85	87
Width (mm)	7	8

The vibrational mode frequency and displacement of the beam model are investigated based on FEM approach through the software ANSYS®-ANSYS 12.1. In the numerical simulation, the element SOLID 186, higher order three-dimensional (3-D) 20-node solid element, is used to model the MFC and CFRP structure. The fixed sup-

port is applied on the fixed end of the beam model. The number of total elements is 1,972 and number of total nodes is 4, 586.

In order to establish the reasonability of the driving model, the mode frequencies from modal analysis are firstly predicted. The simulation results on bending mode frequencies of the beam model are shown in Table 3.3, where the first three mode frequencies are presented. And the corresponding bending mode shapes are shown in Fig. 3.12. At the frequency of about 25Hz, the first bending deformation motion with large displacement occurs.

Table 3.3 Bending Mode Frequencies of Beam Model

Item	**Bending Modes**		
	1	***2***	***3***
Frequency (Hz)	24.8	160.04	457.5

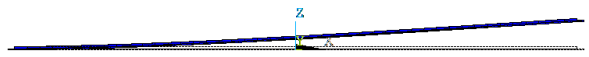

(a) First bending mode

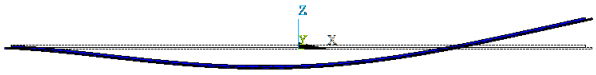

(b) Second bending mode

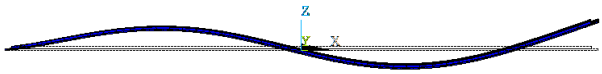

(c) Third bending mode

Fig. 3.12 Bending deformation mode shapes of beam model.

Then, the transient dynamic analysis is carried out in the frequency ranged from 1Hz to 50Hz to evaluate the first bending displacement of the beam model. Also, the corresponding experiments on beam prototype are carried out in the given frequency range for comparison. The range of input voltage with sine waveform on beam prototype is -

500V～+1500V. As shown in Fig. 3.11, one end of the prototype is fixed by experimental devices and the other end is free. The experimental and simulation results on displacement of the free end for beam prototype are shown in Fig. 3.13.

From the Fig. 3.13, the maximum displacement of the beam model happens at about 25Hz in the given frequency range both in simulation and experiments. The simulation result on mode frequency and displacement of first bending deformation mode matches the experimental result well. But displacement difference exists between the simulation and experiments. The minimum difference less than 5% happens at 30Hz. At the natural frequency of first bending mode about 25Hz, the displacement difference is about 14%. The simplified structure model and boundary condition in the numerical analysis make the main effort for difference. The hand-made error and experimental measurement from fixed device on prototype are another source of differences. As a conclusion, the main bending deformation mode frequency and corresponding displacement are evaluated well by the driving model. The feasibility of the driving model based on soft PFC actuator is validated by the experiment on prototype.

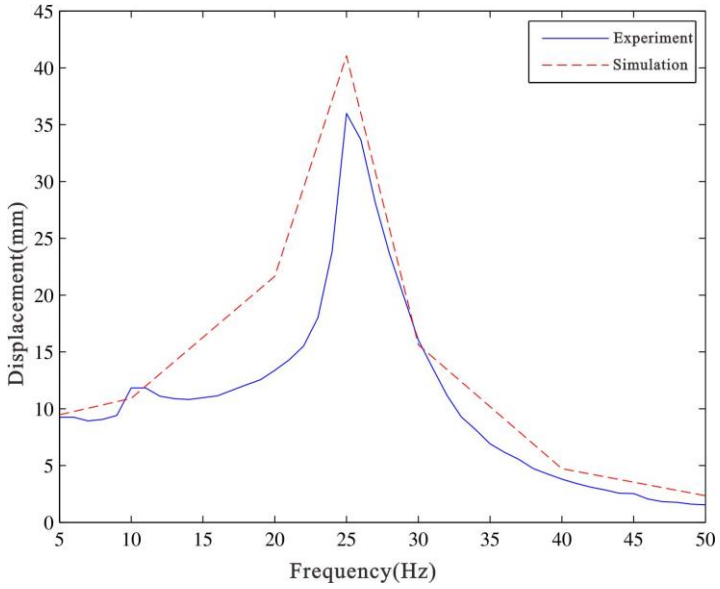

Fig. 3.13 Displacement of beam model in simulation and experiment.

3.3 Modelling of Soft Robotic Fish

According to above established driving model by PFC actuator, the initial structure of the soft robotic fish with BCF propulsion is to be modelled in this part to realize the bending propulsion motion of the soft robotic fish.

The prototype and geometric model of the soft robotic fish is presented in Fig. 3.14 [26]. The emphasis in the research is on BCF propulsion and for that the caudal fin is only considered in the robot model.

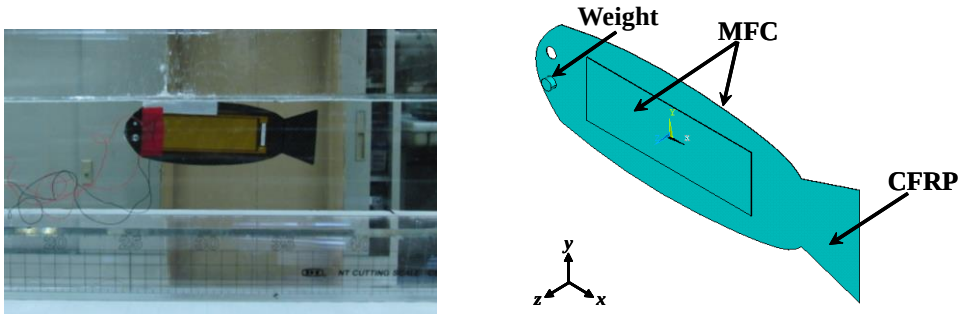

(a) Prototype **(b) Geometry model**

Fig. 3.14 Model of soft robotic fish.

The main body is made by a CFRP plate and two MFC plates. Two MFC plates sandwich the CFRP plate as the actuator structure to generate bending deformation for swimming propulsion motion. One MFC plate is used to control the contraction motion and the other is responsible for the extension motion. Weight made by steel is placed on the head to constrain its motion for increasing the displacement of the tail end for soft robotic fish. This constrains is similar to cantilever structure. The height of fish body is varied toward the tail end and it is smallest at the point where the caudal fin connects to fish body called caudal peduncle.

The MFC with M-8528-P1 type [27] is adopted as the soft actuator for robot structure. The body length of the robot is about 167mm. The thickness of the CFRP plate is 0.2mm. The density of the head weight is 7850 kg/m^3 and its radius is about 2.5mm. The basic structural parameters of the soft robotic fish are shown in Table 3.4.

Table 3.4 Structural Parameters of Soft Robotic Fish

Item	Specification
Body Length (mm)	167
Maximum height of body (mm)	55
Height of caudal fin (mm)	50
Thickness of Main Body (mm)	CFRP 0.2
Type of Actuator	M8528P1
Actuator Dimensions (mm)	112×40
Actuator Active Area (mm)	85×28

3.4 Structure-Acoustic Coupling Analysis of Soft Robotic Fish

Based on the established driving model of PFC actuator and above geometric model of soft robotic fish, the fluid-structural coupling analysis of the soft robotic fish using PFC is developed. In order to predict the dynamic response of the soft robotic fish in the fluid, the coupling between the flexible continuum and surrounding fluid should be considered in the numerical analysis. In this section, the coupling analysis of the soft robotic fish based on the structure-acoustic method is performed to consider the fluid effect for predicting the structural deformation behaviour of the soft robot in the fluid. Through this method, the structural mode frequencies and corresponding mode shapes of the soft robotic fish in the fluid from modal analysis are firstly calculated based on the mentioned numerical simulation system described in Chapter 2. By comparing the deformation motions at corresponding mode frequencies with those of the real fishes, the desired structural bending mode can be identified to realize the corresponding propulsion motion of the soft robotic fish by actuating the robot structure in the fluid. Furthermore, the amplitude of the bending propulsion motion of soft robot is investigat-

ed through transient analysis based on the driving voltage on PFC. It provides the basic foundation for further performance improvement of soft robotic fish.

3.4.1 Overview

To fully investigate the dynamic response of the soft robotic fish, researches must take into the interaction between the soft structure and surrounding fluid field, and model the coupling mechanisms accurately for FSI analysis.

The structure-acoustic coupling method considers the acoustic pressure can be used to solve a broad class of FSI problems involves a fluid domain without significant flow and the main concern in the fluid field is the pressure wave propagation, and predict structural mode and deformation response in the fluid field. Many successful solutions are obtained on prediction of the structural behaviours in the coupling analysis, such as structure mode of underwater cylindrical shell, vibration response of the vehicle and an infinite duct, structure behaviour of spacecraft structures [28]-[32]. From these successful solutions on describing the structural behaviours, a basic of boundary conditions can be obtained for numerical analysis of the soft robotic fish in the fluid. In the present research, the structure-acoustic coupling method is adopted to perform the modal and transient analysis for predicting and identifying the structural behaviour of the soft robotic fish in the fluid.

Addressing the structure-acoustic coupling problems, the FEM analyzed methods is widely used to describe the dynamic response behavior for the structure submerged in a fluid field. The entire problem domain is divided into elements rather than only bounding surface of the domain. The FEM approach is adopted in the research to deal with the coupling problem for soft robotic fish through ANSYS software. Acoustic elements in ANSYS software accomplish the required fluid-structural coupling because they have four degrees of freedom (DOF): three for optional displacement DOFs and one for pressure. Thus, a consistent matrix coupling can be set up between structural and fluid elements in which strongly coupled physics cause no convergence problems.

In the structure-acoustic coupling analysis of the soft robotic fish through ANSYS acoustic program, the acoustic pressure in the fluid is determined by the acoustic wave equation and meets the following basic conditions. Firstly, the fluid is non-flowing, inviscid and compressible, but the change in fluid density is small compared with mean density. Secondly, analyses are allows only relatively small acoustic pressure changes with respect to the mean pressure for small variation in fluid density. Thirdly, the mead density and pressure are uniform though the fluid. Fourthly, there is no heat transfer process. The transfer process between wave propagation and thermodynamics is adiabatic.

3.4.2 Modal Analysis of Soft Robotic Fish

In order to predict the bending deformation mode frequencies and mode shapes of the soft robotic fish in the fluid, the modal analysis of soft robotic fish considering the surrounding fluid based on structure-acoustic coupling method is firstly performed. By comparing the deformation motions at corresponding mode frequencies with those of the real fishes, the bending propulsion mode can be identified to realize the corresponding propulsion motion of the soft robotic fish.

3.4.2.1 Modelling of Computational Domain

In the numerical modal analysis, a spherical surface is set as the computational domain boundary of the enclosed fluid cavity, whose diameter is about 200mm, as shown in Fig. 3.15. The computational domain is in the sphere. The soft robotic fish is placed in the middle of the static fluid domain. The properties of the soft robotic fish in the numerical simulation are shown in Table 3.5.

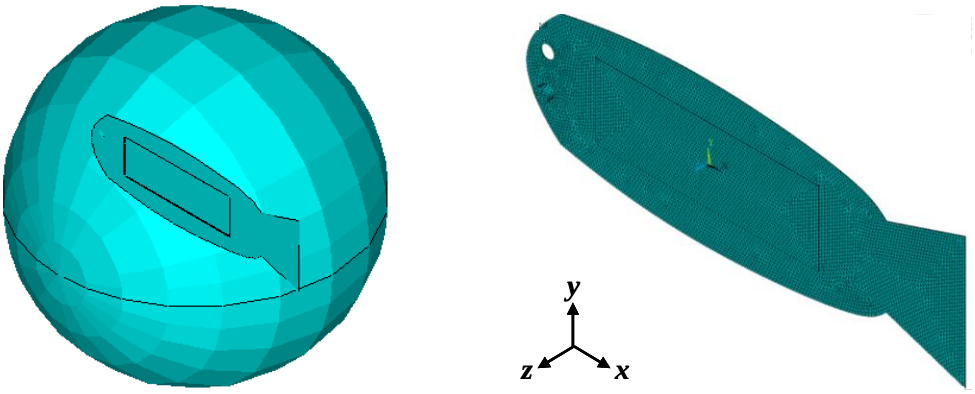

(a) Computational domain **(b) Finite element model of contained soft robot**

Fig. 3.15 Model of soft robot fish in the fluid.

Table 3.5 Properties of Soft Robotic Fish

Item	Material	
	Weight	***CFRP***
Density (kg/m^3)	7850	1643
Elastic Modulus (GPa)	20	20.5
Poisson's ratio	0.3	0.3
Thickness (mm)	2.5	0.2

Due to the high voltage of MFC, the Fluorinert Electronic Liquid FC-3283 is adopted to describe the properties of fluid domain, whose density is 1820 kg/m3 shown in Table 3.6 [33]. It is a fully-fluorinated liquid and primarily a single compound. Its composition will not shift or fractionate with time, which keeps fluid loss to a minimum and insures the fluid transport properties is stable and will not change with time.

Table 3.6 Properties of Fluid Field

Item	Property
Density (kg/m^3)	1820
Average Molecular Weight (g/mol)	521
Kinematic Viscosity (centistokes)	0.75
Absolute Viscosity (centipoises)	1.4

The calculation domain is meshed by ANSYS software. The 3-D solid elements SOLID186 are adopted to describe the soft robot structure, whose finite element model is presented in Fig. 3.15(b). There is no any fixed support on soft robotic fish and the governing equation in finite element formulation described as follows.

$$M_S\ddot{U} + K_S U = F_S + f_F \tag{3-12}$$

$$f_F = RP = \int_{SF} N_S^T n N_F P dS \tag{3-13}$$

where *Ms* and *Ks* are structural mass and stiffness matrices, *U* is displacement, *Fs* is external force, f_F is the force vector describing the coupling to the fluid domain, *P* is fluid pressure, *R* is coupling matrix represents the effective surface area associated with each node on the fluid-structure interface, N_S and N_F contains the finite element shape functions for the structural domain and fluid domain, respectively, *n* is the normal vector at the fluid boundary.

As for the fluid domain, the 3-D FLUID30 elements are used to model the spherical fluid domain and interface between the solid structure and surrounding fluid in the modal analysis of soft robotic fish. It has eight corner nodes with four DOFs on each node. And the pressure constrains are applied on the outer border of the fluid domain. The system of equations for the fluid domain in finite element formation is shown in (3-14) and (3-15), where M_F and K_F are fluid mass and stiffness matrices, respectively, *P* is fluid pressure, F_F is added mass term, ρ_f is fluid static density.

$$M_F\ddot{P} + K_F P = F_F + f_S \tag{3-14}$$

$$f_S = -\rho_f R^T \ddot{U} \tag{3-15}$$

The coupling between the fluid domain and structure domain is descried by boundary force terms, the structure is subjected to a force at the boundary between the domains due to the fluid pressure. The force acting on the fluid due to displacement of the structure can be derived from the boundary term and written in terms of structural

acceleration. At the interface boundary between the structure and fluid domain, defined as Ω_{SF}, the fluid and structure moves together in the normal direction of the interface boundary.

In the computational domain, the grid distribution from the surface of the robot body to the fluid border is sparse gradually. The density of grid nodes near the surface of the robot is largest in the fluid domain. The number of the total grid nodes for whole computational domain is 140,886 and number of the total elements is 244,105. In order to simplify the calculation, there is no buoyancy and heat transfer in the numerical simulation.

3.4.2.2 Numerical Simulation Results

According to above mentioned computational domain, the modal analysis of soft robotic fish with free boundary condition in the fluid is performed. The simulation results on deformation mode frequency of soft robotic fish in the fluid are shown in Table 3.7, where the first six mode frequencies are represented.

Table 3.7 Mode Frequencies of Soft Robot in the Fluid

Item	Mode Frequencies (Hz)					
	1	***2***	***3***	***4***	***5***	***6***
Robot without fluid	43.03	107.2	142.9	219.6	269.4	312.1
Robot in the fluid	5.99	16.55	24.99	36.3	43.8	57.8

The mode frequencies of the soft robotic fish in the fluid field are less than the frequencies without considering the coupling effect of the surrounding fluid. And the decreasing amounts of the high order frequencies are larger than that of the first order frequency. This is mainly due to the increasing of the fluid added mass caused by hydrostatic pressure.

When the geometry size of the fluid domain is changed, the mode frequencies of the soft robotic fish in the fluid are shown in Table 3.8. There is almost no variation on mode frequencies of soft robotic fish. The change in fluid geometry has little effect on mode frequencies of the soft robot. The far-field conditions are applied on the fluid domain successfully.

Table 3.8 Mode Frequencies of Soft Robot in Different Fluid Geometries

Item	Mode Frequencies (Hz)					
	1	***2***	***3***	***4***	***5***	***6***
Geometry-0.20m	5.99	16.55	24.99	36.3	43.8	57.8
Geometry-0.24m	5.95	16.5	24.9	36.1	43.8	57.6
Geometry-0.30m	5.94	16.4	24.8	36	43.8	57.6
Geometry-0.40m	5.92	16.4	24.7	36	43.8	57.7

The structural deformation modes of the soft robotic fish in the fluid at corresponding mode frequencies are shown in Fig. 3.16, where the bending deformation is mainly concerned for soft robot's propulsion motion and the first two bending modes are presented. If the frequency is about 16.5Hz, the first torsion deformation occurs on the caudal fin of the soft robotic fish. When the driving frequencies are about 6Hz and 25Hz, the first and second bending deformation modes are obtained, respectively. The first bending deformation mode is the main propulsion mode of the soft robotic fish for swimming motion. The largest displacement is obtained at the end of the caudal fin. The deformation similar to S-shape occurs on the second bending mode. The minimum displacement all happens at the position where the distance from the edge of head is about one-third of body length. The bending mode frequencies and its corresponding mode shapes of the soft robotic fish are determined by the modal analysis using structure-acoustic coupling method. The suitable bending propulsion motions of the soft robotic fish are obtained through the coupling analysis. The structure-acoustic coupling ap-

proach is suitable to predict the characteristics of deformation mode of the soft robot in the fluid.

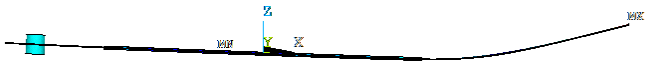

(a) First bending mode (6Hz)

(b) Second bending mode (25Hz)

Fig. 3.16 Bending deformation modes of soft robotic fish in the fluid.

By comparing these deformation motions at corresponding mode frequencies with those of the real fishes, the bending propulsion mode is identified to realize the corresponding propulsion motion of the soft robotic fish by actuation with different frequencies in the fluid.

3.4.3 Transient Analysis of Soft Robotic Fish

To further evaluate the amplitude of the main bending propulsion motion of the soft robotic fish in the fluid, the transient analysis is carried out to determine the displacement response of the soft robot with a time-varying load by structure-acoustic coupling method. The soft robotic fish is also placed in the stationary fluid. The established driving load from (3-10) and (3-11) in sine waveform is applied to soft robot.

The main propulsion mode of the soft robotic fish is first bending mode and mainly focused. The maximum deformation of the soft robot occurs at the end of the caudal fin. Thus, the displacement of the tail end is used to describe the bending deformation response of the soft robotic fish in the present research. The results of 3Hz, where the robot has good flexible fishlike motion due to suitable swimming number S_w [34], is adopted to make the description. The input voltage is in the range of -500V～+1500V. When the driving frequency of input voltage is 3Hz in sine waveform, the simulation results on displacement of the tail end in one cycle are presented in Fig. 3.17. The spe-

cial tested point on the lateral edge of the caudal fin shown in Fig. 3.17(a) is used to describe the deformation of tail end in the present research.

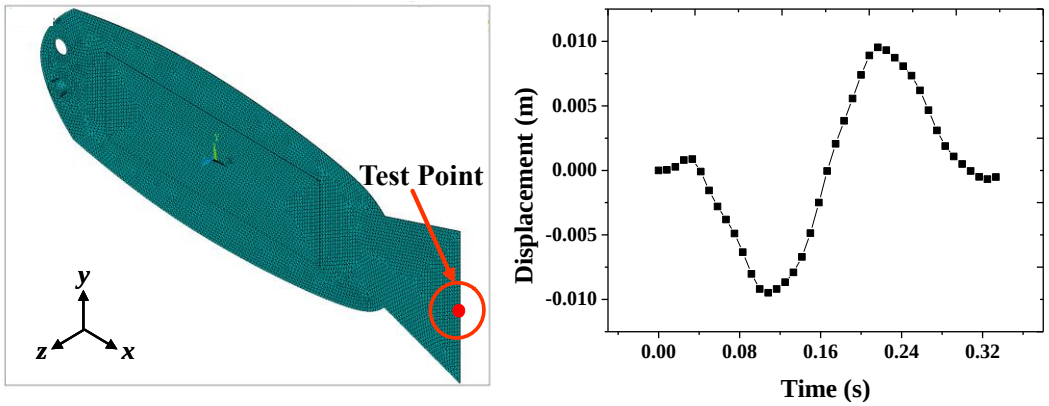

(a) Test point on tail end **(b) Amplitude of test point**

Fig. 3.17 Amplitude of tail end of soft robotic fish.

As shown in Fig. 3.17, the caudal fin of the soft robotic fish makes the oscillating motion similar to a sine wave when the driving loads applied. The maximum amplitude of the tail end is near to 20mm. The amplitude of the bending propulsion motion of the soft robotic fish in the fluid are predicted smoothly through the transient analysis.

As a conclusion, through the structure-acoustic coupling method, the desired bending propulsion modes about the mode frequencies and mode shapes of the soft robotic fish in the fluid are predicted successfully through the modal analysis. The suitable bending propulsion motion is realized on soft robotic fish through the coupling analysis. Also, the amplitude of the main bending propulsion motion of the soft robotic fish in the fluid is calculated through the transient analysis with a time-varying driving loads. The coupling analysis using structure-acoustic coupling method can be used to evaluate the characteristics of structural behavior, propulsion modes and deformation response of the soft robotic fish in the fluid. It provides a way for further optimization and improvement on dynamic deformation modes, motion amplitude or propulsion methods in the design of soft robotic fish. The detailed experiment verification will be presented in next chapter.

3.5 FSI Analysis of Soft Robotic Fish

According to above numerical coupling simulation analysis, the bending deformation modes about mode frequencies and mode shapes of the soft robotic fish in the fluid field have been determined by the structure-acoustic coupling approach. However, in above numerical coupling analysis, the fluid is inviscid and there is no dissipative effect due to viscosity. The hydrodynamic force and wake performance of the soft robotic fish cannot be obtained from above coupling simulation. In order to reveal the hydrodynamic propulsion performances of the soft robotic fish in the fluid, the further hydrodynamics analysis are needed to be investigated in the coupling system for higher motion performances of the soft robot, considering the large deformation of flexible robot structure and complicated coupling dynamics with fluid. This section introduces a FSI analysis based on CFD method to evaluate and enhance the hydrodynamic performances of the soft robotic fish using PFC. According to the scheme of FSI analysis for soft robotic fish shown in chapter 2, by the driving model of the PFC actuator has been mentioned above in this chapter, the FSI analysis of the soft robotic fish is performed. Based on FSI analysis, the relationships of driving frequencies of input signal with propulsive force and displacement of propulsion motion for soft robotic fish are investigated. It provides the basic propulsion characteristics of the soft robotic fish for further improvement.

3.5.1 Overview

Due to the uncompleted understanding of swimming mechanism of the real fish [24] and the limited studies to develop the bionic flexible structure and functions with large deformation, the hydrodynamic performances of robotic fish have not been revealed completely. There is no published report on systematic study for the detailed swimming kinematical performances of the hydrodynamics on robotic fish [35]. Although some mature theories such as large-amplitude elongated-body theory, slender-body theory or

3-D waving plate theory can be used to investigate the hydrodynamic performances of the fishes, these theories are only established on a basis of potential flow, linearized body boundary conditions. They neither get the solution of nonlinear flow-body interaction nor develop the coupling wake dynamics [36].

When a soft robotic fish is contacting a flow fluid is subjected to fluid pressure, the deformation of the soft robotic fish may happen. As a return, a deformed soft robotic fish changes the fluid flow. To fully investigate the hydrodynamic performances of the soft robotic fish, the interaction between the soft robot structure and surrounding fluid must be considered and the coupling mechanism should be modelled accurately for the FSI analysis [37]. In the present research, the CFD numerical method is adopted to predict the hydrodynamic behaviours of the soft robotic fish in FSI system. This coupling method is largely applied into the fields of engineering and biomedicine to solve the FSI problems of the flexible structures and predict their hydrodynamic characteristics [38]-[46]. The FSI analysis based on CFD method is introduced to predict and enhance the propulsive force and amplitude of the soft robotic fish in the fluid in the research.

Addressing the FSI analysis in the research, the data transfers including the deformation results of structural dynamic analysis and fluid pressure loads of surrounding fluid domain occur. According to the scheme of the FSI analysis based on CFD method in chapter 2, in this section, the numerical models of the soft robot structure and surrounding fluid are presented. Through these numerical models, the FSI analysis of the soft robotic fish is performed by CFD method based on the established driving model of the PFC actuator in ANSYS Software. The data transfers of the structural results and fluid pressure loads occur on the interface between the robot structure and surrounding fluid through the interface boundary conditions. From the coupling analysis, the numerical simulation results about propulsive force and amplitude of propulsion motion of the soft robotic fish in the fluid are finally presented for describing its hydrodynamic performance.

3.5.2 Transient Analysis of Soft Robotic Fish

In the numerical FSI analysis, the soft robot structure model is defined through the application of Mechanical and the fluid model is developed in the CFX in ANSYS software. The communicating data between the Mechanical and CFX is calculated by the MFX coupling algorithm of Multi-field solver automatically. The corresponding propulsion characteristics of the soft robotic fish can be obtained from this coupling analysis.

In this part, the numerical models of the solid structure and fluid are firstly presented for FSI analysis, respectively. Then, the detailed solution procedure of the FSI analysis is described for predicting the hydrodynamic performance of the soft robotic fish in the fluid.

3.5.2.1 Modelling of Solid Structure

The geometric model of the solid structure in the numerical FSI analysis, that is, the model of soft robot structure, is shown in Fig. 3.18.

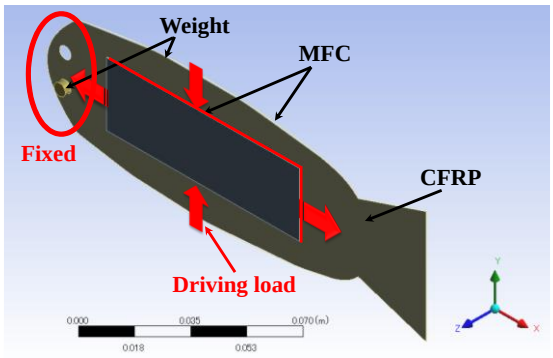

Fig. 3.18 Geometric model of soft robotic fish.

The soft robot model, same as the description mentioned previously in this chapter, is also mainly made by a CFRP plate and two MFC plates. To meet the requirement of measurement platform of propulsion and simplification of calculation, the fixed support applies on the robot head. This structure model of the soft robotic fish is defined as the solid structure domain through the application of Mechanical in the FSI analysis. The

driving voltage from -500V to +1500V is applied on it for robot actuation. By this driving load, the bending deformation generates and the robot makes the oscillating motion in the direction of *z*-axis. The properties of the solid robot structure in the numerical analysis are shown in Table 3.9.

Table 3.9 Properties of Robot Structure

Item	Weight	CFRP
Density (kg/m^3)	7850	1700
Elastic modulus (GPa)	20	29.5
Poisson's ratio	0.3	0.3
Thickness (mm)	2.5	0.2

The finite element model of the soft robot structure is shown in Fig. 3.19. It is modelled by the hexahedral element. The number of the grid nodes is 152,902 and number of the elements is 28,181.

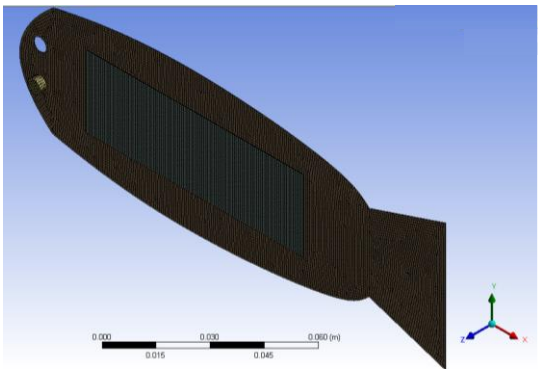

Fig. 3.19 Finite element model of soft robotic fish.

Based on finite element model of the soft robotic fish, the fixed support applies on robot head, and the driving load from (3-10) and (3-11) is applied to the areas of two MFC plates for actuation described in Fig. 3.18 in the Mechanical analysis. Here the driving load is normal to the plane of the area considered on MFC plates. In Fig. 3.18, only one MFC plate's load distribution can be obtained. For the other MFC plate, the driving load is applied in opposite direction based on the corresponding areas of load

distribution. Besides, in the solid structure, the region that defines the interface between the fluid in CFX and structure in ANSYS Mechanical is defined. Data is exchanged across this interface during the execution of the simulation. The basic governing finite element matrix equation of the soft robotic fish is shown as follows [47].

$$M\ddot{U} + KU = F_R \tag{3-16}$$

where M and K are structural element mass and stiffness matrix, respectively; F_R is applied force on the robot structure, including the external driving force and the force describing the coupling to the surrounding fluid; U is displacement.

3.5.2.2 Modelling of Fluid

The 3-D incompressible Navier-Stokes equations and continuity equation are used to model the surrounding fluid domain of soft robotic fish Fig. 3.20 describes, shown as follows. They are solved by the finite volume method in the CFX. By using these equations with additional boundary conditions, the non-linear problems can be solved, and the distribution of fluid velocity and pressure around the soft robotic fish are obtained. To obtain a time-unsteady solution using a relatively simply solver at lower computational cost, the additional turbulence model is adopted and it is the simplified and approximate model, so that the approximate modelling of the fluid in the analysis has the difference with the real conditions. However, it can be employed to calculate the complex flow with high Reynolds numbers and meet the basic demands on physics of turbulent flow.

$$\rho\left(\frac{\partial V_x}{\partial t} + V_x\frac{\partial V_x}{\partial x} + V_y\frac{\partial V_x}{\partial y} + V_z\frac{\partial V_x}{\partial z}\right) = \mu\left(\frac{\partial^2 V_x}{\partial x^2} + \frac{\partial^2 V_x}{\partial y^2} + \frac{\partial^2 V_x}{\partial z^2}\right) - \frac{\partial P}{\partial x} + F_x \tag{3-17}$$

$$\rho\left(\frac{\partial V_y}{\partial t} + V_x\frac{\partial V_y}{\partial x} + V_y\frac{\partial V_y}{\partial y} + V_z\frac{\partial V_y}{\partial z}\right) = \mu\left(\frac{\partial^2 V_y}{\partial x^2} + \frac{\partial^2 V_y}{\partial y^2} + \frac{\partial^2 V_y}{\partial z^2}\right) - \frac{\partial P}{\partial y} + F_y \tag{3-18}$$

$$\rho\left(\frac{\partial V_z}{\partial t}+V_x\frac{\partial V_z}{\partial x}+V_y\frac{\partial V_z}{\partial y}+V_z\frac{\partial V_z}{\partial z}\right)=\mu\left(\frac{\partial^2 V_z}{\partial x^2}+\frac{\partial^2 V_z}{\partial y^2}+\frac{\partial^2 V_z}{\partial z^2}\right)-\frac{\partial P}{\partial z}+F_z \tag{3-19}$$

$$\nabla\cdot V=\frac{\partial V_x}{\partial x}+\frac{\partial V_y}{\partial y}+\frac{\partial V_z}{\partial z}=0 \tag{3-20}$$

where ρ is density; V is velocity; V_x, V_y and V_z are velocity components in the x, y and z direction, respectively; P is pressure; μ is dynamic viscosity; F_x, F_y and F_z are force components in the x, y and z direction, respectively.

As shown in Fig. 3.20, a cubical surface is set as the computational boundary of the fluid field, whose size is 590 × 133 × 440mm same with the liquid tank's in the experiment. The computational domain of the FSI analysis is in the cube. The soft robotic fish is centred in the transverse and the vertical directions of the fluid domain. The Fluorinert Electronic Liquid FC-3283 is also used to describe the properties of the fluid given in Table 3.6 due to the high voltage of the MFC. It is a fully-fluorinated and thermally stable liquid having good electrical insulation properties, meeting insulating requirement in the experiment. It keeps fluid loss to a minimum and insures the fluid transport properties are stable. Besides, it is practically non-toxic orally, and is non-flammable and highly resistant, so that it increases the security in storage and during use.

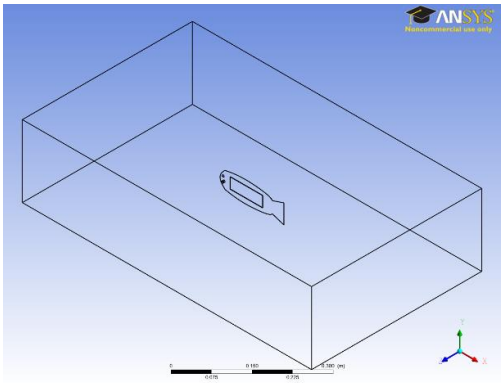

Fig. 3.20 Computational domain of fluid model.

In fluid dynamics, the Reynolds number (*Re*) is a dimensionless number that used to define the characteristics of different flow regimes within a similar fluid, such as lami-

nar flow or turbulent flow. The laminar flow occurs at low Reynolds number. In the fluid flow, the viscous force is dominant and characterized by constant fluid motion. At high Reynolds number, the turbulent flow is generated and dominated by the inertial force. In the turbulent flow, the chaotic eddy, vortices and other flow instabilities. For a fishes with subcarangiform swimming motion, the Reynolds number is often defined as follows [48], [49].

$$R_e = \frac{\rho VL}{\mu} \quad or \quad R_e = \frac{VL}{\nu} \tag{3-21}$$

where ρ is fluid density, V is average forward velocity, μ is dynamic viscosity of the fluid, v is kinetic viscosity of the fluid, L is fish length.

According to (3-21), the Reynolds number of the soft robotic fish at different swimming velocity can be obtained and it is larger than 10^4, characterized by high Reynolds number [48]-[50]. The turbulent flow is generated and the inertial forces dominate the dynamics of the motion in the fluid flow.

In the fluid model, some basic conditions are defined as follows. Firstly, the standard atmosphere and 25°C room temperature are presented as the reference values. Secondly, the buoyancy and heat transfer are not considered. The buoyant force perpendicular to the locomotion direction of the soft robot almost makes no effect on propulsion. The heat transfer in the fluid makes small effect on energy dissipation in the propulsion and can be ignored for simplification in the research. Thirdly, the shear-stress transport (SST) equation model is defined as the fluid turbulence model. It considers the transport of turbulent shear stress, and predicts the fluid flow on curved surface and separated flow on boundary layers accurately.

Two boundary conditions shown in Fig. 3.21, namely opening and nonslip wall boundary, applied to limit the fluid model in the FSI simulation. The nonslip wall boundary condition is applied on the surface of the whole robot body and the borders of the fluid domain expect for the top surface, and the fluid velocity on the wall boundary

is zero. The top surface of the fluid domain is described by the opening boundary condition on which the pressure with zero value is applied.

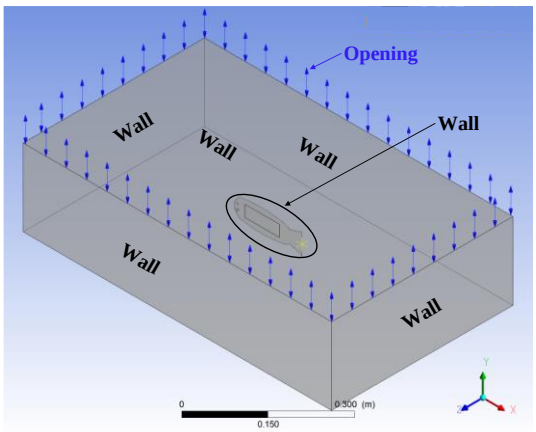

Fig. 3.21 Boundary conditions of fluid model.

The mesh grids of the fluid model are shown in Fig. 3.22. It is meshed through the ANSYS Workbench mesh method. The hexahedral element type is also used. The number of the grid nodes for fluid model is 105,136 and number of the elements is 533,943. The mesh distribution from the surface of the robot body to the fluid border is sparse gradually. The density of the grid nodes around the robot surface is largest in the fluid model.

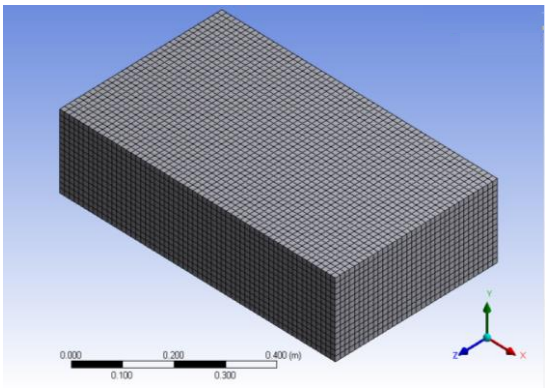

Fig. 3.22 Mesh of fluid model.

3.5.2.3 Solution Procedure

The transient analysis is used into both solid structure and fluid model to determine the hydrodynamic performance of the soft robot for propulsion in the FSI simulation. The FSI analysis through ANSYS program assumes the fluid is an ideal fluid and meets some basic conditions: firstly, the solid structure has flexible behaviour of large deflection; secondly, the fluid is nonflowing and inviscid; thirdly, there is no heat transfer process. The initial values for all variables needed in the analysis are defined as zero.

The interaction between the fluid and robot structure at the interface causes fluid pressure to exert a force on the structure and the structure motion produces an effective fluid load. The governing equations of the robot structure and fluid domain are coupled by the fluid-structure interfacial boundary conditions. The FSI analysis meets the basic principle of the continuity and conservation of velocity, stress, displacement, heat flow and temperature at the interface. The fluid velocity must be equal to the local solid structural wall velocity, including the normal and tangential components, described in (3-22). The Cauchy stress tensor on the interface need to be matched each other in the fluid and solid domain, shown in (3-23) and (3-24). If considering the heat flow, the heat balance at the interface is needed. The heat fluxes at the interface must be equal between the fluid and solid field.

$$v_n^s = v_n^f \qquad v_\tau^s = v_\tau^f \tag{3-22}$$

$$\tau_s + \tau_f = 0 \tag{3-23}$$

$$\sigma_s + \sigma_f = 0 \tag{3-24}$$

where v_n and v_τ are normal and tangential velocity, respectively, τ and σ are normal and shear stress, respectively, subscript s and f are expressed as solid and fluid domain, respectively.

The detailed solution procedure of the FSI analysis between the solid robot structure and fluid is shown in Fig. 3.23.

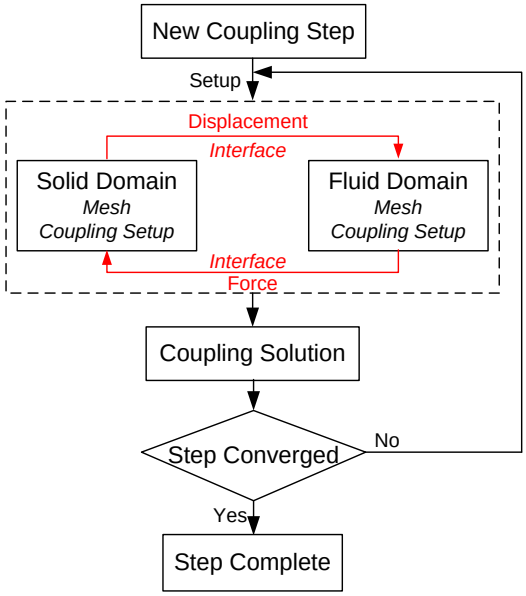

Fig. 3.23 Solution procedure of FSI analysis.

The solid robot structure domain and fluid domain have the separate mesh distribution and boundary conditions. The data transfer occurs on the interface. Each field solver gathers the transfer data require from the other solver, and solves its field equations for the current coupling step. Step calculation is repeated until the data transfer between two solvers and all field equations have converged. After convergence, the current coupling calculation will move to the next step. The transfer data in the analysis are the force from fluid and the displacement from robot structure.

In order to evaluate the hydrodynamic performances of the soft robotic fish, the propulsive force of the robot from this 3-D computation is needed to investigate. In the simulation, the soft robot is oscillating in the direction of *z*-axis and the hydrodynamic force along the *x*-axis is only considered for propulsion. The component of the hydrodynamic force along the *x*-axis can be calculated as the integral of the pressure and viscous stress over the surface of the robot body in the direction of *x*-axis, shown in (3-25) [50].

$$F_x = \oint_A (-\vec{p} \cdot \vec{n}_x + \vec{\tau}_{xi} \cdot \vec{n}_i) dA \tag{3-25}$$

where dA is infinitesimal of surface area of robot body; n_i is the ith component of the unit normal vector of area dA; n_x is unit normal vector of area dA in the direction of x-axis; p is pressure; τ_{xi} is viscous stress tensor in the direction of x-axis.

3.5.2.4 Numerical Simulation Results

According to above mentioned numerical models of solid structure and surrounding fluid, the FSI simulations are carried out to determine the hydrodynamic performances of the soft robotic fish for propulsion. The propulsive force and deformation response play the crucial role in the hydrodynamic propulsion of the soft robotic fish. Thus, the results of propulsive force and displacement of propulsion motion of the soft robotic fish are presented for describe its hydrodynamic performance.

The fluid pressure plays a key role in the propulsion of soft fish robot. Based on specific driving frequency of the robot, the pressure distribution around the robot varies with the time. And the pressure distribution is different with different driving frequencies of the soft robotic fish. Figure 3.24 presents the fluid pressure in the x-z mid-plane in half cycle at 3Hz where the robot has the good flexible fishlike motion due to the suitable swimming number S_w [34]. Here the pressure relative to one standard atmosphere is used to express the static pressure in the fluid.

As shown in Fig. 3.24, the robot makes the oscillating bending motion. The pressure of flow field near the robot has the obvious disturbance and the dynamic pressure is determined by the motion of the robot. The pressure contours are crowded near the robot body, where the higher pressure is obtained. The pressure peak and trough appear at the tail part of the robot, where the largest deformation of the robot occurs. Due to the oscillating bending motion of the robot, the obvious pressure differential between the left and right part around the robot generates. However, there is very low pressure difference between the front and back part of the robot, benefits from its streamlined body shape. Fig. 3.24(b) shows the fluid pressure where the maximum deformation of the robot happens. When the robot displacement goes larger, the area of fluid disturbance will be expanded.

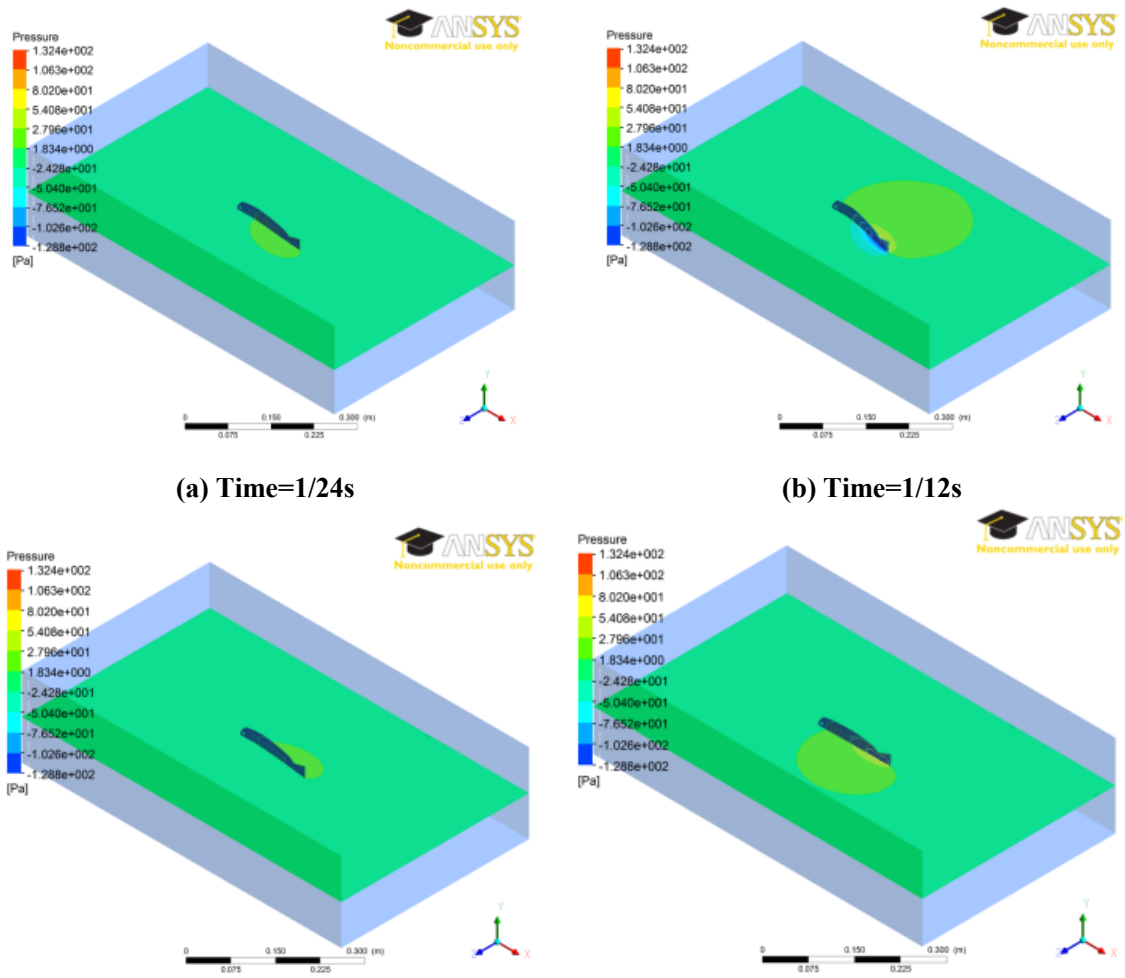

(a) Time=1/24s **(b) Time=1/12s**

(c) Time=4/8s **(d) Time=1/6s**

Fig. 3.24 Fluid pressure contours in the *x*-*z* mid-plane in half cycle at 3Hz.

The results on hydrodynamic force along the *x*-axis are presented in Fig. 3.25. The input voltage range on robot is -500V～+1500V and the range of driving frequency is 1Hz～25Hz.

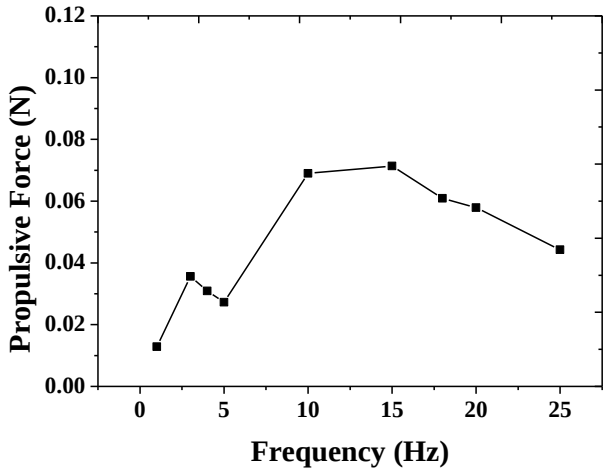

Fig. 3.25 Propulsive force of soft robotic fish in the simulation.

In Fig. 3.25, the propulsive force of the soft robotic fish for the case of fixing robot head at different driving frequencies is predicted by the FSI analysis. At different driving frequencies, the propulsive force is different. There is no direct proportional relationship between the propulsive forces and driving frequencies of the soft robot occurs. Through investigating the propulsion motion of the soft robotic fish, there are some minimum points can be used to describe the propulsion mode of the soft robot in its locomotion. The propulsion mode of the soft robot in one cycle at 3Hz and 5Hz are shown in Fig. 3.26. From the Fig. 3.26, it can be found that there are some points with minimum deformation exist on the propulsion mode of the soft robotic fish at different frequencies. It can be found that the similar bending mode occurs on soft robot at 3Hz and 5Hz, but the point with minimum deformation generates at different position of the tail part. By comparison of propulsion mode at 3Hz and 5Hz, the minimum node point at 5Hz happens near the place where the body length is about 130mm, larger than that of 3Hz whose minimum point occurs at the place where the body length is about 120mm described in Fig. 3.26(a). The proportion of robot body utilizing for propulsion near the tail part at the frequency of 3Hz is larger than that of 5Hz. Thus, the propulsive force of the soft robot at 5Hz is smaller due to the node point near the caudal fin part which does not contribute to the propulsion of the robot.

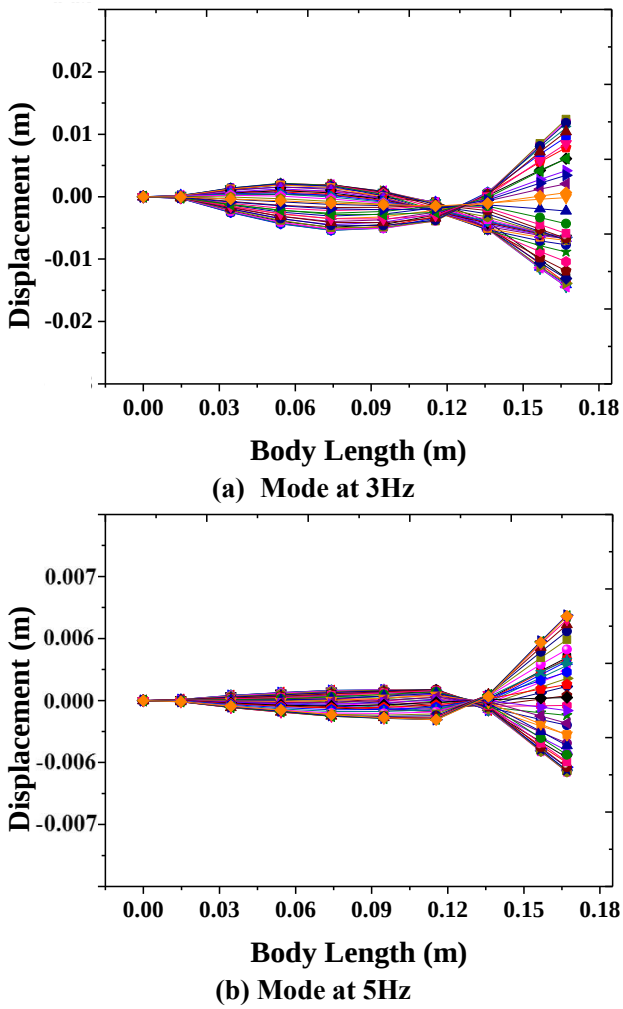

Fig. 3.26 Propulsion modes of soft robotic fish at 3Hz and 5Hz.

The corresponding displacement of the soft robotic fish at different driving frequencies also can be obtained from FSI analysis. The soft robot makes the oscillating motion. At different driving frequencies, the similar bending deformation modes occur on the soft robot for propulsion. The results at 3Hz where the robot has the good flexible fish-like motion is adopted to present its bending deformation modes, shown in Fig. 3.27. The results in quarter of one cycle are adopted for description. As shown in Fig. 3.27, the bending deformation mode occurs in the oscillating motion of the soft robot, and the displacement is increasing gradually from 0.005s to 0.0845s at 3Hz. At 0.0845s, the deformation reaches the maximum value. At different time values, the maximum deformation of the robot is all obtained at the caudal fin end. The bending propulsion motion is realized on soft robot through the FSI analysis.

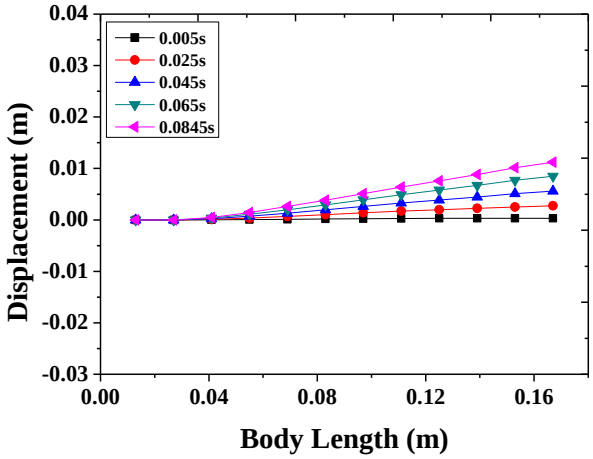

Fig. 3.27 Deformation modes of soft robotic fish in quarter of one cycle at 3Hz.

The results on displacement of the caudal fin end at different driving frequencies are presented in Fig. 3.28. The maximum displacement is obtained at 1Hz and it is about 34mm. With the increase of the driving frequency on soft robot, the displacement of the tail end of the soft robotic fish is decreasing. The relationship between the driving frequencies and displacement of the propulsion motion for the case of fixing robot head of the soft robotic fish is determined through the FSI analysis.

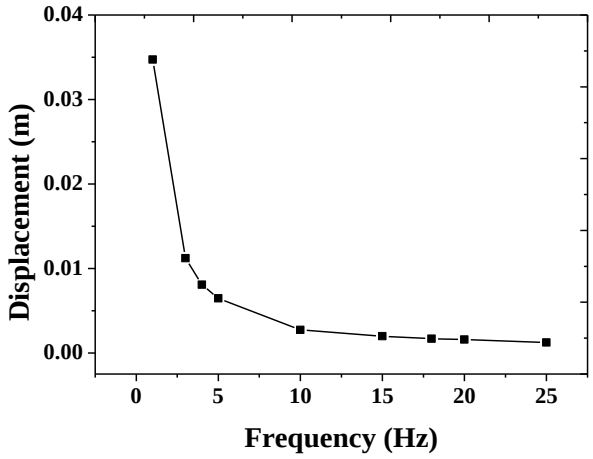

Fig. 3.28 Displacement of caudal fin end in the simulation.

As a conclusion, the propulsive force and deformation trajectory of the soft robotic fish at different driving frequencies can be calculated through the FSI simulation. The relationships of the driving frequency of input voltage with the propulsive force and displacement of the propulsion motion for the case of fixing robot head of the soft ro-

botic fish in the fluid are obtained. The FSI analysis can be used to predict the propulsion performances of the soft robotic fish for further performance improvement.

In order to evaluate these results about propulsive force and displacement of the soft robotic fish in the fluid and feasibility of the FSI analysis, the corresponding experiments on robot prototype will be carried out to make the verification in next chapter.

3.5.3 Vortex Analysis around Soft Robotic Fish

In fluid dynamics, a wake is the region of disturbed flow (usually called turbulent) downstream of a solid body moving through a fluid field, which is caused by the fluid flow around the solid body. In the wake structure of the object moving in a fluid, the vortex is a region within a fluid where the flow is mostly a spinning motion. This motion pattern is called a vortical flow. Vortices phenomenon often can be observed in the wake of the swimming fishes and they are a major component of wake development of swimming fishes for propulsion.

In order to further investigate and improve the propulsion performance of the soft robotic fish, the wake around the soft robotic fish is investigated by the FSI analysis in the research. The continuous swimming motion of the body and tail of the robotic fish provides an excitation of the fluid and hence the unsteady flow patterns are expected to produce, including any organized vortical patterns shed by the body or tail of the robotic fish. Besides, in the turbulent flow, unsteady vortices appear on many scales and interact with each other and the structure and location of boundary layer separation often changes with swimming motion and flowing fluid. Vortex is a form of transmission, transformation and dissipation of energy caused by the interaction between the soft robotic fish and surrounding fluid [51], [52]**.** It is a major component of turbulence flow**.** Therefore, it is necessary to further study the vortex in the wake performance around the soft robotic fish for performance improvement on propulsion by FSI analysis.

Turbulence is a non-linear fluid motion which is irregular spatially and chaotic, and appears very complex flow patterns. It is a very difficult problem in fluid dynamics due

to its randomness, rotationally and dissipation. In the CFD, the Navier-Stokes (N-S) equations is used to describe the turbulence for solution. Depending on the scale of the flow, the method using direct numerical simulation (DNS), Reynolds-averaged Navier-Stokes equations (RANS) and larger eddy simulation (LES) are presented for numerical solution of the Navier-Stokes equations for turbulent flow, described in Fig. 3.29.

Through DNS analysis, the accurate solution and information about turbulent flow can be obtained, and it is an effective method to investigate the mechanism of turbulence. The Navier-Stokes equations are numerically solved without any turbulence model in this analysis. That is, the whole range of spatial and temporal scales of the turbulence is all resolved. However, due to the significantly different mixing-length scales involved in turbulent flow, the stable and accurate solution of this requires such a fine mesh resolution that the computational time becomes significantly infeasible for DNS analysis [53]-[55]. Attempts to make a solution of turbulent flow using a laminar solver typically result in a time-unsteady solution, which fails to converge appropriately. To solve this problem, the RANS method, supplemented with turbulence models, is used for modelling the turbulent flows. This method is used in the previous FSI analysis for describing the fluid flow around the soft robotic fish. The time-averaged equations of motion are solved for fluid flow. The additional modelling is required to close the RANS equation for solving and many different turbulence models are created. Although it can calculate the complex flow with high Reynolds numbers, the average solution cannot describe the turbulence of fluid flow on details such as pressure fluctuations, which cannot be obtained from a RANS analysis [47]. The vortex is not observed in the motion of the soft robotic fish based on previous FSI analysis using RANS method.

LES is an approach which solves for large-scale motions explicitly while the small-scale motions are represented approximately by a model. Turbulent flows contain a wide range of length and time scales, with large scale motions being generally more energetic than the small scale ones. The prediction of industrially important fluctuating flow problems can be performed using the technique of LES [55]. This approach can also be used to solve the equations in RANS method numerically [47]. Although it is

computationally more expensive in time than RANS method, it produces more and better results about flow field solution and larger-scale vortex structure. Besides, compared with the DNS method, the computational cost is also largely reduced [54]. As a conclusion, the LES method can resolve large scales of the flow field solution allowing better fidelity than alternative RANS methods. It also models the smallest scales of the solution, rather than resolving them as DNS method, and has a relatively reduced computational cost compared with DNS method. The LES method will be adopted to make the FSI analysis of soft robotic fish in this part to investigate the fluid flow and vortices around the soft robotic fish. The model of the soft robotic fish described in Fig. 3.14 is also used as object in the simulation.

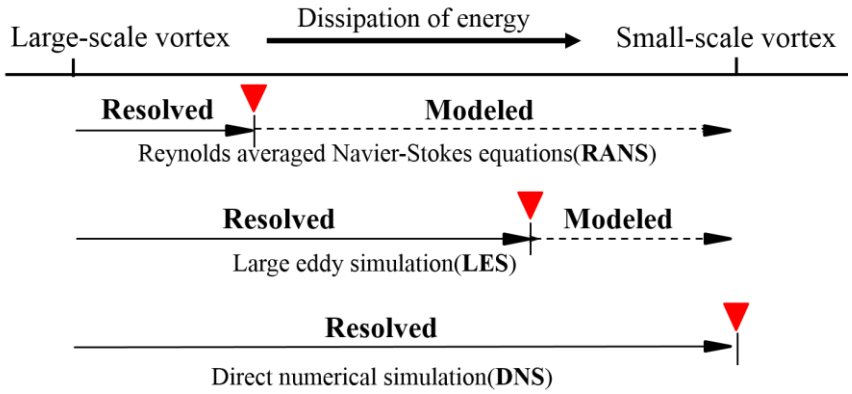

Fig. 3.29 Different simulation methods of turbulent flow in CFD.

In the FSI analysis, a cubical surface is also set as the computational boundary of the fluid field, whose size is 590 × 133 × 440mm. The soft robotic fish is also centred in the transverse and the vertical directions of the fluid domain and fixed support is applied on robot head described in Fig. 3.18. The Fluorinert Electronic Liquid FC-3283 is also used to describe the properties of the fluid given in Table 3.6. In the LES analysis, the fine mesh is needed for solution, but it has higher cost in computational time than RANS method. In order to make the comparison and identify the existence of the vortex in the wake of the old soft robot, the same modelling, mesh method and number of grids described in Section 3.5.2 of this Chapter are also adopted for this FSI analysis using LES method. For whole computational domain, the hexahedral element type is also adopted

to mesh the interface between robot and fluid. The boundary conditions of the fluid domain are defined as shown in Fig. 3.20. In the fluid domain, the standard atmosphere and 25℃ room temperature are also presented as the reference values. The buoyancy and heat transfer are also not considered.

Based on FSI analysis of soft robotic fish using LES method, the vortices generate with the motion of the soft robotic fish at the frequency of 10Hz. The simulation results about vortex distribution in the wake around the soft robotic fish at 10Hz are described in Fig. 3.30. The pressure gradient as contour lines at the tail part when the soft robot makes the motion from maximum deformation to minimum deformation in half cycle is described. The pressure gradient plays the key role on vortex distribution in the wake of soft robot. Due to obvious variation of adverse pressure gradient near the boundary layers, the fluid flow is separated and generates different fluid pattern [56], [57]. When the adverse pressure gradient is increasing, the separation of the fluid flow is strong and it is possible that vortex distribution is enlarged in the wake.

From the Fig. 3.30, it can be known that the pressure gradient with non-zero value occurs around soft robot, obviously observed at the place near tail end of the soft robotic fish. The body posterior to the tail end produces relatively large pressure gradient in the wake structure. Due to obvious variation of adverse pressure gradient near the tail end, the separation of fluid flow is stronger at this place and vortex is possible to be obtained in the wake of soft robotic fish. The single row of vortices may mainly generate near the tail end. At the maximum deformation of soft robotic fish, the obvious pressure gradient occurs at the lower side and described as A in Fig. 3.30(a). The large pressure gradient causes the fluid flow is instable and separated easily near the boundary layers. Due to the larger adverse pressure gradient at the lower side, the separation of fluid flow is relatively stronger at this place. It is possibility that the vortex distribution can be obtained at this lower side. When the robot makes the motion from maximum deformation to minimum deformation, the pressure gradient at the lower side is obviously decreased and it reduces to small scale gradually described as B and C in Fig. 3.30(b) and (c). In this stage, the pressure gradient is reduced to relatively small scales, but maximum pres-

sure gradient still generates near the tail end. The large variation of pressure gradient may cause the vortices generates near the tail end in the wake. At the minimum deformation of soft robotic fish, the pressure gradient is largely increased and maximum pressure gradient described as D in Fig. 3.30(d) generates at the upper side near the tail end of the soft robotic fish. It is possibility that the vortex can be obtained at the upper side near tail end. Thus, due to pressure gradient distribution in the propulsion motion of soft robotic fish, the vortex is possible to be obtained near the tail end in the wake.

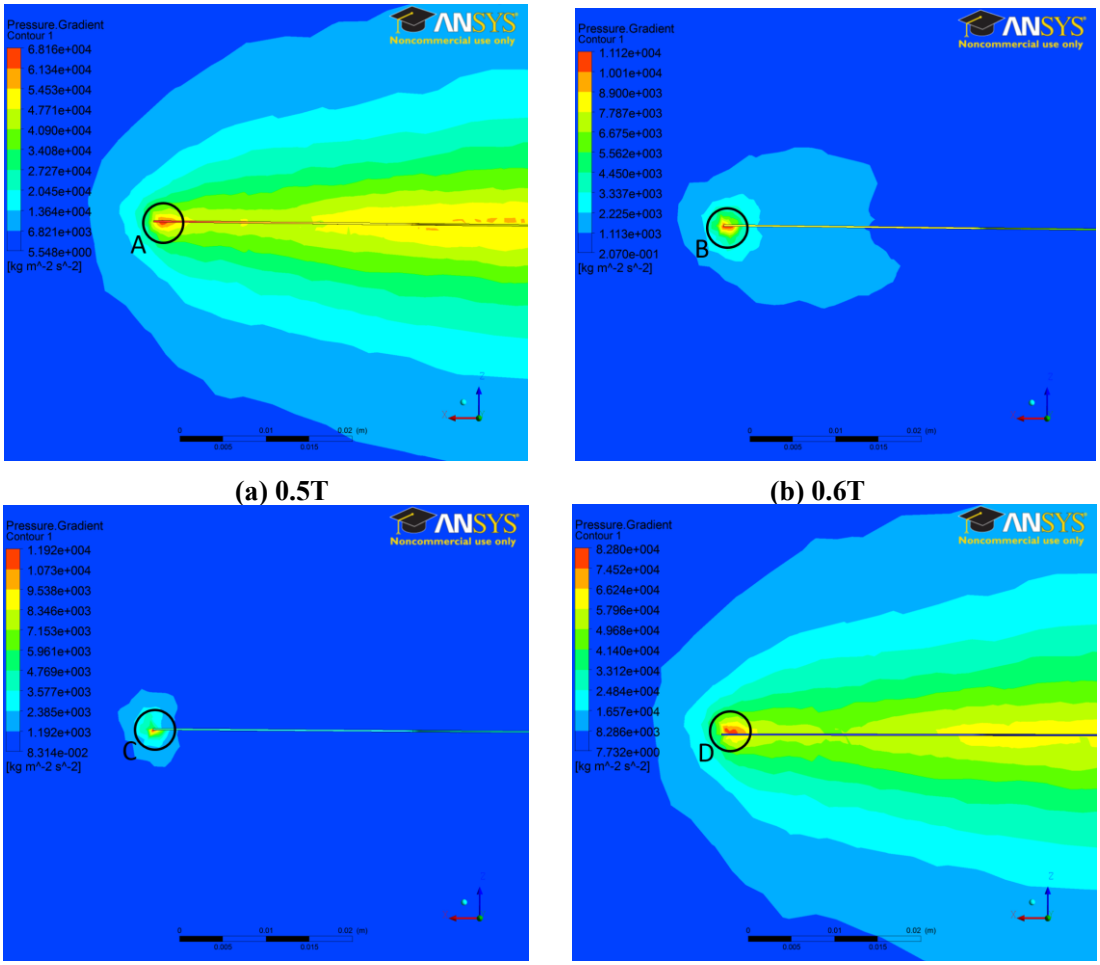

(a) 0.5T **(b) 0.6T**

(c) 0.8T **(d) 1T**

Fig. 3.30 Pressure gradient contours at horizontal mid-plane (*x*-*z* mid-plane) at 10Hz.

In this motion process, obvious pressure gradient occurs near the tail end. The pressure and propulsion force variation of soft robotic fish near the tail end in one cycle are presented in Fig. 3.31, where the point on robot surface near the tail end at which obvi-

ous pressure gradient occurs is adopted for description of pressure variation. From this figure, it can be found the similar trend of variation happens between the curves of pressure and propulsive force of soft robot.

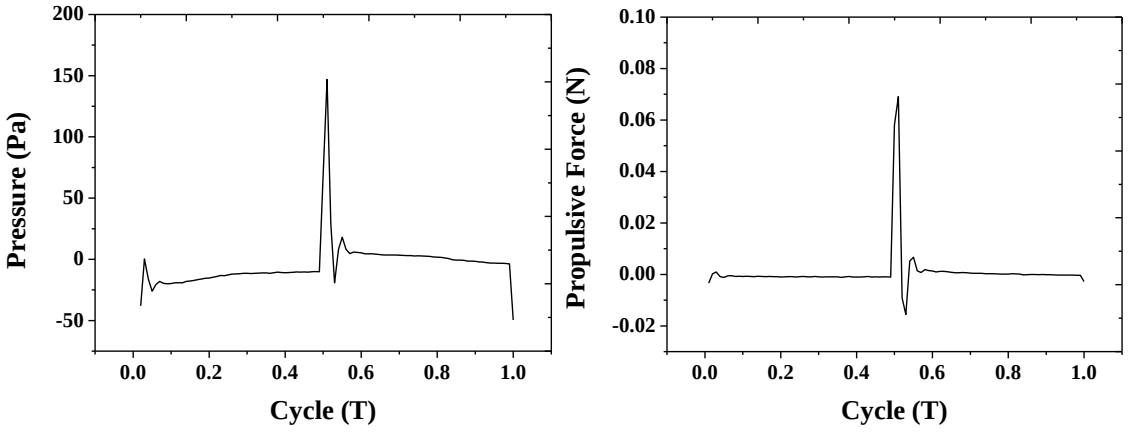

(a) Pressure of point near the tail end **(b) propulsive force of robot**

Fig. 3.31 Pressure and propulsive force variation of soft robotic fish in one cycle at 10Hz.

The corresponding fluid streamlines near the tail end of the soft robotic fish at 10Hz are presented in Fig. 3.32. The streamline near the tail end when the soft robot makes the motion from maximum deformation to minimum deformation in half cycle at 10Hz are described. Based on streamline distribution in the wake of soft robotic fish, the vortex generation can be identified and represented. From this figure, it is confirmed that vortex generates obviously near the tail end of soft robotic fish in the propulsion based on FSI analysis.

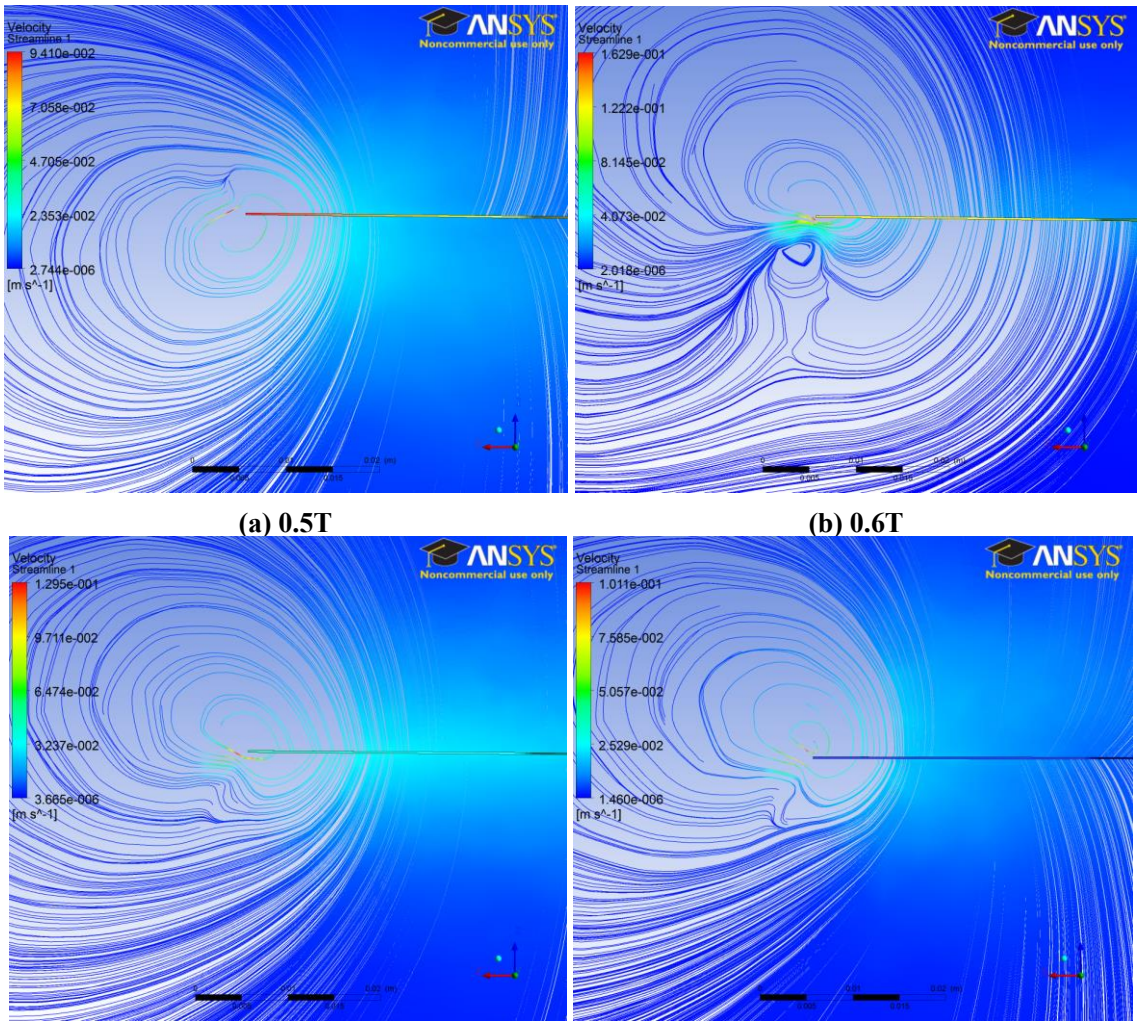

(a) 0.5T **(b) 0.6T**

(c) 0.8T **(d) 1T**

Fig. 3.32 Fluid streamline near tail end at horizontal mid-plane (*x*-*z* mid-plane) at 10Hz.

Compared with corresponding pressure gradient contours described in Fig. 3.30, the vortex is obtained at the place where obvious adverse pressure gradient occurs. It also can be found that if fluid velocity is relatively larger, the smaller pressure gradient generates. The vortex structures and scales are varied as the motion amplitude varies. The transmission, transformation and dissipation of energy on vortex happen in the interaction between soft robotic fish and surrounding fluid through the FSI analysis. With the oscillating motion of soft robotic fish, the vortex generates near the tail end in its wake is identified and verified by the FSI analysis using LES method. Due to vortex generation, the smaller propulsive force of soft robotic fish in the propulsion occurs compared

with previous simulation. It is possible to retrieve the energy contained in vortex to enhance propulsive force or efficiency of the soft robotic fish for improvement.

As a conclusion, based on distribution of pressure gradient and fluid streamline around the soft robotic fish, it can be found that vortex generates near the tail end in the wake at 10Hz based on FSI analysis using LES method. Compared with previous FSI analysis described in Section 3.5.2, this method is better for identifying the vortex distribution of the soft robotic fish. It provides the basic flow conditions for further performance improvement of soft robotic fish in robot design.

3.6 Motion Control Analysis of Soft Robotic Fish

Until now, the mentioned swimming motion of the soft robotic fish is only confined to the straight ahead motion of the soft robot in the research. Therefore, in order to make the soft robot realize not only motion of turning left but also motion of turning right, the motion control analysis of the soft robotic fish is investigated for achievement of turning motion of soft robot by the established coupling analysis using structure-acoustic coupling method.

By controlling the amplitude of input voltage signals of the soft actuators, the soft robotic fish can implement the straight ahead and turning motion in the fluid. In this part, the soft robotic fish with input voltage of 3Hz in sine and square waveform is taken as an example in the numerical simulation for description of straight ahead motion and turning motion of the soft robotic fish. The input voltage is in the range of -500V～+1500V.

In the present research, the soft robotic fish is composed of two soft actuators. When the input voltage signals on both left and right MFC actuators have the same voltage amplitude and are distributed in the opposite directions from each other, the straight ahead motion can be realized on the soft robotic fish. Figure 3.33 describes the input voltage of 3Hz in sine and square waveform on both left and right MFC actuators for

straight ahead motion of the soft robotic fish. The input voltage on both actuators is all in the range of -500V～+1500V, but they are applied on the soft robotic fish in the opposite directions.

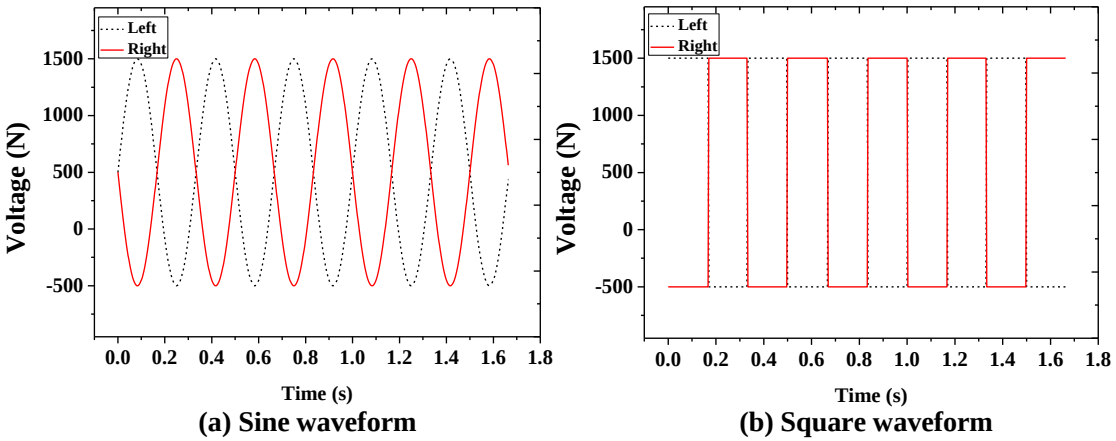

Fig. 3.33 Input voltage on both MFC actuators for straight ahead motion at 3Hz.

Based on these input voltage signals on both MFC actuators, the straight ahead motion of the soft robotic fish is generated and the corresponding propulsion mode of the soft robotic fish in the straight ahead motion in one cycle at 3Hz is presented in Fig. 3.34.

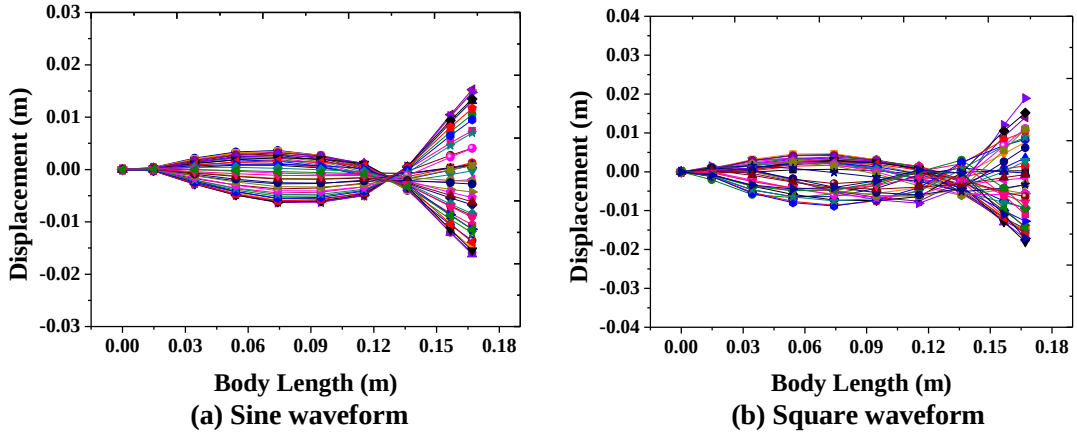

Fig. 3.34 Propulsion mode of straight ahead motion of soft robotic fish at 3Hz.

In Fig. 3.34, the positive displacement describes the displacement on the left side of swing for the soft robot. Otherwise, it describes the right-side displacement of swing. From the Fig. 3.34, it can be known that the swing of the caudal fin in the propulsion of

straight ahead motion is in symmetrical distribution around the midline of the soft robotic fish (centreline of thickness of robotic fish) in both sine and square waveform. The displacement on the left side and right side of swing for the tail part is symmetrical. Through characterizing this propulsion mode, the straight ahead motion of the soft robotic fish is realized. Besides, through comparing the results from sine and square waveform, although the displacement track based on square waveform is not as smooth as the track from sine waveform, the displacement at tail end based on square waveform is larger than that from sine waveform. This is because sine wave is representation of a single frequency, while the square wave not only considers fundamental frequency component but also contains harmonics of fundamental frequency. It is possibility that the soft robotic fish has the faster swimming velocity for propulsion based square waveform than that using the sine waveform.

In order to realize the turning motion of the soft robotic fish, the asymmetric signals are applied on the soft robotic fish based on the conditions of the straight ahead motion of the soft robotic fish. If the input voltage signals on both left and right actuators are asymmetric, the turning motion of the soft robotic fish is realized due to the asymmetrical output from these MFC actuators. Furthermore, based on the controllability of input voltage signals on MFC actuators, when the input voltage on left MFC actuator is larger than that on right MFC actuator, the motion of turning right is obtained on the soft robotic fish. On the contrary, the motion of turning left is realized.

To obtain the motion of turning right of the soft robotic fish, the input voltage signals on both MFC actuators are presented in Fig. 3.35, where the voltage of 3Hz in sine and square waveform is also adopted for description. The input voltage on left MFC actuator is in the range of -500V～+1500V, larger than the voltage on right MFC actuator which is in the range of -500V～+500V. The distributions of the input voltage on both MFC actuators are also in the opposite directions.

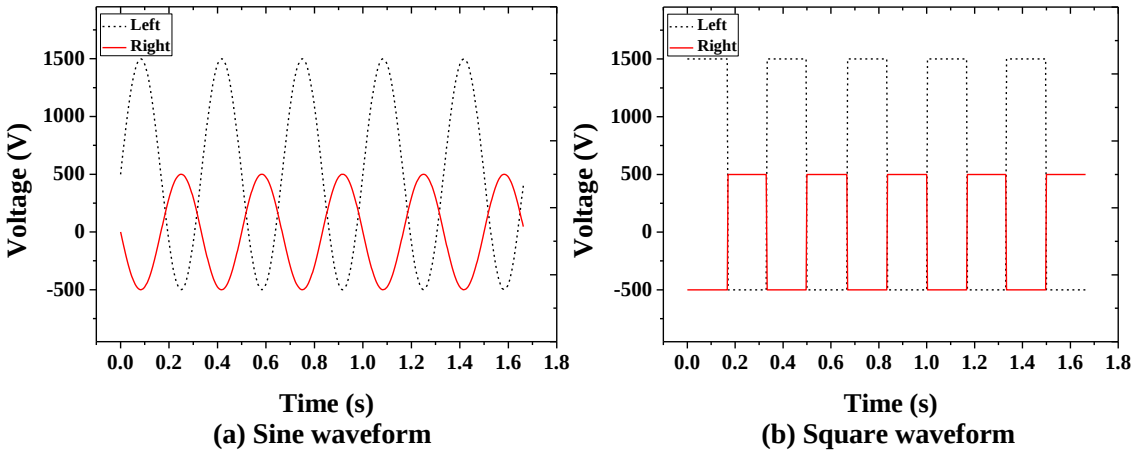

Fig. 3.35 Input voltage on both MFC actuators for motion of turning right at 3Hz.

Through this asymmetrical distribution of input voltage on both actuators, the motion of turning right of the soft robotic fish is achieved and the corresponding propulsion mode of the soft robotic fish in the motion of turning right in one cycle at 3Hz is presented in Fig. 3.36. From the Fig. 3.36, it can be known that the swing of caudal fin in the propulsion of turning right motion is in asymmetrical distribution around the midline of soft robotic fish in both sine and square waveform compared with the results of the straight ahead motion of the soft robotic fish described in Fig. 3.34. In Fig. 3.36, the positive displacement also describes the displacement on the left side of swing for the soft robot, otherwise it describes the displacement on the right side of swing. Thus, the displacement on the right side of swing is larger than that on the left side for the caudal fin part. The swing of caudal fin for the soft robotic fish mainly occurs on the right side. Due to this asymmetrical propulsion mode of the swing on the left and right side for the tail part of soft robot, caused by asymmetrical input voltage signals on both actuators, the motion of turning right of the soft robotic fish generates. Besides, due to the sine wave only considering the fundamental frequency, the displacement at tail end by using sine waveform is smaller than that from the square waveform. By using the square waveform in the propulsion for actuation, it is possible to obtain the larger turning velocity than that from sine waveform.

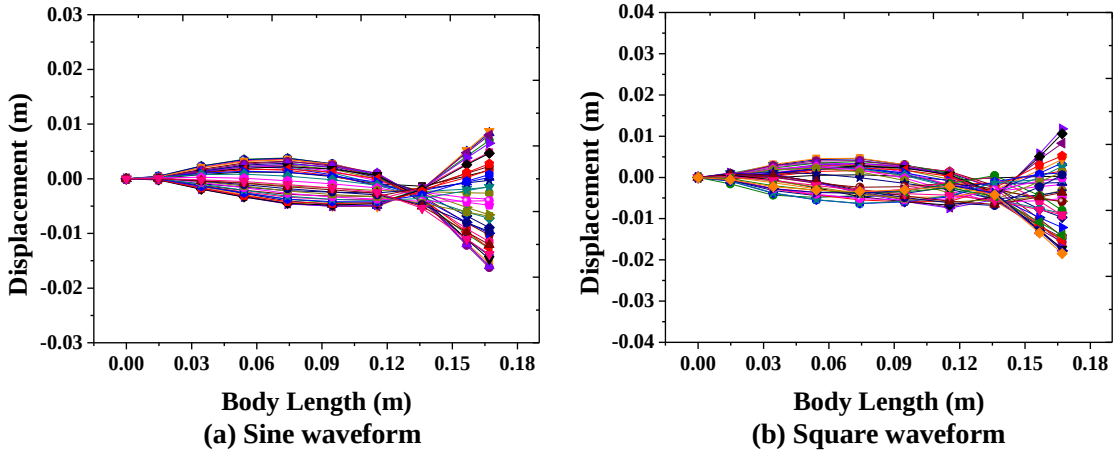

Fig. 3.36 Propulsion mode of the motion of turning right of soft robotic fish at 3Hz.

For the motion of turning left of the soft robotic fish, the applied approach of the input voltage signals on both MFC actuators is contrary to that of motion of turning right. When the input voltage on left MFC actuator is smaller than that on right MFC actuator, the motion of turning left is obtained on the soft robotic fish. The input voltage signals on both MFC actuators are presented in Fig. 3.37, where the voltage of 3Hz in sine and square waveform is also adopted. The input voltage on left MFC actuator is in the range of -500V～+500V, and the voltage on right MFC actuator which is in the range of -500V～+1500V. The input voltage on left MFC actuator is smaller than that on right MFC actuator and the input voltage on both actuators are also distributed in the opposite directions. Based on the asymmetrical input voltage signals on both actuators, the motion of turning left of the soft robotic fish is achieved and the corresponding propulsion mode of the soft robotic fish in the motion of turning left in one cycle at 3Hz is presented in Fig. 3.38. The displacement on the left side of swing is larger than that on the right side for the caudal fin of the soft robotic fish in both sine and square waveform. The asymmetrical propulsion mode of swing of the caudal fin generates on the soft robotic fish. Due to this asymmetrical propulsion mode of swing on the tail part of soft robot, the motion of turning left is realized on the soft robotic fish. Besides, due to representation of only fundamental frequency in sine wave, it can also be found that the displacement at tail end by using sine waveform is smaller compared with than that

from square waveform. The larger turning velocity of the soft robotic fish can be obtained by using square waveform for robot actuation.

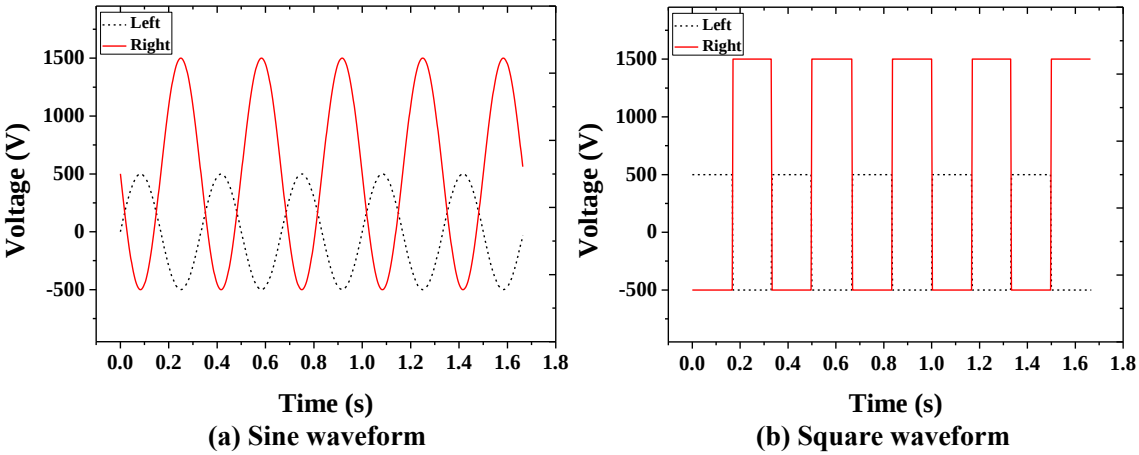

Fig. 3.37 Input voltage on both MFC actuators for motion of turning left at 3Hz.

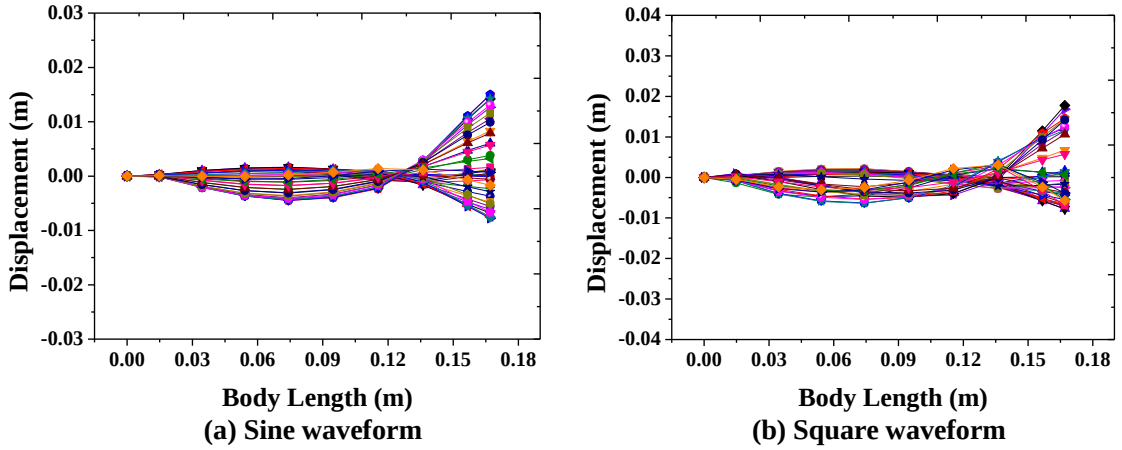

Fig. 3.38 Propulsion mode of the motion of turning left of soft robotic fish at 3Hz.

In the swimming of the soft robotic fish, the input signals on soft robotic fish can be designed and controlled to realize the desired the swimming motions. Based on the controllability of the input signals on soft robotic fish, the different swimming motions such as forward and turning motion are realized on the soft robotic fish. In the present research, in order to realize the turning motion of the soft robotic fish, the motion control of the soft robotic fish is analysed. If the input voltage on both actuators has same voltage amplitude and applied in the opposite directions from each other, the straight ahead motion is obtained and the swing for the tail part of soft robot in its propulsion is in

symmetrical distribution around the midline of the soft robotic fish. The displacement on the left side and right side of the swing for the tail part is symmetrical. By characterizing this propulsion mode of the soft robotic fish, the straight ahead motion of the soft robotic fish is identified and established. By controlling the input voltage on both actuators to achieve that the voltage amplitude of the input signal on left actuator is larger than that on right actuator, the turning right motion of the soft robotic fish is realized in the swimming, and its swing of tail part in the propulsion mainly occurs on the right side for the soft robotic fish. Due to this asymmetrical swing of tail part on the left and right side in the propulsion mode, the motion of turning right of the soft robotic fish generates. When the input voltage amplitude on left actuator is smaller than that on right actuator, the motion of turning left generates on the soft robotic fish. The propulsion mode in the turning left motion is characterized that the swing of tail part is mainly focused on the left side of the midline; in contrary to that in the turning right motion. Therefore, the straight ahead, turning left and turning right motion can be identified and established through the characteristics of swing in the propulsion mode of the soft robotic fish.

In the motion control of the turning motion of the soft robotic fish, there is a special case that the input voltage signal is applied to only one MFC actuator, that is, the input voltage on one actuator is in the range of -500V～+1500V and the voltage on the other actuator is zero. Although the turning motion is realized in this special case, the turning speed of the soft robotic fish is lower compared with the input signal conditions described in Fig. 3. 35 and Fig. 3.37. The difference on voltage amplitude of the input signals between two actuators can be controlled freely for different requirements in practice.

3.7 Summary

In this chapter, the numerical analyses are described to predict the propulsion performance of the soft robotic fish using PFC for further optimization and improvement. Based on the established driving model of the soft robotic fish, the numerical analysis based on structure-acoustic coupling method and FSI method are performed to investigate the propulsion motion and propulsive force of the soft robotic fish. From the numerical simulation analysis of the soft robotic fish, the following important conclusions are obtained. They provide the basic foundation for further performance improvement of soft robotic fish.

Firstly, the effectiveness of the driving model of soft robotic fish using PFC as soft actuator is verified by comparing the experimental results on simple cantilever beam structure. The relationship between the input voltage and generated stress of the PFC is obtained.

Secondly, the deformation mode frequencies and mode shapes of the soft robotic fish in the fluid are predicted and determined by the modal analysis using structure-acoustic coupling method. By comparing these deformation motions at corresponding frequencies with those of the real fishes, the fish-like propulsion mode is identified to realize the corresponding propulsion motion of the soft robotic fish. Furthermore, through this coupling method, the amplitude of the bending propulsion motion of soft robotic fish is calculated based on the driving load.

Thirdly, the relationship of driving frequencies of input voltage with propulsive force and displacement of the propulsion motion for the case of fixing robot head of the soft robotic fish in the fluid are obtained through the FSI analysis. The displacement is decreasing with the increase of driving frequencies of the soft robotic fish in certain range.

Fourthly, vortices created by the motion of the soft robotic fish are identified by FSI analysis using LES method. Through the LES method, the vortices generate in the wake around the soft robotic fish at 10Hz. It can be used to identify the vortex distribution of

the soft robotic fish compared with the previous simulation method. It provides the basic flow conditions for further performance improvement of soft robotic fish.

Finally, the motion control of the soft robotic fish is investigated to obtain the turning motion of the soft robotic fish. Through controlling the voltage amplitude of input signals on both actuators, the motion of turning right of the soft robotic fish is realized in its swimming when the input voltage amplitude on left actuator is larger than that on right actuator, otherwise the motion of turning left generates on the soft robotic fish. The difference on voltage amplitude of the input signals between two actuators can be controlled freely for different requirements of the soft robotic fish in practice.

References for Chapter 3

[1] A. J. Schönecker, T. Daue, B. Brückner, C. Freytag, L. Hähne and T. Rödig, "Overview on macrofiber composite applications," Proc. Of the SPIE, Vol. 6170, pp. K1-K8, 2006.

[2] R. J. Werlink, R. G. Bryant and D. Manos, "Macro fiber piezocomposite actuator poling study," NASA Technical Reports Server (NTRS), Nonmetallic Materials, NASA/TM-2002-211434, pp. 1-22, 2002.

[3] W. Wilkie, J. High, P. Mirick, R. Fox, B. Little, R. Bryant, R. Hellbaum and A. Jalink, "Low-cost piezocomposite actuator for structural control applications," Proc. Of the SPIE's 7th International Symposium on Smart Structures and Materials, Newport Beach, California, March 5-9, 2000.

[4] H. T. Banks, R. C. Smith and Y. Wang, "Smart material structures: modeling estimation and control," John Wiley & Sons, Masson, Paris, 1996.

[5] N. W. Hagood and A. A. Bent, "Development of piezoelectric fiber composites for structure actuation," AIAA-1993-1717-CP, 199S3.

[6] A. K. Jha, "Vibration analysis and control of an inflatable toroidal satellite component using piezoelectric actuators and sensors," Doctoral Dissertation of Virginia Polytechnic Institute and State University, Blacksburg, Virginia, 2002.

[7] R. W. Moses, C. D. Weiseman, A. A. Bent and A. E. Pizzochero, "Evaluation of new actuators in a buffet loads environment," Proc. Of the SPIE 8th Annual International Symposium on Smart Structures and Materials, Newport Beach, CA, 2001.

[8] H. Manz and K. Schmidt, "On the application of smart materials in automotive structures," Volkswagen AG Vehicle Research, Paper Number Z00.519.2.20.20, 2000.

[9] Continuum Control Corp., "Electronic Tennis Racket Improves Performance," Reinforced Plastics, p. 4, 2000.

[10] D. Rotman, “Materials science getting active-new ceramics: smarter, tougher,” Technology Review, p. 25, 1999.

[11] A. A. Bent, “Active Fiber Composite Material Systems for Structural Control Applications,” Proc. Of the SPIE’s 6th International Symposium on Smart Structures and Materials, Newport Beach, CA, March 1-5, 1999.

[12] R. B. Williams, “Nonlinear mechanical and actuator characterization of piezoelectric fiber composites,” Doctoral Dissertation, Virginia Polytechnic Institute and State University, 2004.

[13] A. A. Bent, “Active fiber composites for structural actuation,” Doctoral Dissertation, Massachusetts Institute of Technology, 1997.

[14] A. A. Bent and N. W. Hagood, “Piezoelectric fiber composites with interdigitated electrodes,” Journal of Intelligent Material Systems and Structures, Vol. 8, No. 11, pp. 903-919, 1997.

[15] W. Keats Wilkie, et al, “Piezoelectric macro-fiber composite actuator and method for making same,” U.S. Patent Application Publication US 2003/0056351 A1, March 27, 2003.

[16] S. Yoshikawa, M. Farrell, D. Warkentin, R. Jacques, E. Saarmaa, “Monolithic piezoelectric actuators and vibration dampers with interdigitated electrodes,” Proc. Of the SPIE’s 6th International Symposium on Smart Structures and Materials, Newport Beach, CA, March 1-5, 1999.

[17] J. S. Bevan, “Piezoceramic actuator placement for acoustic control of panels,” Doctoral Dissertation, Old Dominion University, December 2001.

[18] M. S. Azzouz, C. Mei, J. Bevan and J. J. Ro, “Finite element modeling of MFC/AFC actuators and performance of MFC,” Journal of Intelligent Material Systems and Structures, Vol. 12, pp. 601-612, 2001.

[19] H. A. Sodano, G. Park and D. J. Inman, “The use of macro-fiber composites in structural vibration applications,” Mechanical Systems and Signal Processing, in press, 2003.

[20] E. Ruggiero, G. Park, D. J. Inman and J. Wright, “Multi-input, multi-output modal testing techniques for a gossamer structure,” Proc. Of the ASME IMECE Adaptive Structures Symposium, pp. 167-175, 2002.

[21] Http://www.smart-material.com/MFC-product-main.html. MFC Properties, accessed 2012.

[22] M. Li, W. Chen, L. Jia, “Drive characteristics and stiffness influence with piezoelectric fiber composite actuators on airfoil surface,” Acta Aeronautica Et Astronautica Sinic, Vol. 31, No. 2, pp. 418-425, 2010.

[23] G. Luan, et al, “Piezoelectric transducer and transducer array,” Beijing, the Press of Perking University, 2005.

[24] L. Jia and X. Yin, “Passive oscillations of two tandem flexible filaments in a flowing soap film,” Physical review letters, Vol. 100, No. 22, pp.1-4, 2008.

[25] W. Zhao, J. Shintake, A. Ming, M. Shimojo, “Structural design and dynamic analysis of robotic fish with piezoelectric fiber composite,” Proc. Of the 9th France-Japan & 7th Europe-Asia Congress on Mechatronics (MECATRONICS)/13th Int'l Workshop on Research and Education in Mechatronics (REM), Paris, France, pp.161-168, 2012.

[26] J. Shintake, A. Ming and M. Shimojo, “Development of flexible underwater robots with caudal fin propulsion,” Proc. Of the IEEE/RSJ International Conference on Intelligent Robots and Systems (IROS), pp. 940-945, 2010.

[27] Http://www.smart-material.com/MFC-product-main.html. MFC P1 Std. Sizes, accessed 2012.

[28] M. B. Xu, “Three method for analysis forces vibration of a fluid-filled cylindrical shell,” Applied Acoustics, Vol. 64, No. 7, pp. 731-752, 2003.

[29] S. G. Ai and L. P. Sun, “Fluid-structure coupled analysis of underwater cylindrical shells,” Journal of Marine Science and Application, Vol. 7, No. 2, pp. 77-81, 2008.

[30] S. H. Sung and D. J. Nefske, “A coupled structural acoustic finite element model for vehicle interior noise analysis,” Transaction of the ASME, Journal of Vibration, Acoustics, Vol. 106, No. 2, pp. 314-318, 1984.

[31] C. Howard, “Coupled structural-acoustic analysis using ANSYS,” Internal Report of the University of Adelaide, 2000.

[32] H. Djojodihardjo, “BEM-FEM acoustic-structure interaction for modeling and analysis of spacecraft structures subject to acoustic excitation,” Proc. Of the International Conference on Recent Advances in Space Technologies, pp. 165-170, 2007.

[33] Http://www.3m.com/fluids. Product Information of Fluorinert Electronic Liquid FC-3283, accessed 2012.

[34] I. Tanaka and M. Nagai, “Hydrodynamic of resistance and propulsion-learn from the fast swimming ability of aquatic animals,” Ship & Ocean Foundation, pp. 14-19, 1996.

[35] D. Xia, J. Liu, W. Cheng, and L. Han, “Numerical simulation of the hydrodynamics of fishlike robot swimming based on converged speed,” Journal of Mechanical Engineering, Vol. 46, No. 1, pp. 48-54, 2010.

[36] H. Liu and K. Kawachi, “A numerical study of undulatory swimming,” J. Comput. Phys., Vol. 155, No. 2, pp. 223-247, 1999.

[37] H. J. Bungartz and M. Schäfer, “Fluid-structure interaction: modelling, simulation, optimization,” Springer-Verlag, 2006.

[38] W. Dettmer and D. Peric, “A computational framework for fluid-structure interaction: finite element formulation and applications,” Computer Methods in Applied Mechanics and Engineering, Vol. 195, pp. 5754-5779, 2006.

[39] S. Gong, L. Ren, H. Liu, L. Li and Z. Zou, “Fluid-solid interaction of rotor blade in last stage of steam turbine,” Thermal Turbine, Vol. 36, No. 3, pp. 153-157, 2007.

[40] D. Tang, C. Yang, S. Kobayashi, and D. N. Ku, “Effect of a lipid pool on stress/strain distributions in stenotic arteries: 3-D fluid-structure interactions (FSI) models,” J. Biomech. Eng., Vol. 126, No. 3, pp. 363-370, 2004.

[41] D. Tang, C. Yang, S. Mondal, F. Liu, G. Canton, T. Hatsukami and C. Yuan, “A negative correlation between human carotid atherosclerotic plaque progression and plaque wall stress: in vivo MRI-based 2D/3D FSI models,” J. Biomech., Vol. 41, No. 4, pp. 727-736, 2008.

[42] J. Leach, V. Rayz, M. Mofrad and D. Saloner "An efficient two-stage approach for image-based FSI analysis of atherosclerotic arteries," Biomech. Model Mechanobiol, Vol. 9, No. 2, pp. 213-223, 2010.

[43] H. J. Bungartz, M. Mehl and M. Schäfer, "Fluid-structure interaction II: modelling, simulation, optimization," Springer-Verlag, 2010.

[44] H. Schmucker, F. Flemming and S. Coulson, "Two-way coupled fluid structure interaction simulation of a propeller turbine," The 25th IAHR Symposium on Hydraulic Machinery and Systems/ IOP Conf. Series: Earth and Environmental Science, Vol. 12, No.1, pp. 1-10, 2010.

[45] R. L. Campbell, "Fluid-structure interaction and inverse design simulations for flexible turbomachinery," Doctoral Dissertation of the Pennsylvania State University, 2010.

[46] M. Hsu and Y. Bazilevs, "Fluid-structure interaction modeling of wind turbines: simulating the full machine," Computational Mechanics, Vol. 50, No. 6, pp. 821-833, 2012.

[47] ANSYS Inc., ANSYS theory reference 12.1, ANSYS Inc., 2009.

[48] M. S. Triantafyllou, G. S. Triantafyllou and D. K. P. Yue, "Hydrodynamics of fish-like swimming," Annu. Rev. Fluid Mech., Vol. 32, pp. 33-53, 2000.

[49] G. V. Lauder and E. D. Tytell, "Hydrodynamics of undulatory propulsion," Fish Physiol, Vol. 23, pp. 425-468, 2006.

[50] I. Borazjani and F. Sotiropoulos, "Numerical investigation of the hydrodynamics of carangiform swimming in the transitional and inertial flow regimes," Journal of Experimental Biology, Vol. 211, pp. 1541-1558, 2008.

[51] M. Sfakiotakis, D. M. Lane and J. Bruce C. Davies, "Review of fish swimming modes for aquatic locomotion," Journal of Oceananic Engineering, Vol. 24, No. 2, pp. 237-252, 1999.

[52] M. S. Triantafyllou, A. H. Techet, Q. Zhu, D. N. Beal, F. S. Hover and D. K. P. Yue, "Vorticity control in fish-like propulsion and maneuvering," Integr. Comp. Biol., Vol. 42, pp. 1026-1031, 2002.

[53] X. Shi, “A survey of direct numerical simulation of turbulence,” Journal of Hydrodynamics, Vol. 7, No. 1, pp. 103-109, 1992.

[54] J. Kim, P. Moin and R. Moser, “Turbulence statistics in fully developed channel flow at low Reynolds number,” Journal of Fluid Mechanics, Vol. 177, pp. 133-166, 1987.

[55] G. Cui, C. Xu and Z. Zhang, “Progress in large eddy simulation of turbulent flows,” Acta Aerodynamic Sinica, Vol. 22, No. 2, pp. 121-129, 2004.

[56] C. V. Seal, C. R. Smith and D. Rockwell, “Dynamics of the vorticity distribution in endwall junctions,” J. AIAA, Vol. 33, No. 7, pp. 1273-1278.

[57] H. Zhang and Z. Lu, “Experimental investigation of vortex characteristics in swept wing/body junctions,” Experiments and Measurements in Fluid Mechanics, Vol. 14, No. 2, pp. 16-20, 2000.

Chapter 4. Experiment Validation of Soft Robotic Fish

In order to validate the simulation results of numerical coupling analysis of the soft robotic fish obtained in Chapter 3, the experiment implement and evaluation are developed in this chapter. The mode shapes, amplitude of propulsion motion, propulsive force for the case of fixing robot head and vortex distribution around the soft robotic fish are measured by using the actual robot prototype. The turning motion control of the soft robotic fish is also measured through the controllability of the input voltage signals on robot prototype. The present numerical simulation results are congruent with experimental results by comparisons between them. The effectiveness of the modelling method and numerical coupling analysis used in the present research is verified and it's useful to predict the propulsion characteristics of the soft robotic fish in the fluid for performance improvement by the numerical analysis. In the chapter, the experiment evaluation of modal and transient analysis considering the surrounding fluid is firstly described. Then, to support the FSI analysis of the soft robotic fish, the comparisons on propulsive force and displacement for the case of fixing robot head and vortex distribution around the soft robotic fish are carried out between the simulation and experiment for evaluation. Finally, the experiments for turning motion control of the soft robotic fish are presented for validation.

4.1 Prototype of Soft Robotic Fish

The prototype of the soft robotic fish for experiment evaluation is shown in Fig. 4.1 [1].

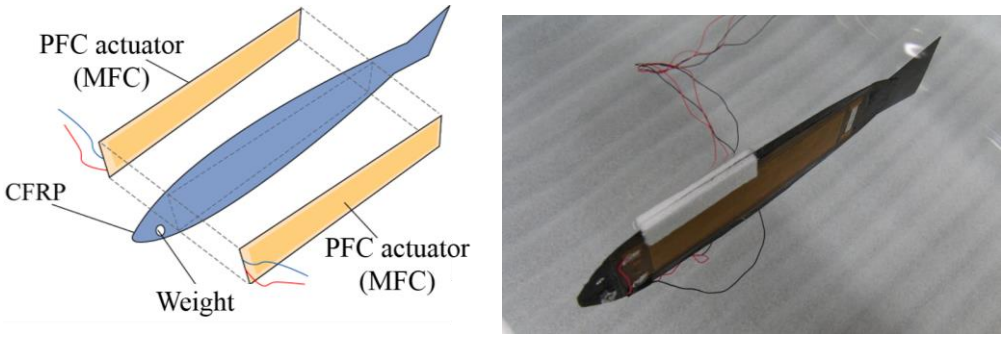

Fig. 4.1 Prototype of soft robotic fish.

Two MFC plates sandwich the CFRP plate as actuator structure to generate bending deformation for swimming motion. Weight made by steel is placed on the head to increase the displacement of the tail end. In order to make the prototype stable in the fluid, low density blowing agent is used as float and placed on the top part of prototype to balance its body weight and stabilize it. The MFC with M-8528-P1 type is adopted for soft robot. The detailed specifications of the prototype are shown in Table 4.1. The epoxy 3M-DP460 is used to make the MFC plate bonded on the CFRP plate. In the experiment, a cubical fluid tank described by the Fluorinert Electronic Liquid FC-3283 is used due to the high input voltage of the MFC.

Table 4.1 Specifications of Prototype

Item	Specification
Body Length (mm)	167
Maximum Height (mm)	55
Minimum Height (mm)	30
Body Thickness (mm)	CFRP-0.2
PFC Actuator	MFC 8528P1 ×2
Robot Weight (g)	15.98
Adhesive	Epoxy 3M-DP460

In the experiment platform of soft robotic fish, high-speed camera is adopted for prototype measurement. The Digital Camera EX-F1 made by Casio Company [2] is used in the experiment platform. The EX-F1 is Casio's most advanced high-speed camera. It is capable of shooting video up to 1200 frames per second (fps) for high-speed movies and

equipped with a powerful 12× zoom. The operating speed of high-speed continuous shutter can reach up to 60fps and the maximum speed of flash continuous shutter is 7fps (up to 20 images). The driving system of the prototype in the experiment is shown in Fig. 4.2. The main signal generation is controlled by the computer and basic signal waveforms such as sine, square and triangle are designed for application. The signal processing circuit uses a voltage follower between the high-voltage amplifier (AMP PA05039) and the computer to reduce output impedance. The high-voltage amplifier capable of delivering an output voltage of -500V to +1500V at an output current up to 50mA DC is adopted to drive the MFCs [3]. The high-voltage output is controlled through the amplifier input voltage of -2.5V to 7.5V DC or peak AC corresponds to -500V to +1500V output.

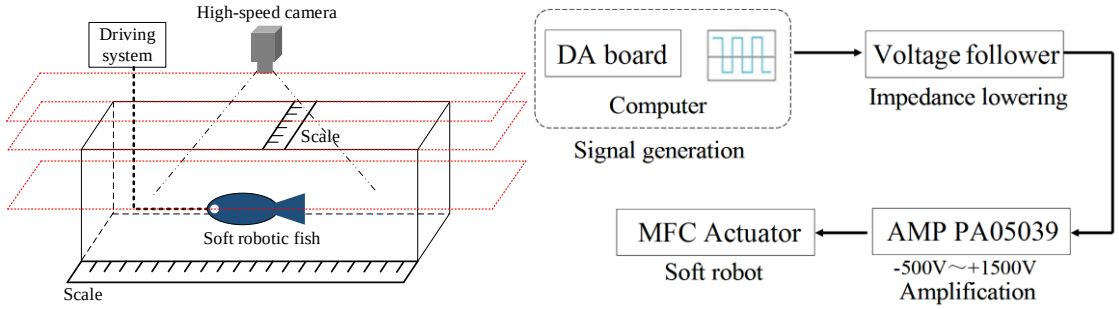

(a) Experiment platform **(b) Driving system**

Fig. 4.2 Driving system of robot prototype in the experiment.

4.2 Validation of Structure-Acoustic Coupling Analysis of Soft Robotic Fish

According to above prototype of the soft robotic fish, the experiment evaluation of structure-acoustic coupling analysis is described in this section. The bending deformation motion of the soft robotic fish is mainly considered in the research. Thus, the experiment evaluation of the bending propulsion modes described in Chapter 3 from modal analysis of soft robotic fish is developed by robot prototype. The bending mode

frequencies and mode shapes are firstly verified by comparing with the experimental results. Then, the amplitude of the main propulsion mode of the soft robotic fish is evaluated through prototype.

4.2.1 Swimming Mode of Soft Robotic Fish

In Chapter 3, the bending propulsion modes of the soft robotic fish in the fluid are predicted through the modal analysis using structure-acoustic coupling method. In order to support the modal analysis, the corresponding experiments about swimming mode frequencies and mode shapes are developed on prototype. In the experiment, the platform on measurement of swimming mode is described in Fig. 4.3(a). The high-speed camera (Casio Digital Camera EX-F1) placed on the top of fluid tank is adopted for observation and measurement. The input voltage in sine waveform on prototype is in the range of -500V～+1500V and the range of the driving frequency is 1Hz～25Hz. The experiment measurement is performed in the liquid tank whose size is 590 × 133 × 440mm.

The swimming mode frequencies of the prototype in the fluid are firstly presented in Table 4.2. The first bending mode frequency is 6Hz and second bending mode frequency is 25Hz. Compared with the simulation results, there is small difference between the simulation and experiment. The swimming bending mode frequencies of the soft robotic fish in the fluid are predicted successfully through the modal analysis using structure-acoustic coupling method.

Furthermore, at the corresponding mode frequencies, the swimming mode shapes of the prototype in the fluid are shown in Fig. 4.3. The circle marks the relatively obvious location bending deformation occurs.

Table 4.2 Swimming Mode Frequencies of Prototype in the Fluid

Item	Mode Frequewncies (Hz)	
	1^{st} Bending	2^{nd} Bending
Simulation	5.99	24.99
Experiment	6.0	25.0

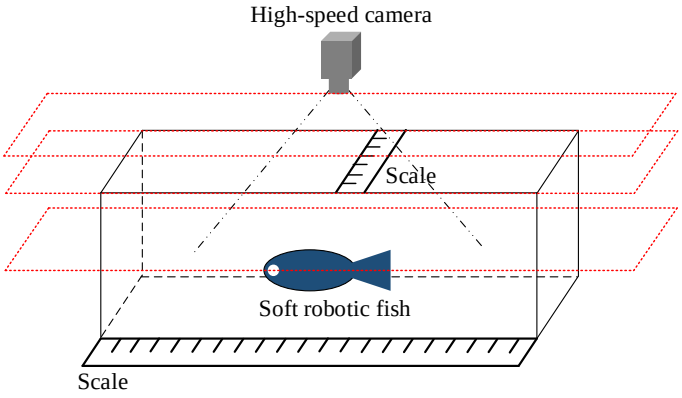

(a) Experimental platform on measurement of swimming mode

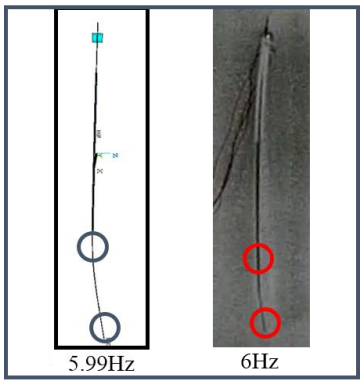

(b) First bending mode (6Hz)

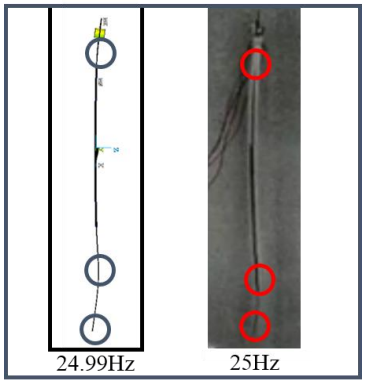

(c) Second bending mode (25Hz)

Fig. 4.3 Swimming modes of prototype in the fluid.

When the driving frequencies of the prototype are about 6Hz and 25Hz, the first and second bending modes occurs on robot prototype for propulsion, respectively. There are similar swimming modes at the corresponding mode frequencies happen between the simulation and experiment. At the first bending mode, the largest displacement of the prototype is obtained at the end of the caudal fin. This first bending mode is the main swimming mode of the prototype for its propulsion motion. At 25Hz, the second bending mode similar to S-shape occurs on prototype. The fish-like swimming modes are realized successfully on prototype. The calculated results on mode frequencies and mode shapes are congruent well with experiments on prototype. The swimming modes of the soft robotic fish in the fluid are predicted exactly by the modal analysis described

in Chapter 3. The modal analysis is verified feasible by comparing with the experimental results of prototype. It is suitable to identify the mode characteristics of the soft robotic fish in the fluid.

4.2.2 Amplitude of Soft Robotic Fish

In order to further evaluate the amplitude of the main bending propulsion motion of the soft robotic fish in the fluid, the amplitude of the prototype are measured. Above mentioned first bending mode of the prototype is the main swimming mode for its propulsion and focused in this part to make the verification. The input voltage on prototype is in the range of -500V～+1500V.

At the first bending mode, the maximum deformation of the prototype occurs at the end of the caudal fin. Thus, the displacement of the tail end is used to describe the amplitude of the prototype. To verify the simulation results from transient analysis of soft robotic fish using structure-acoustic coupling method described in Chapter 3, the corresponding driving frequency of 3Hz in sine waveform is also applied on prototype where the prototype has the good performance similar to those of real fishes to make the description. When the driving frequency is 3Hz, the experimental results on amplitude of the tail end in one cycle are presented in Fig. 4.4. The experimental platform and test point on prototype are shown in Fig. 4.4(a). The high-speed camera (Casio Digital Camera EX-F1) is adopted in the experiment. To determine the oscillating amplitude of the prototype by the scale which is located on the top of the fluid tank, the distance L_1 between the test point on prototype and camera and distance L_2 between the scale and camera are measured firstly. According to the ratio between L_1 and L_2, the real oscillating amplitude of the test point is calculated.

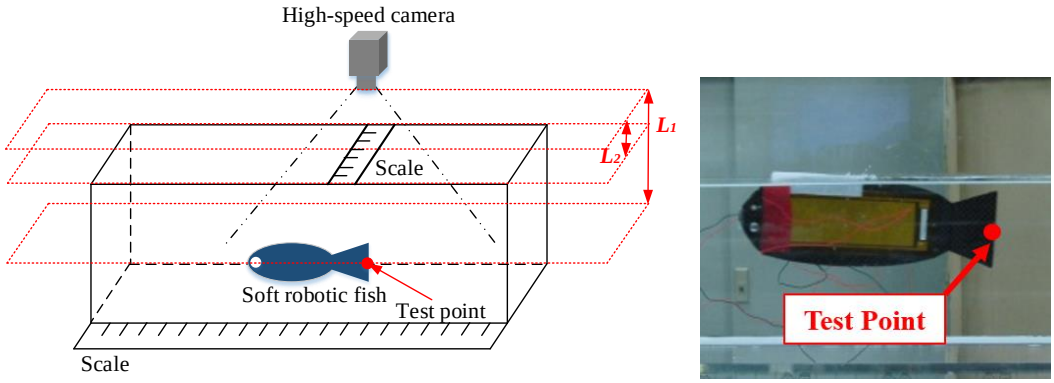

(a) Experimental platform and test point on tail end

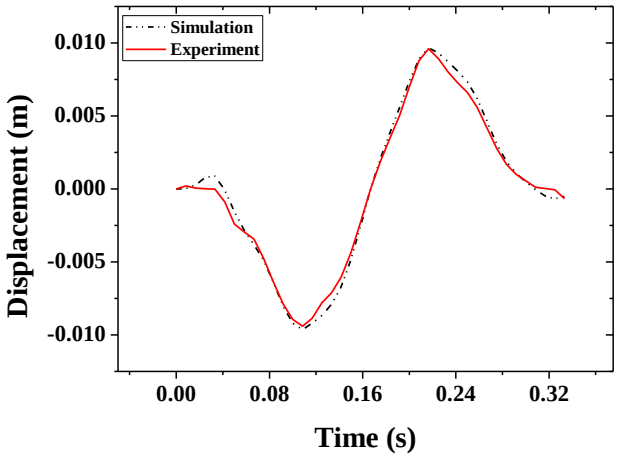

(b) Amplitude of test point

Fig. 4.4 Amplitude at the tail end of prototype.

There is very similar deformation curve occurs in simulation and experiment based on the driving load. The caudal fin of the prototype makes the motion similar to a sine wave. The maximum displacement at the tail end of prototype is about 19mm. Compared with the simulation results about 20mm obtained from Chapter 3, there is very small difference and it is about 5%. The simulation results are congruent well with the experimental results.The reason why there is small difference between simulation and experiment is mesh optimization performed in the numerical coupling analysis. The numerical results of displacement at the tail end of the soft robotic fish at 3Hz based on different number of mesh grids are shown in Table 4.3. After mesh optimization of the computational domain which is described in Fig. 3.14, the displacement of the tail end

is determined well by the numerical coupling analysis through comparing with the experimental results from prototype.

Table 4.3 Displacement at Tail End of Soft Robot at 3Hz in the Fluid by Different Grids Number

Item	No. of Nodes	No. of Elements	Displacement of tail end (m)
1	12,189	27,132	0.016
2	24,911	48,067	0.0166
3	37,915	72,738	0.0174
4	140.886	244,105	0.02

As a conclusion, the numerical simulation results based on structure-acoustic coupling method coincide with experimental results well. The coupling analysis using structure-acoustic coupling method is verified reasonable by comparing with the experiments on prototype, and fish-like swimming modes are obtained successfully on prototype. Also, the amplitude of the main swimming mode for soft robotic fish in the fluid is determined well through this coupling method based on the experimental results from prototype. The coupling analysis using structure-acoustic coupling method can be used to evaluate the vibration characteristics, fish-like swimming modes and amplitude of the propulsion motion of soft robotic fish in the fluid. It provides a way for further optimization and improvement on deformation response or propulsion approach in the design of soft fish robot.

4.3 Validation of FSI Analysis of Soft Robotic Fish

In order to further validate the effectiveness of the FSI analysis for predicting the propulsion characteristics of the soft robotic fish in the fluid, the comparison between the FSI simulation and experiment is carried out. According to the simulation results of the FSI analysis described in Chapter 3, the propulsive force of the soft robotic fish are

firstly evaluated by the experiment for the case of fixing robot head. Then, the verification of displacement of the soft robotic fish in the fluid are performed. The calculated results from FSI analysis on propulsive force and displacement are congruent with experiments for the case of fixing robot head of the soft robotic fish.

4.3.1 Propulsive force of Soft Robotic Fish

In the measurement of the propulsive force of the prototype, the range of input voltage in square waveform on prototype is -500V～+1500V and the range of driving frequency is 1Hz～25Hz. The measurement is also performed in the liquid tank whose size is 590 × 133 × 440mm.

The experimental platform on propulsive force of prototype is shown in Fig. 4.5. A force gauge (single-axis load cell) and a stick are adopted. The type of the load cell is WBJ-05N [4]. The rated capacity of load cell is 500mN. The load cell is fixed to the upper part of the stick which rotates with rotation axis and the lower part is contacted to the head of robot prototype. When the input voltage is applied on robot structure, the robot generates force for propulsion motion and the stick contacting the robot head rotates with the rotation axis. Through the rotation axis, the force for propulsion motion is transferred to the upper part of the stick. Based on the force F_s from the load cell fixed on the upper part of the stick, the prototype's propulsive force F_t can be calculated by $F_t = (l_1 F_s)/l_2$. Here the distance between the rotation axis and the upper part of the stick where the stick is fixed on the force gauge is expressed as l_1 and the distance of the rotation axis away from the lower part of the stick where the stick contacts the prototype is l_2. In the experiment, l_1 is 45mm and l_2 *is* 210mm. The propulsive force is the averaged value in the measured time.

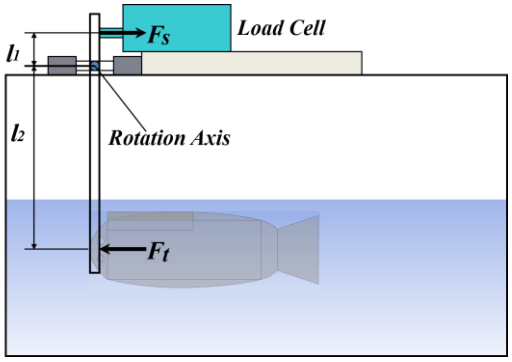

Fig. 4.5 Experimental platform of propulsive force for prototype.

According to this experimental platform, the results on propulsive force of the prototype at different driving frequencies are presented in Fig. 4.6. The maximum propulsive force of the prototype happens at 18Hz.

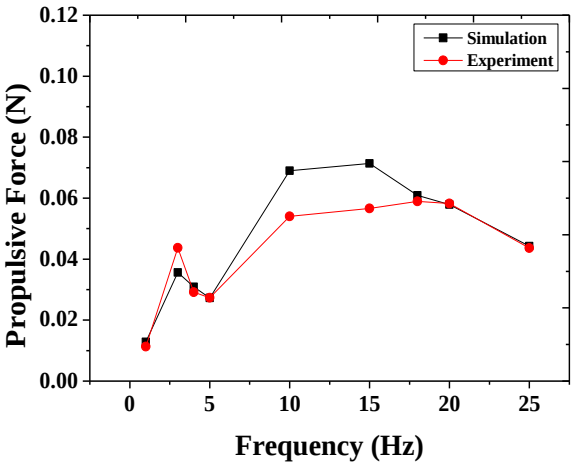

Fig. 4.6 Propulsive force of prototype in the experiment.

From this figure, it is known that there is no direct proportional relationship between the propulsive force and the driving frequency of the robot prototype. However, compared with the simulation results from FSI analysis, the similar variation of propulsive force happens in the experiment of prototype. Due to the fluid model and boundary conditions in the simulation, the force difference is relatively large in the frequency ranged from 10Hz to 18Hz. In the simulation, the numerical fluid model is modelled approximately to represent the physics of turbulent flow for FSI solution. Many parameters in the governing equations of the fluid model are determined by the experiences.

This approximate fluid model reduces the accuracy of simulation and cause the difference on fluid flow compared with the real conditions in practice. The real physics of the turbulent flow is not described accurately. The load acting on the robot structure caused by the fluid are all the approximate solution and this will cause the error between the simulated and measured results. Furthermore, in the numerical analysis, the uniform fluid model and boundary conditions are selected for avoiding the systematic errors. In this frequency range, the uniform model and boundary conditions causes the larger difference. Besides, compared with the real conditions in the experiment, the simplified model including the fluid and structure model and boundary conditions in the numerical analysis are another source of difference. The experimental measurement from fixed device and hand-made error in the manufacture of the prototype also make the effort for difference between the simulation and experiment. As a conclusion, the simulation results are close to the experimental results. The trends in variations in propulsive force of the soft robotic fish at different frequencies are determined and results similar to experiments are achieved successfully through the useful FSI analysis.

4.3.2 Displacement of Soft Robotic Fish

After establishing the propulsive force of the prototype in the given range, the corresponding measurement on displacement of the prototype at different driving frequencies are carried out. In the experiment, the fixed support is applied on the head of the prototype. The input voltage in square waveform on prototype is ranged from -500Vto +1500V and the range of driving frequency is 1Hz～25Hz. The experimental results are obtained by the high-speed camera (Casio Digital Camera EX-F1).

In the experiment, the similar bending deformation modes of the prototype are obtained at different driving frequencies. The results at 3Hz are adopted to present its bending deformation modes, shown in Fig. 4.7. The results in quarter of one cycle are adopted for description. The difference of displacement between the simulation and experiment at 3Hz are also described.

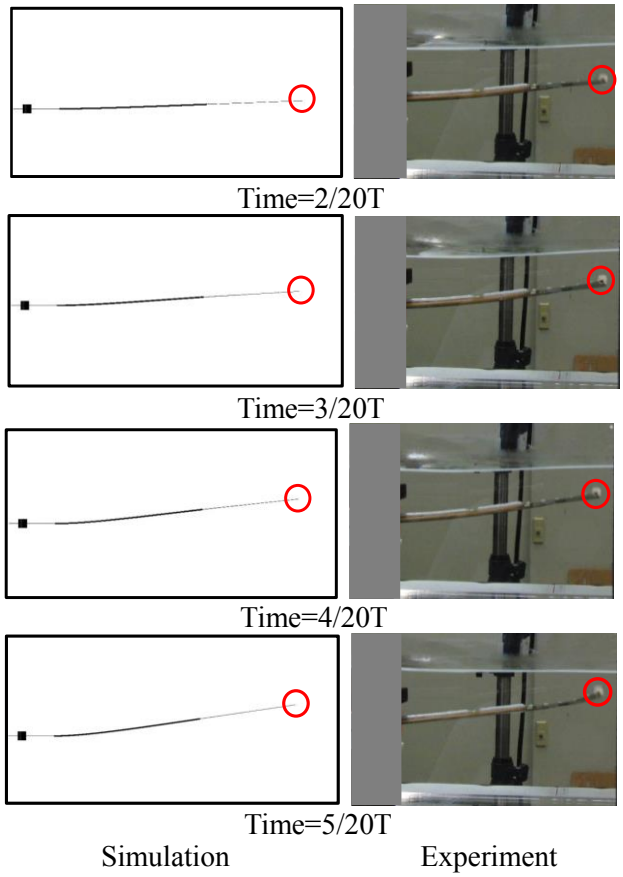

(a) Bending deformation modes

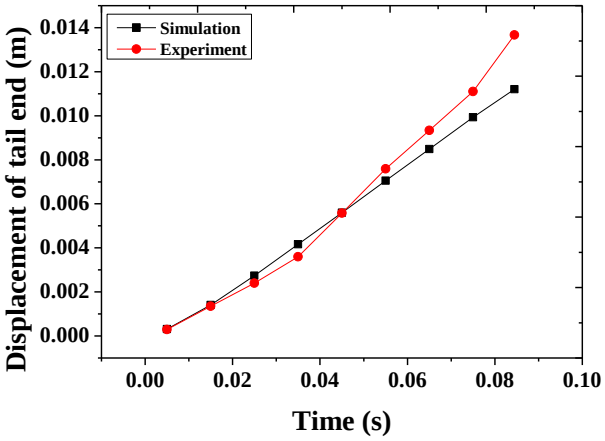

(b) Displacement at the tail end

Fig. 4.7 Deformation mode and displacement of prototype in the experiment at 3Hz.

As shown in Fig. 4.7, at different time values, the maximum displacement of the prototype is all obtained at the end of the caudal fin described in Fig. 4.7(a). The almost same bending deformation mode shapes occur at the corresponding time values in the

simulation and experiment. The corresponding displacement of the tail end is described in Fig. 4.7(b). At the frequency of 3Hz, the maximum displacement difference at the tail end is about 18% between them. The displacement of the soft robotic fish can be determined well through the FSI analysis by comparing simulation results with experimental results.

The experiment results on displacement at the caudal fin end of the prototype at different driving frequencies are presented in Fig. 4.8.

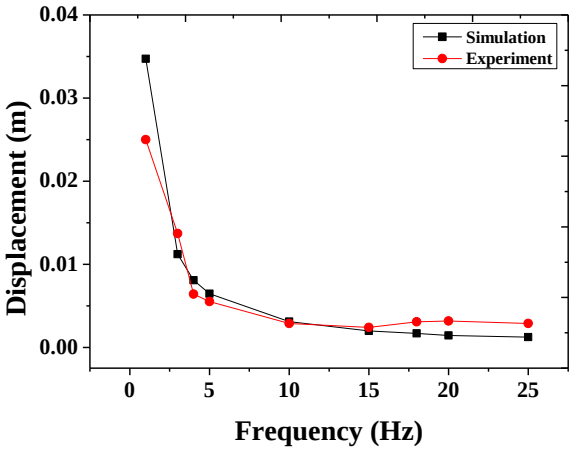

Fig. 4.8 Displacement at the caudal fin end of prototype.

From this figure, it can obtain the similar displacement curve in the simulation and experiment. The displacement of the tail end is decreasing with the increase of the driving frequency in certain range. The maximum displacement in the simulation and experiment are all obtained at 1Hz rather than the frequency where the maximum propulsive force generates. This is because the fluid absorbs the energy from the resonance and the resonance energy is not transferred completely to the robot structure. At 1Hz, the maximum deformation at the tail end is about 34mm in the simulation and 24.7mm in the experiment, and the maximum displacement difference about 39% happens. The minimum difference occurs at the frequency of 10Hz and it is about 5%. The simulation results on displacement of the tail end are close to those from the experiments of prototype. The effectiveness of the FSI analysis described in Chapter 3 is verified by

comparison with experiments. The FSI analysis can be used to predict the deformation characteristics of the soft robotic fish.

According to the experimental results from prototype, the relationships of driving frequencies with propulsive force and displacement of prototype are obtained. By comparing these results in the numerical FSI simulation and experiment, the FSI analysis meets the initial demands of design and control for soft robotic fish from the view of morphology. However, from the view of dynamics, the differences of propulsive force and displacement exist in the simulation and experiment. The model of soft robotic fish and boundary conditions play the key role to describe the hydrodynamic performance of the soft robotic fish accurately. Compared with the real conditions in experiment, the simplified model including the fluid and structure model and boundary conditions in the numerical analysis will cause the difference. Besides, to avoid the systematic errors, the selection of the uniform fluid model, wall function and mesh size of the computation domain make the difference in different trend at different frequencies. The accuracy of the numerical simulation is needed to be improved for accurate design. The float on robot prototype, hand-made error from manufacture and experimental measurement on prototype are another source of differences. These actors will be considered in the further optimization and improvement for accurate design. In a word, the simulation results from FSI analysis on propulsive force and displacement coincide with experimental results. The effectiveness of the FSI analysis is verified by the experiments on prototype. It is useful to predict the propulsion characteristics of the soft robotic fish in the fluid for improvement.

4.3.3 Vortex Distribution around Soft Robotic Fish

In order to further validate the feasibility of the FSI analysis on identification of vortex around the soft robotic fish in the propulsion presented in Chapter 3, the corresponding measurement on vortex distribution around the prototype at the driving frequency of 10Hz are carried out. In the experiment, the input voltage in square waveform on proto-

type is ranged from -500Vto +1500V. The high-speed camera (Casio Digital Camera EX-F1) is adopted to observe the vortex around the prototype.

In the swimming motion of prototype at the driving frequency of 10Hz, the fluid flow patterns around the robot can be observed by high-speed camera. With the tail motion of the prototype, the vortex generates in its wake around the robot and it is gradually developed to be larger scale until it disappears due to dissipation. Figure 4.9 describes the obvious vortex generating in the wake around the prototype.

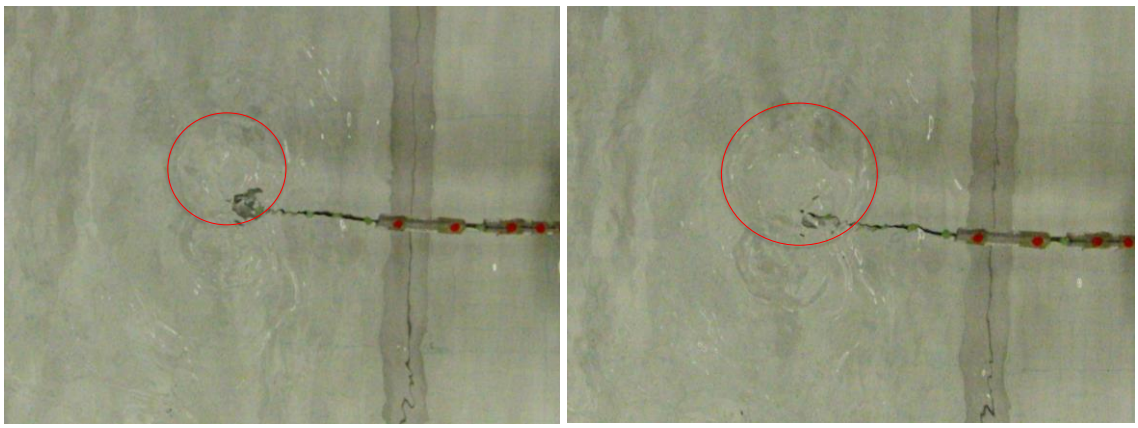

Fig. 4.9 Vortex around the prototype of soft robotic fish at 10Hz.

From this figure, it can be known that the obvious vortices are obtained in the wake around the prototype at 10Hz. They created by the robot motion are left near the tail of the prototype. Although the detailed vortex structure is not observed from its wake development in the experiment, the existence of vortex near the tail part in the wake at the frequency of 10Hz verifies the effectiveness of FSI analysis using LES method to a certain extent. The FSI analysis using LES method is suitable for identifying the vortex in the wake around the soft robotic fish. It provides the basic flow conditions for further performance improvement of soft robotic fish.

As a conclusion, for the case of fixing robot head of the prototype, the deformation mode, propulsive force and displacement of the soft robotic fish in the fluid at different driving frequencies are measured through the prototype. And the vortex distribution created by the robot motion is observed around the prototype. From these experimental

results, the simulation results from FSI analysis described in Chapter 3 are close to those of experiments. The feasibility of numerical FSI analysis are verified. It is useful to identify the hydrodynamic performance of the soft robotic fish in the fluid for further optimization and performance improvement.

4.4 Swimming Velocity of Soft Robotic Fish

In the experiment implement and evaluation of prototype, the measurement on swimming velocity of the prototype at different driving frequencies is developed. The input voltage signals on both actuators of prototype are all in the range of -500V～+1500V and distributed in the opposite directions, as shown in Fig. 3.33. Based on this symmetrical distribution of input voltage signals on both actuators, the straight ahead motion is achieved on robot prototype. Due to achievement of larger displacement and swimming velocity by using square waveform in robot actuation, the input voltage in square waveform is applied on prototype to describe the swimming velocity of straight ahead motion. The driving frequency of input voltage in the experiment is ranged from 1Hz to 25Hz. The prototype is also placed in the liquid tank whose size is 590 ×133×440mm for measurement.

The platform on measurement of the swimming velocity of the prototype is described in Fig. 4.10. The high-speed camera (Casio Digital Camera EX-F1) is used in the experiment. To determine the moving distance of the prototype on the scale which is located on the side of the fluid tank, the distance L_1 between the prototype and camera and distance L_2 between the scale and camera are measured firstly. According to the ratio between L_1 and L_2, the real moving distance of the prototype is calculated. In order to decrease the measurement error, the oblique motion of the prototype should be avoid as much as possible in the experiment.

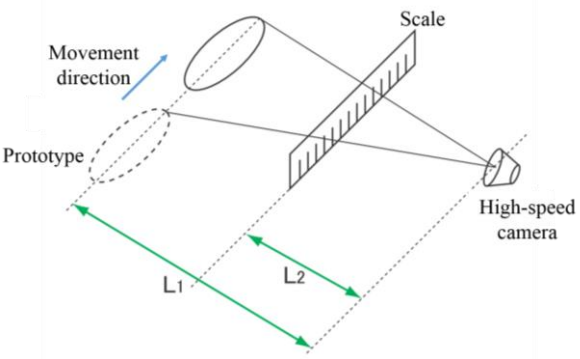

Fig. 4.10 Experimental platform on measurement of swimming velocity of prototype.

The results of swimming velocity of the prototype at different driving frequencies are presented in Fig. 4.11. At different driving frequencies, the swimming velocity of the prototype is different. The maximum swimming velocity of the robot prototype is 0.72m/s at 18Hz.

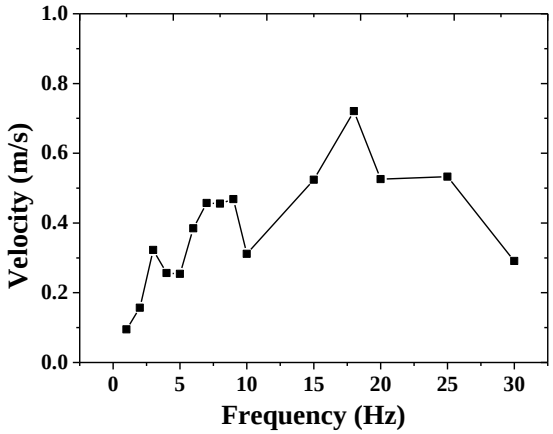

Fig. 4.11 Swimming velocity of prototype.

4.5 Validation of Motion Control of Soft Robotic Fish

To validate the motion control on turning motion of the soft robotic fish, the corresponding experiments are performed on robot prototype based on the input voltage signals proposed in section 3.6 of Chapter 3.

By applying input voltage signals with bias to actuators of the soft robotic fish, turning motion is realized in the experiments. Figure 4.12 describes the experimental

platform on measurement of the turning motion of robot prototype by high-speed camera (Casio Digital Camera EX-F1). The high-speed camera is placed on the top of fluid tank for measurement. Due to achievement of larger velocity by using square waveform in robot actuation, the input voltage in square waveform is also applied on prototype to describe the turning motion of the soft robotic fish. In the experiment, the input voltage of 18Hz in square waveform applied to the prototype is taken as an example to present the turning motion of the robot, where the maximum swimming speed of the soft robotic fish is obtained.

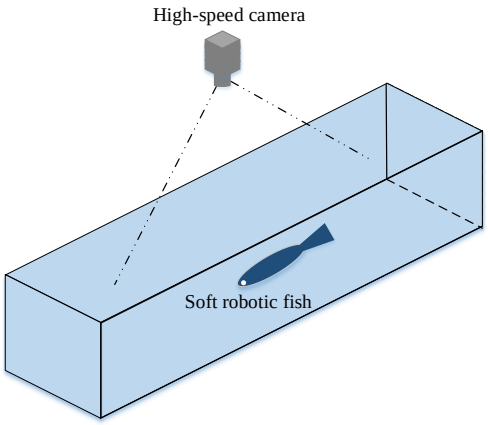

Fig. 4.12 Experimental platform on measurement of turning motion of prototype.

Based on the analysis on motion control of the soft robotic fish in Chapter 3, to obtain the motion of turning right, the input voltage signals with 18Hz on both MFC actuators in square waveform in Fig. 4.13 are adopted for description. The input voltage on left MFC actuator is in the range of -500V～+1500V and the voltage on right MFC actuator is in the range of -500V～+500V. The input voltages on both actuators are distributed in the opposite directions. Through this asymmetrical distribution of input voltage on both actuators, the motion of turning right of the soft robotic fish is achieved on robot prototype. Figure 4.14 describes the corresponding turning right motion of the soft robotic fish at different time values in one second at 18Hz. Based on asymmetric input voltage signals shown in Fig. 4.13, the swing of soft robotic fish mainly occurs on the right side for the soft robotic fish, and asymmetrical propulsion mode of the swing

on the left and right side for the soft robot generates (that is, the displacement on the right side of swing is larger than that on the left side for the tail part of the soft robot). By the asymmetrical propulsion mode, motion of turning right of the soft robotic fish is achieved successfully, and the maximum turning velocity is about 27deg/s. The motion control on turning right motion of the soft robotic fish is validated through controlling the input voltage signals on robot.

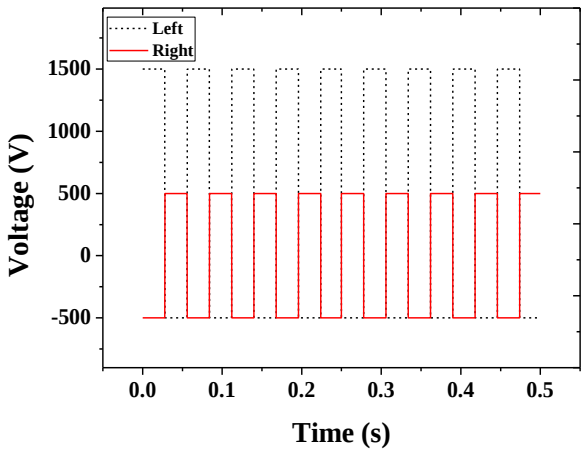

Fig. 4.13 Input voltage on both MFC actuators for motion of turning right at 18Hz.

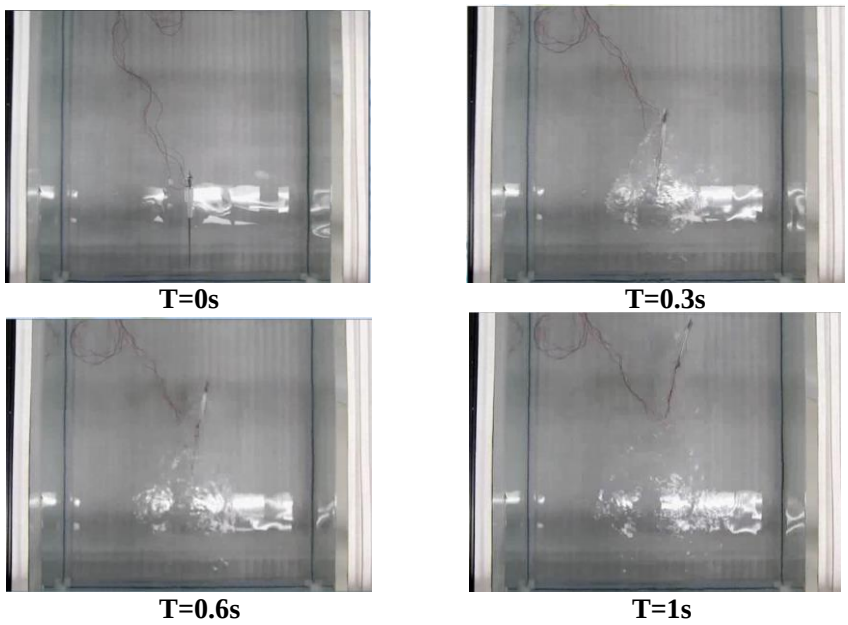

Fig. 4.14 Motion of turning right of prototype at 18Hz.

For the motion of turning left of prototype, the applied approach of the input voltage signals on both MFC actuators is contrary to that of motion of turning right. The input voltage signals with 18Hz in square waveform are also adopted and presented in Fig. 4.15. On left MFC actuator, the input voltage is in the range of -500V～+500V, and it is in the range of -500V～+1500V on right MFC actuator. The distributions of the input voltage on both actuators are also in the opposite directions.

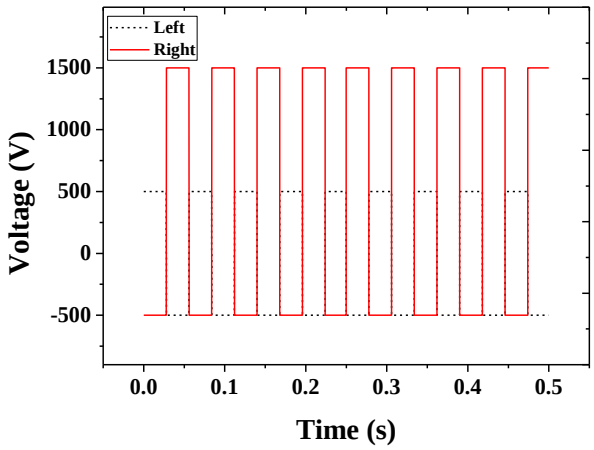

Fig. 4.15 Input voltage on both MFC actuators for motion of turning left at 18Hz.

Based on these asymmetrical input voltage signals, the motion of turning left is achieved and descried in Fig. 4.16.

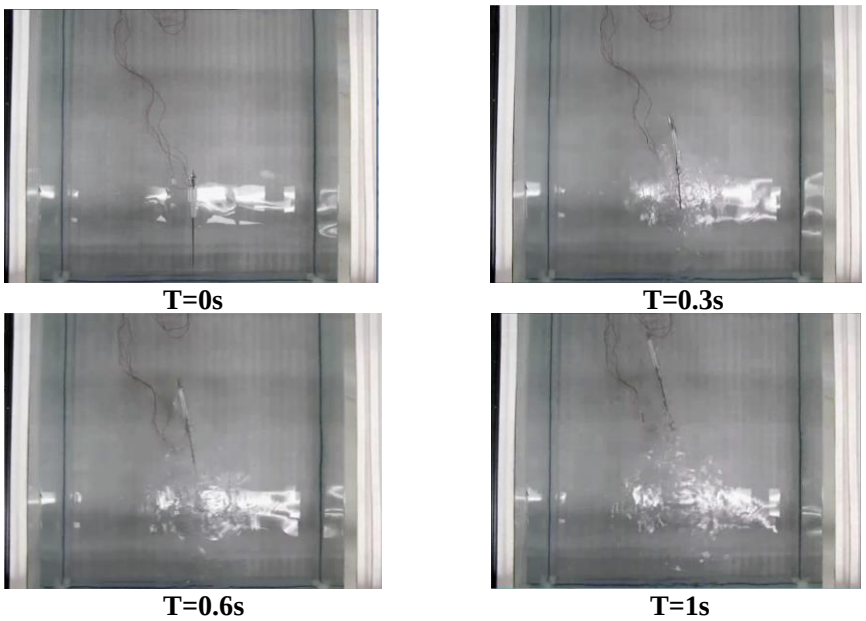

Fig. 4.16 Motion of turning left of prototype at 18Hz.

From this figure, it can be known that when the input voltage on left MFC actuator is smaller than that on right MFC actuator, the swing of the soft robotic fish is mainly focused on the left side of the midline of the robot, which is in contrary to the turning right motion of the soft robotic fish. Based on this asymmetrical input signals on robot prototype, the motion of turning left of the soft robotic fish is realized successfully and the maximum turning velocity is about 27deg/s. The input signal control on turning left motion of the soft robotic fish is validated through the experiments on prototype.

As a conclusion, the turning left and turning right motion of the robot prototype are realized by controlling the input voltage amplitude on actuators of the soft robotic fish. When the input voltage amplitude on left actuator is larger than that on right actuator and applied in the opposite directions, the turning right motion of the soft robotic fish is obtained. Otherwise, the motion of turning left generates on the soft robotic fish. If the input voltage on both actuators have same voltage amplitude and applied in the opposite directions from each other, the straight ahead motion is realized. The motion control on turning motion of the soft robotic fish described in Chapter 3 is validated successfully.

4.6 Summary

In order to validate the simulation results of numerical coupling analysis of the soft robotic fish in Chapter 3, the mode shapes, amplitude of propulsion motion, propulsive force of soft robot in the fluid for the case of fixing robot head and vortex distribution around the prototype are measured by using the actual robot prototype. The relationship of input signal with the propulsion mode and amplitude of the propulsion motion and propulsive force of the soft robotic fish for the case of fixing robot head are determined and established by prototype. Similar variation trend of propulsive force and displacement of the soft robotic fish can be obtained between the simulation and experiment. Besides, the vortex created by the robot motion generates in the wake around the robot prototype. Through controlling the input voltage amplitude on actuators of the robot

prototype, the motions of turning right and turning left are obtained successfully on soft robotic fish. The present numerical simulation results are congruent with experiments on prototype. The effectiveness of the modelling method and numerical coupling analysis used in the present research are verified and it is useful to predict the propulsion performance of the soft robotic fish in the fluid for performance improvement.

References for Chapter 4

[1] J. Shintake, A. Ming and M. Shimojo, “Development of flexible underwater robots with caudal fin propulsion,” Proc. Of the IEEE/RSJ International Conference on Intelligent Robots and Systems (IROS), pp. 940-945, 2010.

[2] Http://www.casio.com/products/archive/Digital_Cameras/High-Speed/EX-F1/. Exilim EX-F1.

[3] Http://www.smart-material.com/PiezoElectronics-product-main.html. High Voltage Power Amplifier, model PA05039.

[4] Http://www.showa-sokki.co.jp/Product_manual/WBJ_2011.pdf. WBJ-05N.

Chapter 5. Improvement by Design Optimization of Soft Robotic Fish

According to the experiment evaluation on actual robot prototype described in Chapter 4, the numerical simulation analysis performed in Chapter 3 is verified feasible and it can be used to identify and establish the fish-like propulsion motion of the soft robotic fish in the fluid effectively for performance improvement. Thus, to enhance the performance of the soft robotic fish, new biomimetic soft robot with high performance is developed based on effective modelling method and numerical analysis by optimization in this chapter. Firstly, the basic propulsion principle of soft robotic fish is introduced. Then, the structural parameters of the robot are allowed to vary within a range and the amplitude of the propulsion motion for the soft robot is calculated at different parameters by the numerical analysis. The structural parameters of the robot capable of propulsion motion with larger-amplitude are chosen for improvement. Based on this result, new soft robots are designed and evaluated by the experiments. From the experiment results of new soft robots, it is confirmed that the higher swimming speed, better fish-like swimming performance and larger turning velocity are realized. It can be said that the new soft robotic fish has been developed successfully for improvement.

5.1 Theoretical Background of Optimization of Soft Robotic Fish

Creatures that have a long and slender shape called cylindrical object or a thin and long ribbon shape called belt object move forward by making transformation waves generat-

ed by a meandering motion. The transformation is obtained by the bending moment generated from the muscles along the body axis of creatures. In cylindrical and belt objects of the creatures where the height, width or diameter is small compared with the body length, it is known that slender body theory holds. A transformation towards the rear of the body has little influence to the front end. The fluid force that works at a certain length is decided only by the cross-section shape and crossing velocity [1]. In the forward motion of the creatures, the transformation wave is travelled to the rear of the body.

Figure 5.1 shows the inertia force for the meandering motion of creatures in the case of constant vibration amplitude and increased vibration amplitude. In the case of constant vibration amplitude, due to the motion of creature body, the inertia force from the apparent increase in mass of the fluid cancels each other, described in Fig. 5.1(a). However, the inertial force becomes a propulsive force in the case of increased amplitude, described in Fig. 5.1(b). The net positive force can be obtained for locomotion direction when motion amplitude is increased toward the tail. Therefore, to achieve the propulsive force from inertial force of the fluid, the motion amplitude of the designed soft robot is needed to be increased toward the tail.

Slender body theory also approves for the fishes with slender body such as trout fishes, the subcaragiform type focused in the research [1]. These fishes make propulsion by caudal fin transformation together with body transformation. The propulsion motion is dominated by inertial force of fluid [1]. In their propulsion motion, the mode shapes is presented in Fig. 5.2. The amplitude of the undulation is limited anteriorly, and increases only in the posterior half of the fish body. To achieve the larger propulsive force for higher propulsive velocity of the soft robotic fish, the slender body theory as mathematical model is adopted to investigate the propulsive force of the soft robotic fish in the present research.

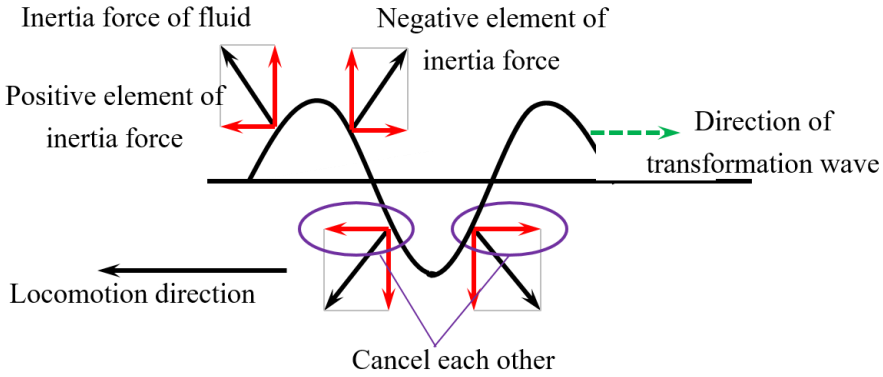

(a) Constant vibration amplitude

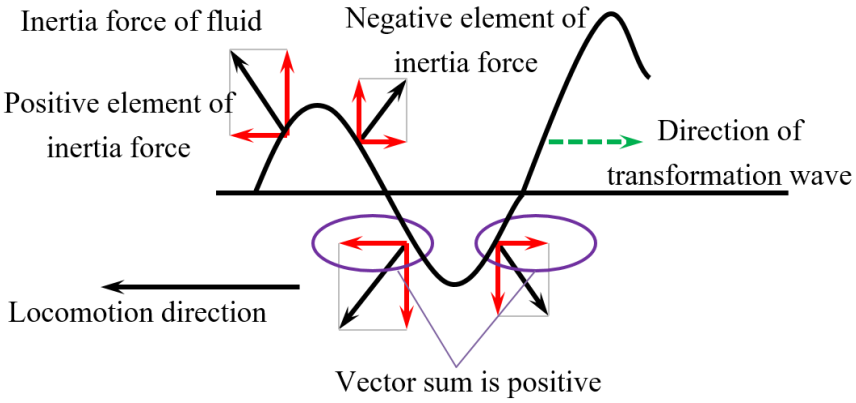

(b) Increase of vibration amplitude

Fig. 5.1 Inertial force for wave transformation motion.

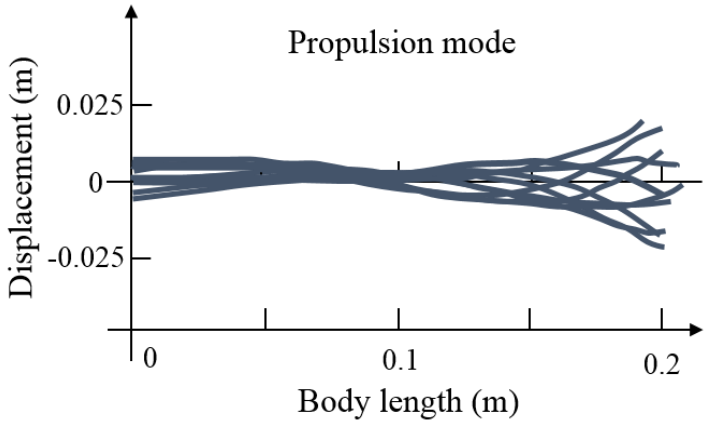

Fig. 5.2 Propulsion mode of slender trout fish.

In Fig. 5.3, a slender fish is moving in the negative direction along the *x*-axis at velocity *V*. The lift distribution in the direction of body axis can be calculated from the pressure difference Δp that is the change of kinetic momentum in the direction of *y*-axis [1]. From the head end to the maximum body height, the lift distribution can be calculated by (5-1), and (5-2) describes the lift distribution from the minimum body height to the caudal fin.

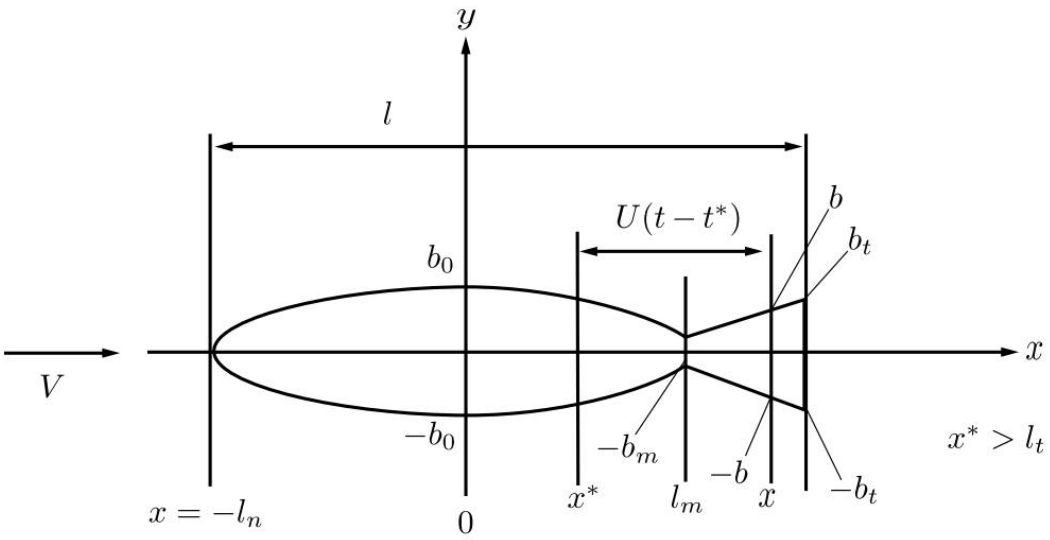

(a) Side view

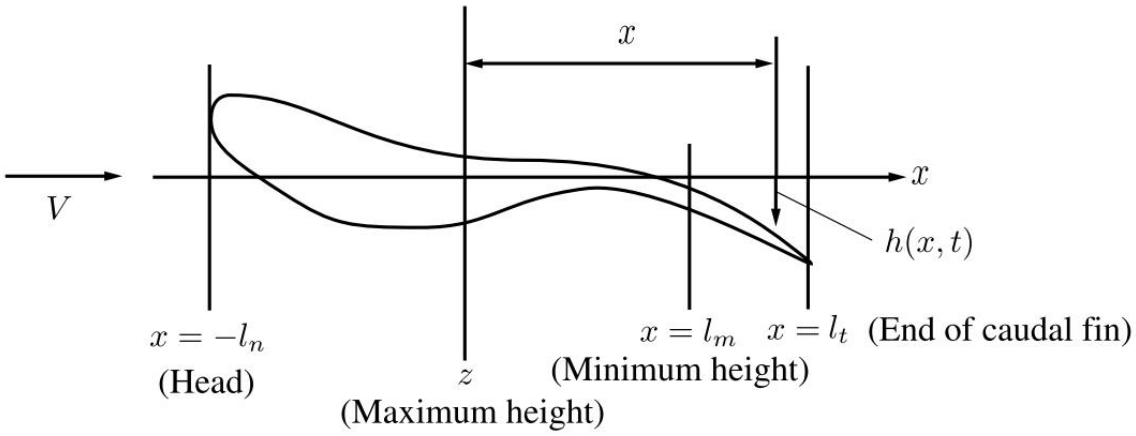

(b) Top view

Fig. 5.3 Coordinate system of slender fish.

$$l(x,t) = \int_{-b}^{b} (-\Delta p)dy = -\frac{d}{dt}\{A_{33}(x)w(x,t)\}; (-l_n < x < 0) \quad \textbf{(5-1)}$$

$$l(x,t) = -\frac{d}{dt}\{A_{33}(x)w(x,t)\} + w^{*}\frac{d}{dt}\{A_{33}(x)\}; (l_m < x < l_t) \quad \textbf{(5-2)}$$

where

$$A_{33}(x) = \rho\pi b^2(x)\gamma \quad \textbf{(5-3)}$$

$$w(x,t) = \frac{d}{dt}h(x,t) = \left(\frac{\partial}{\partial t} + V\frac{\partial}{\partial t}\right)h(x,t) \quad \textbf{(5-4)}$$

$$A_{33}(-l_n) = 0 \quad \textbf{(5-5)}$$

$$\left|\frac{\partial h}{\partial x}\right| << 1 \qquad \left|\frac{\partial h}{\partial t}\right| << V \quad \textbf{(5-6)}$$

A_{33} (x) is added mass, ρ is fluid density, γ is coefficient of added mass. And w^{*} is the velocity of the vortex come from the end of caudal fin at an arbitrary position after the point with maximum body height $x = x^{*}(0 < x^{*} < l_{\mathrm{m}})$, can be defined as follows.

$$w^{*} = w(x^{*}, t^{*}) \quad \textbf{(5-7)}$$

$$t^{*} = t - (x - x^{*})/V \quad \textbf{(5-8)}$$

Assume that the slender body theory, distribution of lift between the points with maximum body height and minimum body height is

$$l(x,t) = -\frac{d}{dt}\{A_{33}(x)w(x,t)\}; (0 < x < l_m) \quad \textbf{(5-9)}$$

Propulsive force T, consists of the part due to the above mentioned of distribution of lift and the part by suction force that works at the front edge (T_s), can be calculated by

$$T = \int_{-l_n}^{l_t} l(x,t)\frac{\partial h}{\partial x}(x,t)dx + T_s \quad \textbf{(5-10)}$$

Thus,

$$T_s = \int_{-l_n}^{0} \frac{1}{2} w^2 \frac{\partial A_{33}}{\partial x} dx + \int_{l_m}^{l_t} \frac{1}{2} (w - w^*)^2 \frac{\partial A_{33}}{\partial x} dx \quad \textbf{(5-11)}$$

$$\begin{aligned} T = & -\frac{\partial}{\partial t} \int_{-l_n}^{l_t} A_{33} w \frac{\partial}{\partial x} h dx + [A_{33} (\frac{1}{2} w^2 - Vw \frac{\partial h}{\partial x})]_{x=l_t} \\ & - \int_{0}^{l_m} (\frac{1}{2} w^2 - Vw \frac{\partial h}{\partial x}) \frac{\partial A_{33}}{\partial x} dx \\ & + \int_{l_m}^{l_t} (\frac{1}{2} (w - w^*)^2 - \frac{1}{2} w^2 + Vw^* \frac{\partial h}{\partial x}) \frac{\partial A_{33}}{\partial x} dx \end{aligned} \quad \textbf{(5-12)}$$

The suction power that works at the front edge is generated due to the fluid flow around the fish body changes by motion of the caudal fin, and fluid velocity becomes large at the front edge. Generally, the suction power is small for the slender object. Therefore, first term in (5-10) is dominant. And from this first term, the following conditions can be obtained and are important to achieve the larger propulsive force in the case of the slender object.

Firstly, the velocity of the transformation wave must be larger than that of the locomotion velocity.

Secondly, body height toward the tail should be changed and should be decreased at the stem of caudal fin which is called as caudal peduncle for fishes. As for the caudal fin, the maximum height and maximum motion amplitude should be located at the end of the caudal fin.

Thirdly, the amplitude of motion in propulsion should be increased toward the tail.

In a certain oscillating frequency range, the swimming velocity of the fish has the approximately proportional relationship with the oscillating frequency. When the oscillating frequency is decided, the approximately proportional relationship occurs between the swimming velocity and motion amplitude in a certain range. However, for some kind of fishes such as tuna, the oscillating frequency is more important for increasing the swimming speed than the motion amplitude. The swimming speed is improved by increasing the oscillating frequency of the fish.

Therefore, aiming to design the soft robotic fish with larger propulsive force and high swimming speed, the maximum motion amplitude should be located at the end of the

caudal fin and the motion with larger amplitude at the end of the caudal fin is necessary for propulsion. In the research, in order to improve the performance of the old prototype described in Chapter 4 for larger swimming velocity, based on its bending propulsion motion, the amplitude at the caudal fin end is needed to be increased by optimization for improvement.

5.2 Optimization Scheme of Soft Robotic Fish

For the old robot prototype, the main propulsion motion with first bending mode is focused. The maximum amplitude of the propulsion motion for old prototype is obtained at the caudal fin end, meets the required conditions for achieving the larger propulsive force. Therefore, in order to obtain the higher performances of the soft robotic fish based on old prototype, the structure optimizations in the fluid are carried out to increase the amplitude at the end of the caudal fin by the established coupling analysis using structure-acoustic coupling method. Thus, the amplitude of the caudal fin end, that is, the bending displacement of the tail end, should be increased when the driving frequency decided.

The caudal fin shape, head weight and body thickness of the soft robot play the important role in the motion of the robot for propulsion[1], [2], and they are viewed as the key structural parameters needed to optimize for improvement in the present research.

The dashed lines in Fig. 5.4 describe the locations of the optimization on robot structure. The caudal peduncle height and caudal fin height are considered for optimization of the caudal fin shape. CFRP carbon plate is the main body of the actuation structure of the soft robotic fish. Its thickness is important for large amplitude of the soft robotic fish. Weight placed on the head is used to constrain the head motion for increasing the amplitude of the caudal fin end. The optimization of the head weight is needed to carry out for optimal structure of the soft robotic fish.

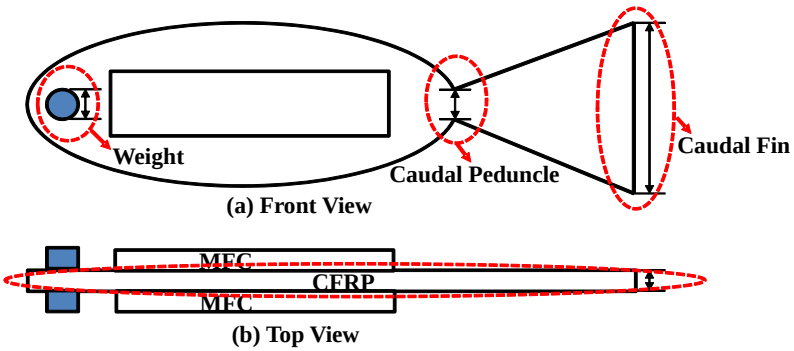

Fig. 5.4 Locations of the optimization on soft robotic fish.

5.3 Serial Optimization of Soft Robotic Fish

According to above mentioned optimization scheme, it is possible to design an optimal soft robot model for high performance by optimization of these key structural parameters. In order to verify the optimization scheme is feasible or not, the serial method is firstly carried out to make the optimization for simplifying the calculation. In the optimization, the height of the caudal peduncle where the caudal fin connects to the fish body is optimized firstly. Then the caudal fin height is optimized based on the optimal caudal peduncle height. Next, the thickness of the CFRP plate is optimized for improvement based on the optimal caudal fin shape of the soft robotic fish. Finally, the optimization of the head weight is developed based on above optimal structure parameters. After the optimization of these key structural parameters, it is possible to obtain the relatively optimal robot structure for performance improvement.

5.3.1 Optimization of Key Parameters

In the serial optimization, the driving load of 3Hz in sine waveform is applied in the simulation for comparison with old prototype. The input voltage is in the range of -500V～+1500V

The caudal fin shape is firstly presented to optimize the robot's structure, where the height of the caudal peduncle and height of caudal fin are considered. At first, the width of caudal peduncle is presented to make the optimization. The simulation results of dis-

placement at the end of the caudal fin in one cycle are shown in Fig. 5.5. The caudal peduncle height is ranged from 3mm to 30mm. For different height, there are almost identical tracks similar to a sine wave occur. The caudal peduncle height is in inverse proportion to the displacement of the caudal fin end. The maximum displacement occurs when the caudal peduncle height is 3mm and it is about 48.3mm in the given range. It is greatly larger than the old robot with 20mm. The caudal peduncle height plays the significant effect on amplitude of the caudal fin end. The caudal peduncle height of 3mm is used for further optimization.

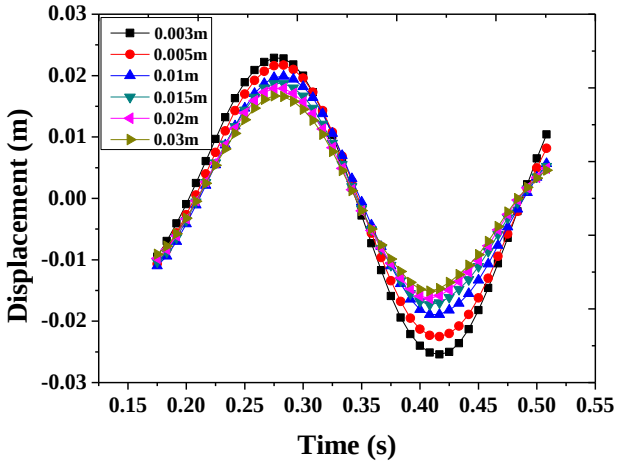

Fig. 5.5 Displacement of tail end at different caudal peduncle heights.

Then the caudal fin height of the soft robotic fish is optimized in the range of 30mm ～60mm based on caudal peduncle height of 3mm. The simulation results on displacement of the tail end in one cycle are shown in Fig. 5.6. Due to the weakened stiffness, the deformation track has a little irregular when the height is 30mm. If the height is 60mm, the displacement reaches the maximum value about 52mm. The height of the caudal fin is proportional to the displacement of the caudal fin end in the given range. The optimal caudal fin height is 60mm for propulsion motion with larger-amplitude. Thus, the relatively optimal caudal fin shape of the soft robotic fish is obtained through above optimization.

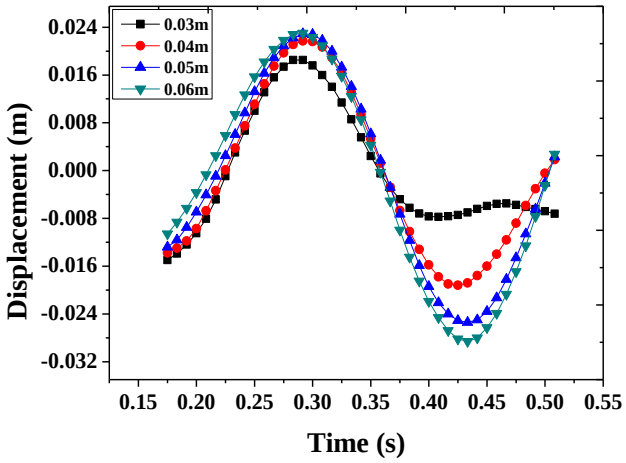

Fig. 5.6 Displacement of tail end at different caudal fin heights.

Next, based on above optimal caudal fin shape of the soft robotic fish, that is, the optimal height of the caudal peduncle and caudal fin, the thickness of the main robot body (CFRP plate) are concerned to make further optimization. The thickness range of the CFRP plate from 0.1mm to 1mm is considered in the simulation. Figure 5.7 shows the displacement results of the caudal fin end in one cycle. When the thickness is 0.2mm, the maximum deformation occurs and it is about 52mm. The CFRP plate with 0.2mm thickness is adopted as the fish body components for soft robot structure.

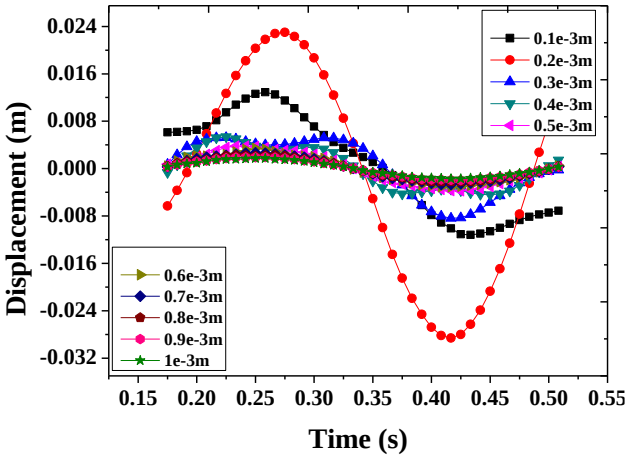

Fig. 5.7 Displacement of tail end at different thicknesses of CFRP plate.

In the present research, the weight is placed on the robot head for larger displacement of the tail end. Thus, the optimizations of the head weight are finally carried out through different volumes for improvement based on optimal key parameters of the caudal fin

shape and robot body thickness. In the simulation, the radius of head weight is ranged from 1mm to 7mm. Figure 5.8 presents the simulation results of displacement of the tail end and head tip at different radii of head weight.

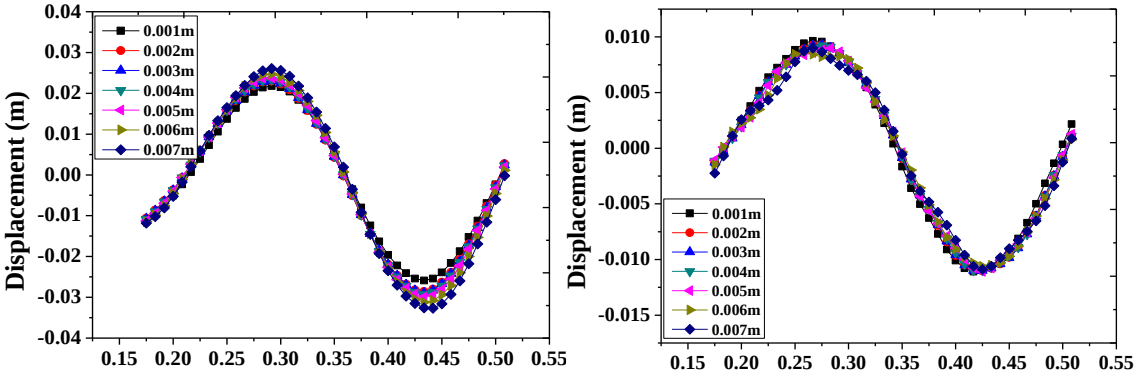

(a) Displacement of tail end (b) Displacement of head end

Fig. 5.8 Displacement at different radii of head weight.

There are almost identical displacement curves happen at the different volumes of head weight both on caudal fin end and head tip. The displacement difference among different volumes is small, especially on the head tip. The displacement of the tail end is proportional to the volume of the head weight. When the radius of the head weight is 7mm, it obtains a maximum displacement. The radius of head weight with 7mm is optimal for propulsion with larger-amplitude.

Finally, caudal peduncle height with 3mm, caudal fin height with 30mm, CFRP plate with 0.2mm thickness and radius of the head weight with 7mm are adopted to design the new soft robotic fish with larger-amplitude for improvement.

5.3.2 Serial Optimized Model of Soft Robotic Fish

According to above serial optimization results of key structural parameters, the model of new soft robotic fish is designed and described in Fig. 5.9. The main body is also made by a CFRP plate and two MFC plates. Two MFC plates sandwich the CFRP plate

as the actuator structure. Weight is also placed on the robot head to increase the displacement of the tail end.

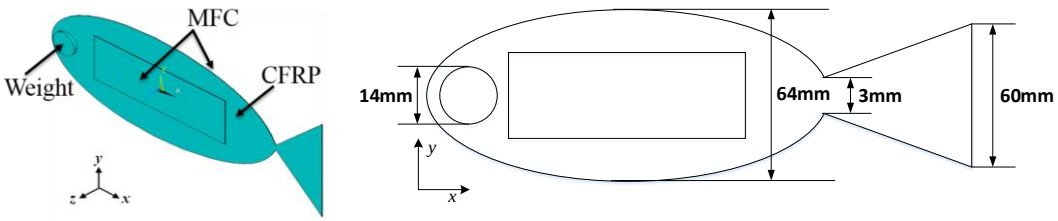

Fig. 5.9 Model of new soft robotic fish from serial optimization.

Based on above new model from serial optimization, the bending deformation track of the new robot structure is shown in Fig. 5.10. The old robot's result is also presented for comparison. Here the results of 3Hz are taken as an example to describe, and the results in quarter of one cycle are presented due to motion symmetry.

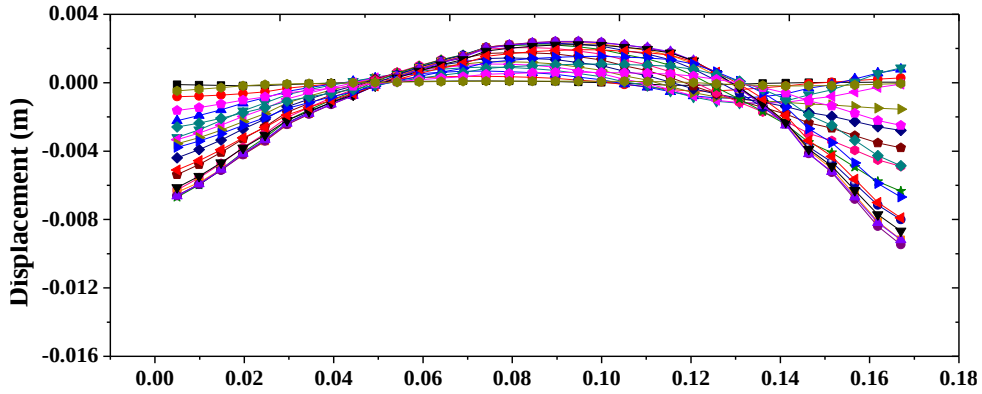

(a) Deformation track of old robot

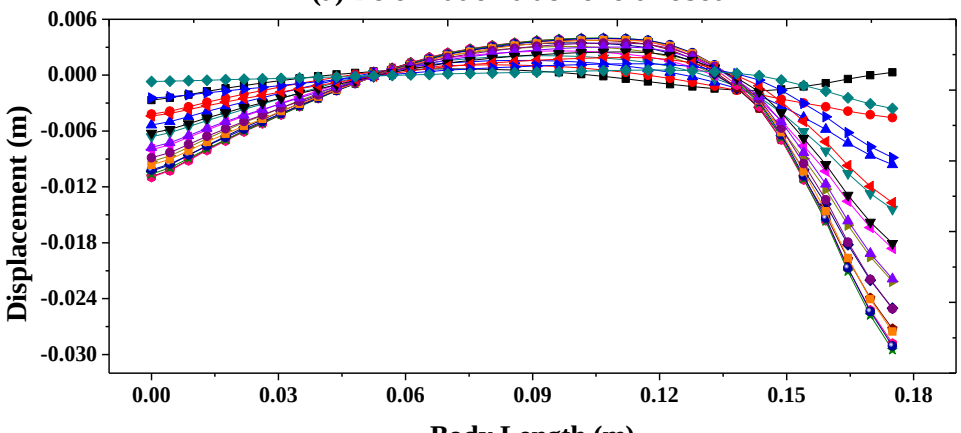

(b) Deformation track of new robot from serial optimization

Fig. 5.10 Deformation track of new robot from serial optimization in quarter of one cycle.

From this figure, it can be known that the maximum amplitude of the propulsion motion for the new and old robot structure occurs at the end of the caudal fin. The minimum deformation all happens at the position where the distance from the edge of robot head is about one-third of body length. They have the similar first bending deformation mode for both soft robots in the swimming motion. However, the displacement at the caudal fin end of the new robot is larger than the old robot, meets the desired purpose for larger amplitude at the end of the caudal fin.

Furthermore, the mode frequencies of serial optimized soft robot with a free boundary condition are shown in Table 5.1. The first five mode frequencies are presented.

Table 5.1 Mode Frequencies of Serial Optimized Soft Robot in the Fluid

Item	Mode Frequencies (Hz)				
	1	***2***	***3***	***4***	***5***
Old robot	5.99	16.55	24.99	36.3	43.8
New robot	3.95	10.7	20.5	29.0	37.9

Compared with the results of old robot, the mode frequencies of the serial optimized soft robot are smaller due to the different distribution in structure stiffness and weight. The first bending mode frequency is about 4Hz for the serial optimized soft robot and 6Hz for the old robot, and its maximum deformation occurs at the tail end. The second bending mode similar to S-shape is obtained at about 20.5Hz for the serial optimized soft robot and 25Hz for the old robot. If the frequency is 29Hz, the third bending mode occurs on the serial optimized soft robot. When the frequencies are about 11Hz and 37.9Hz, the torsion deformation will generate on the serial optimized soft robot.

5.3.3 Experiment Evaluation

Figure 5.11 presents the prototype of the serial optimized soft robotic fish. In the experiment, the blowing agent is also placed on the top to balance the robot weight. The type of the MFC is M8528P1 same to the old robot's. The detailed specifications of the prototype are shown in Table 5.2. The epoxy 3M-DP460 is used to make the MFC plate

bonded on the CFRP plate. In the experiment, a cubical fluid tank described by the Fluorinert Electronic Liquid FC-3283 is used to build the platform of measurement due to high input voltage of the MFC. The driving system of the prototype in the experiment shown in Fig. 4.2 is also adopted. The high-speed camera (Casio Digital Camera EX-F1 [3]) is also used for observation and measurement. The input voltage on new prototype is in the range of -500V～+1500V and the range of the driving frequency is 1Hz～30Hz.

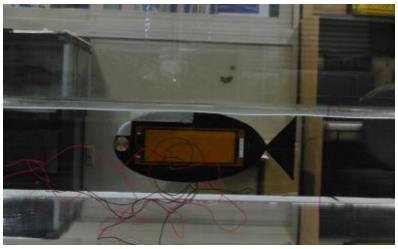

Fig. 5.11 Prototype of serial optimized soft robotic fish.

Table 5.2 Specifications of Serial Optimized Soft Robotic Fish

Item	Specification
Caudal peduncle height (mm)	3
Caudal fin height (mm)	60
Radius of head weight (mm)	7
Maximum body height (mm)	64
Type of actuator	MFC 8528P1×2
Actuator dimensions (mm)	112×40
Actuator active area (mm)	85×28
Actuator for adhering	CFRP-0.2mm thickness
Adhesion bond	Epoxy 3M-DP460

According to the deformation track of the serial optimized soft robotic fish shown in Fig. 5.10, Fig. 5.12 describes the difference of bending mode at 3Hz for the serial optimized soft robot between the simulation and experiment. The results in quarter of one cycle are also presented. The deformation of the serial optimized soft robot in the experiment is observed by high-speed camera. The maximum displacement of the soft robotic fish is all obtained at the tail end at different time values. There is almost same

bending mode exists in the simulation and experiment. The simulation results are congruent with experimental results. From this figure, it can be known that fish-like bending propulsion motion is realized on prototype of serial optimized soft robotic fish.

Based on the prototype of serial optimized soft robotic fish, the bending mode frequencies in its swimming motion can be obtained. Table 5.3 presents the first three bending mode frequencies of the serial optimized soft robotic fish in the fluid. At 4Hz, the main bending propulsion mode occurs. The second and third bending mode happens at the frequency of 21Hz and 29Hz, respectively. Compared with the old robot, the mode frequencies of the serial optimized soft robotic fish in the fluid is smaller.

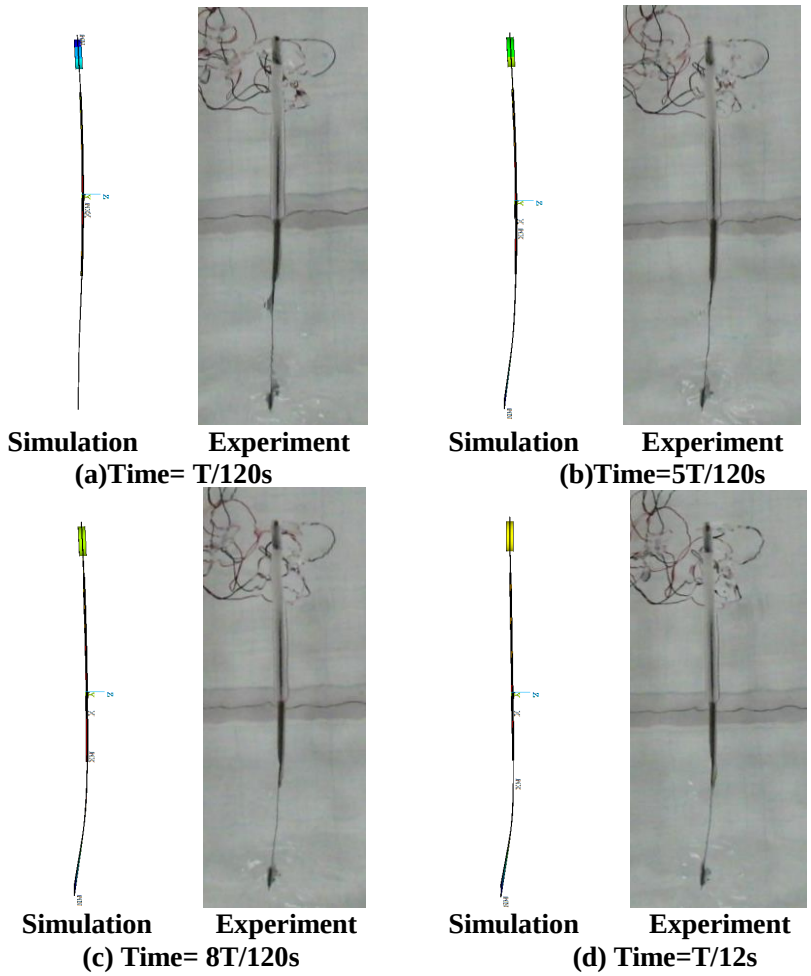

Fig. 5.12 Deformation modes of serial optimized soft robotic fish between simulation and experiment in quarter of one cycle at 3Hz.

Table 5.3 Bending Mode Frequencies of Prototype for Serial Optimized Soft Robotic Fish in the Fluid

Item	Bending Mode Frequewncies (Hz)		
	1	***2***	***3***
Old robot	6	25	36
Serial optimized robot	4	21	29

At different bending mode frequencies of the serial optimized robot prototype in the fluid, the corresponding bending propulsion modes in the fluid by high-speed camera are shown in Fig. 5.13.

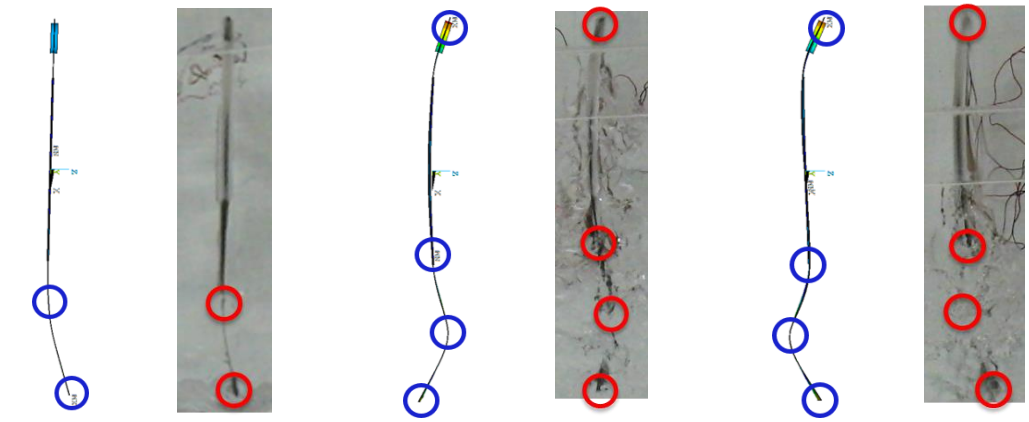

(a) First order-4Hz **(b) Second order-21Hz** **(c) Third order-29Hz**

Fig. 5.13 Bending propulsion modes of prototype for serial optimized soft robotic fish.

The serial optimized soft robotic fish has the very similar bending deformation modes at the corresponding bending mode frequencies compared with the experimental results. At the different mode frequencies, they have the different bending deformation modes. When the frequency of 4Hz is applied, the maximum displacement is obtained at the end of the caudal fin. If the second and third bending modes occur based on the frequency of 21Hz and 29Hz, the different propulsion modes generate and the maximum deformation happens at different part of robot body. As a conclusion, the simulation results on bending propulsion modes about frequencies and mode shapes co-

incide with experimental results well and fish-like bending propulsion motion is realized on the prototype of the serial optimized soft robotic fish.

Furthermore, the larger displacement at the caudal fin end of the serial optimized soft robotic fish at different driving frequencies is evaluated. The results of comparison between the prototype of serial optimized robot and old prototype are described in Fig. 5.14. The serial optimized robot and old robot have the similar displacement curves in the given frequency range. And the serial optimized robot has larger displacement at the caudal fin end than the old robot. The displacement at the caudal fin end of the serial optimized soft robotic fish is increased by 1.5 times averagely in the given range. The serial optimized soft robotic fish has the larger amplitude for propulsion than old robot.

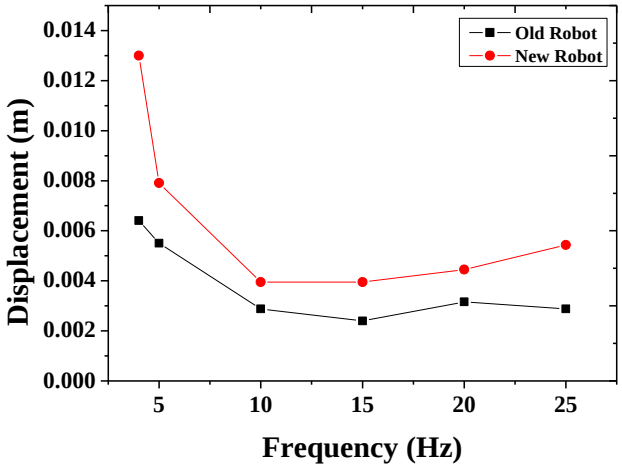

Fig. 5.14 Displacement of tail end for serial optimized soft robot at different frequencies.

According to above results of displacement of the tail end for the serial optimized soft robotic fish at different frequencies, the serial optimized soft robot can make the basic swimming motions in the fluid, such as forward motion. The swimming velocity of the serial optimized soft robot at different frequencies ranged from 1Hz to 30Hz are described in Fig. 5.15. Old robot's velocity is also presented for comparison.

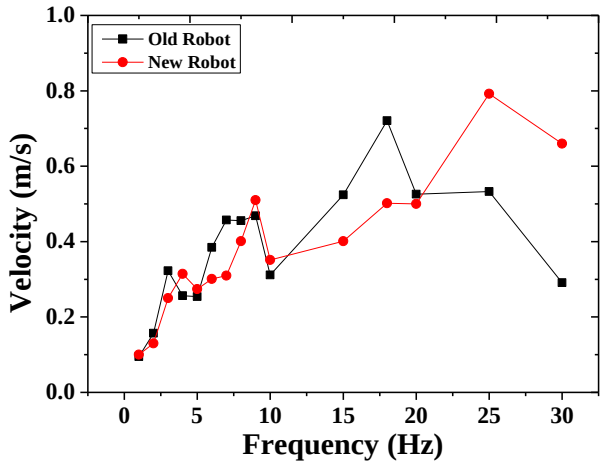

Fig. 5.15 Swimming velocity of serial optimized soft robotic fish at different frequencies.

By comparison between the serial optimized robot and old robot, there is similar velocity curve occurs. However, the maximum swimming velocity of the serial optimized robot is larger than the old robot about 0.72m/s. The serial optimized soft robot can reach up to about 0.792m/s at the frequency of 25Hz. The relatively higher performances are obtained from the serial optimized soft robotic fish.

In the robotics, the energy efficiency of the robot is adopted to evaluate the efficiency performance of the robot. The energy used per distance is presented to describe the efficiency of the soft robotic fish, and it can be estimated by the following equation.

$$H = \frac{W}{V} \tag{5-13}$$

where H is energy used per distance, whose unit is J/m; W is electrical energy; V is swimming velocity of the soft robotic fish.

To calculate the efficiency, the electrical energy of the soft robotic fish at different frequencies is measured by measuring the voltage and current of the MFC actuators and shown in Fig. 5.16. The electrical energy of the soft robotic fish increases with the growth of the driving voltage frequency. Compared with the old soft robotic fish, the serial optimized soft robot has the larger electrical energy at different frequencies for swimming motion.

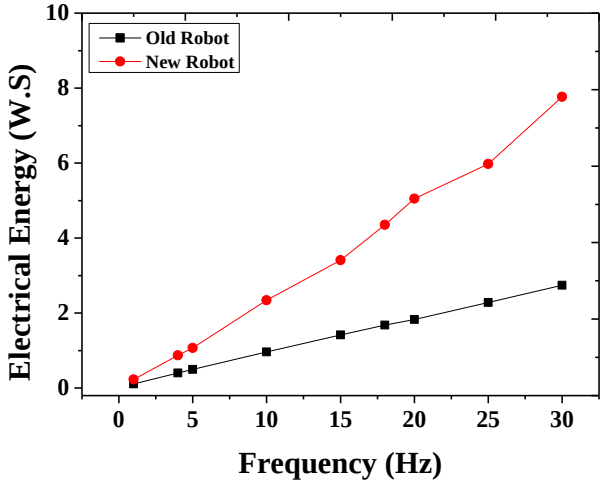

Fig. 5.16 Electrical energy of serial optimized soft robotic fish at different frequencies.

According to the measured results of swimming velocity and electrical energy of the serial optimized soft robotic fish described in Fig. 5.15 and Fig. 5.16, respectively, the energy used per distance for the soft robotic fish can be calculated by (5-13) and the results at different frequencies are presented in Fig. 5.17.

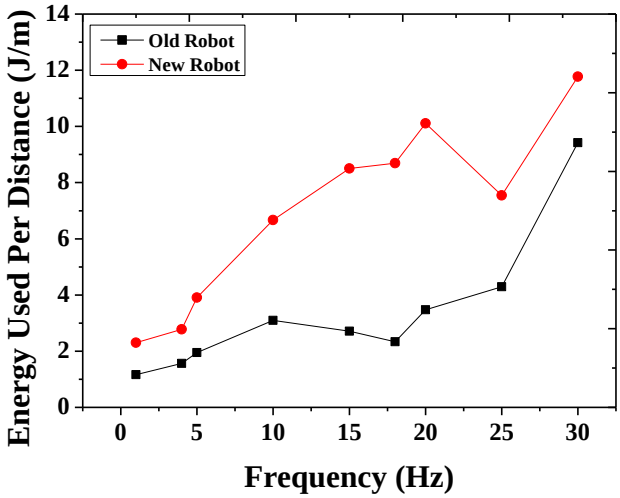

Fig. 5.17 Energy used per distance for serial optimized soft robotic fish.

In Fig. 5.17, with the growth of the driving frequency of the soft robotic fish, the energy used per distance is increasing in the given range. Compared with the old soft robotic fish, the energy used per distance for the serial optimized soft robotic fish is larger at different frequencies due to larger amplitude. The minimum energy used per

distance for the serial optimized soft robotic fish is about 2.3J/m in the given range. At 25Hz where the largest swimming speed of the serial optimized soft robot is obtained, the energy used per distance for the serial optimized soft robot is decreasing. The corresponding energy efficiency of the serial optimized soft robot at this frequency is increased.

The maximum output work energy efficiency for the MFC actuator is about 0.16 [4]. Thus, the maximum 16% of the input electrical energy can be converted into useful output work for an MFC actuator. Therefore, the maximum electrical energy used per distance for the serial optimized soft robotic fish are about 0.37J/m, obtained by (5-14), respectively. Compared with the maximum energy used per distance for the old soft robotic fish about 0.16J/m, the serial optimized soft robot's maximum energy used per distance is increased up to about two times.

$$H^{\max} = \frac{0.16W}{V} \tag{5-14}$$

In the biomimetic field, swimming number S_w of the fish is widely used to evaluate the swimming performances of the designed robotic fish. S_w, related to velocity V, frequency f, body length L, can be expressed by (5-15),

$$Sw = \frac{V}{fL} \tag{5-15}$$

where V is velocity, f is frequency, L is body length.

Swimming number of fish describes the distance fish moved per tail beat. The S_w of the fishes is generally about 0.6 for high performances with good flexibility and mobility [5], described in Fig. 5.18.

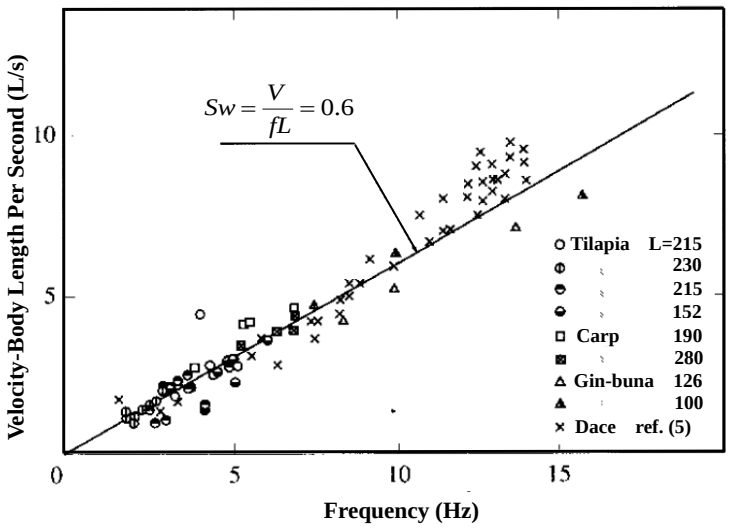

Fig. 5.18 S_w of fishes [5].

It means that there is a representation of the premise of similarity law in the biomimetic field. Swimming number is sufficient to describe the performance related to swimming motion of fish [5]. It can be utilized to evaluate the performance of the soft robot having fish like swimming motion in the biomimetic by biomimetic approach.

The swimming number S_w of the serial optimized soft robot at different frequencies is shown in Fig. 5.19.

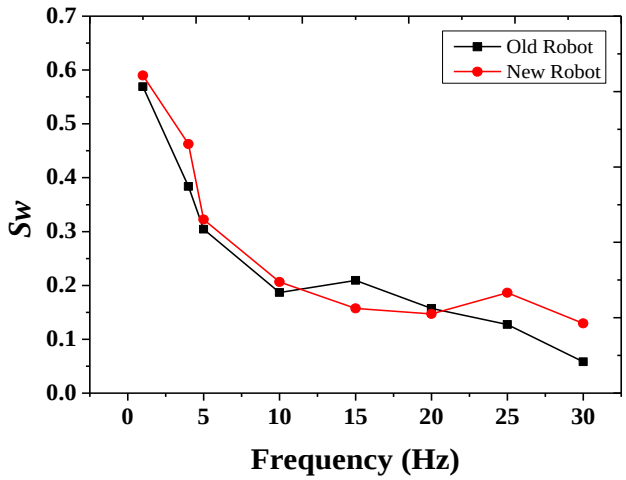

Fig. 5.19 S_w of serial optimized soft robotic fish at different frequencies.

The S_w of the serial optimized soft robot is larger than the old robot both near the frequencies where the first, second and third bending propulsion modes occur. Near the

frequency of first bending mode, the S_w is increased by 1.1 times compared with the old robot. And it is increased by 1.8 times near the frequency of second and third bending modes. The S_w of the serial optimized robot is much close to the value of real fishes about 0.6 where the good flexibility and mobility of the real fishes happen compared with the old robot. It can be considered that the serial optimized soft robot has the better propulsion performances similar to those of fishes than the old robot.

As a conclusion, a new soft robotic fish with higher performance is developed by the serial optimization for improvement of old prototype. The larger deformation and higher swimming velocity of the serial optimized soft robotic fish are evaluated and verified successfully by the prototype of the serial optimized soft robotic fish. Compared with the old robot, this new soft robotic fish from serial optimization, that is, the serial optimized soft robotic fish, has the better fish-like propulsion performances. The optimization scheme of the soft robotic fish is feasible and it is possible to develop a relatively optimal robot model by optimization of key structural parameters effectively.

5.4 Integrative Optimization of Soft Robotic Fish

Although the new soft robotic fish obtained by serial optimization has the larger swimming velocity and displacement than the old prototype, the serial optimization simplifies the calculation in which only few points are considered. Therefore, to further improve the propulsion performance of the soft robotic fish, the integrative optimization on soft robotic fish is performed in this part based on structure-acoustic coupling method.

5.4.1 Optimization of Key Parameters

According to optimization scheme and above serial optimization, the caudal peduncle height, caudal fin height, body thickness and head weight of the soft robotic fish are the key structural parameters for robot propulsion and needed to be optimized for further

improvement. The integrative optimization is also performed to increase the displacement at the end of the caudal fin for improvement.

In the integrative optimization, these key parameters of the robot are allowed to vary within a relatively better range than that of serial optimization for further optimization. The varied range of these key parameters is described in Table 5.4. The maximum body height of the mentioned new soft robot is 64mm. Thus, the caudal peduncle height and the caudal fin height is optimized in the range of 1mm～64mm. The body thickness is also ranged from 0.1mm to 1mm for softness and radius of the head weight is still in the range of 1mm～7mm due to structural dimensions of the robot. These key parameters are arranged and combined at random in the given range to achieve the optimal and maximum displacement of the caudal fin end for improvement.

Table 5.4 Range of Key Structural Parameters of Soft Robot for Improvement

Key Structural Parameters of Soft Robot	**Range of Optimization**
Caudal Peduncle Height (mm)	1～64
Caudal Fin Height (mm)	1～64
Body Thickness (CFRP Thickness) (mm)	0.1～1
Radii of Head Weight (mm)	1～7

In the integrative optimization, the driving load of 3Hz in sine waveform is still applied in the numerical simulation for comparison. The input voltage is in the range of -500V～+1500V. The simulation results of the displacement at the caudal fin end based on different parameter arrays in the given range are described in Fig. 5.20.

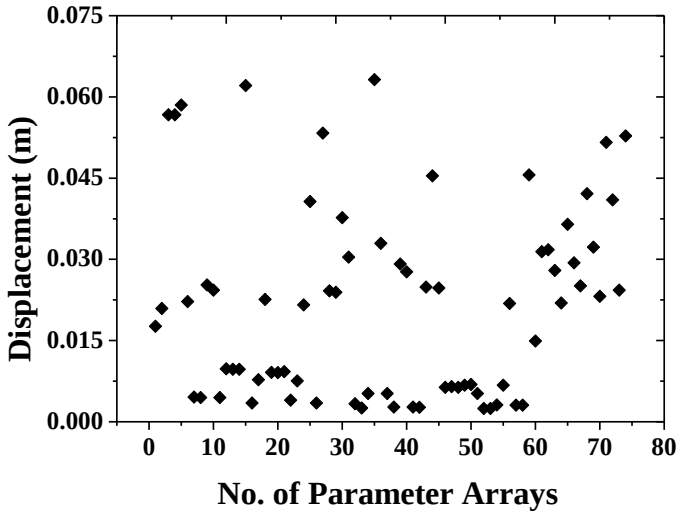

Fig. 5.20 Displacement of caudal fin end based on different parameter arrays.

From this figure, the maximum displacement about 62mm can be obtained at 3Hz. It is larger than the new soft robotic fish whose displacement of the caudal fin end is 52mm at 3Hz. Based on this maximum displacement, the corresponding optimal structural parameters can be obtained, that is, the caudal peduncle height of 3mm, the caudal fin height of 20mm, the body thickness with 0.1mm and radius of head weight with 7mm. Therefore, based on these optimal structural key parameters for relatively largest displacement of the tail end, the new numerical model of the soft robotic fish can be obtained. Through this new numerical model from integrative optimization, it is possible to improve the performance of the new soft robotic fish.

5.4.2 Integrative Optimized Model of Soft Robotic Fish

According to simulation results obtained from the integrative optimization of the soft robotic fish, the new model of the soft robotic fish can be designed and shown in Fig. 5.21. Two MFC plates also sandwich the CFRP plate as the actuator structure. Through this new model, it is possible to further improve the performance of the soft robotic fish.

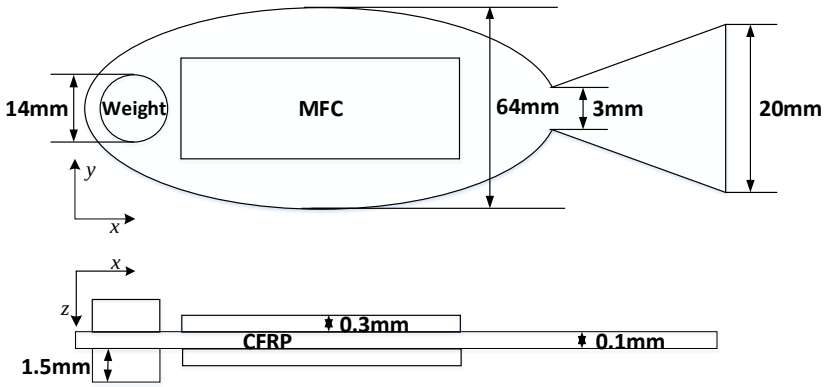

Fig. 5.21 Model of integrative optimized soft robotic fish.

According to this integrative optimized model, the mode frequencies of the integrative optimized soft robotic fish with a free boundary condition are shown in Table 5.5. The first five mode frequencies are presented.

Table 5.5 Mode Frequencies of Integrative Optimized Soft Robot in the Fluid

Item	Bending Mode Frequencies (Hz)		
	1	***2***	3
Serial optimized robot	3.95	20.5	29.0
Integrative optimized robot	2.5	9.5	11.8

Compared with the results of robot obtained from serial optimization, the mode frequencies of the integrative optimized robot are smaller due to the different distribution in structure stiffness and weight. The first bending mode frequency is about 2.5Hz for the integrative optimized robot, and its maximum deformation occurs at the tail end described in Fig. 5.22. The second bending mode similar to S-shape is obtained at about 9.5Hz for the integrative optimized robot. If the frequency is near 12Hz, the third bending mode occurs on robot obtained from integrative optimization. The similar bending mode shapes happen on both new soft robots obtained from serial optimization and integrative optimization.

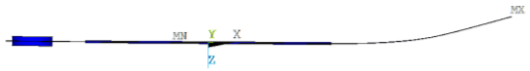

(a) First bending mode

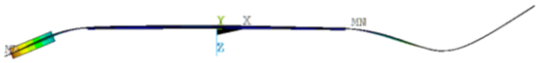

(b) Second bending mode

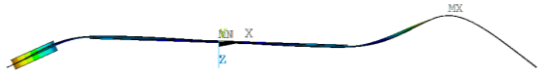

(c) Third bending mode

Fig. 5.22 Bending modes of integrative optimized soft robotic fish.

5.4.3 Experiment Evaluation

Figure 5.23 presents the prototype of the integrative optimized soft robot. In the experiment, aiming to balance the robot weight, the blowing agent is placed on the head and top part of the robot. The MFC with M8528P1 type is adopted as soft actuator. The detailed specifications of the prototype obtained from the integrative optimization are shown in Table 5.6. The epoxy 3M-DP460 is used to make the MFC plates bonded on the CFRP plate. A cubical fluid tank described by the Fluorinert Electronic Liquid FC-3283 is also used for measurement due to the high input voltage of the MFC. The driving system of the prototype in the experiment shown in Fig. 4.2 is also adopted. In the experiment, the input voltage in square waveform applied on prototype is ranged from -500V to +1500V and the driving frequency is in the range of 1Hz～30Hz.

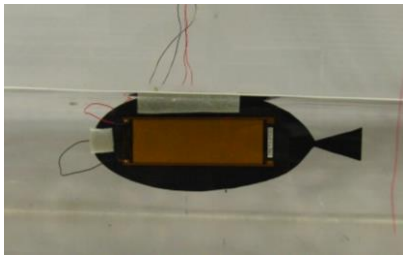

Fig. 5.23 Prototype of integrative optimized soft robotic fish.

Table 5.6 Specifications of Integrative Optimized Soft Robotic Fish

Item	Specification
Caudal peduncle height (mm)	3
Caudal fin height (mm)	20
Radius of head weight (mm)	7
Maximum body height (mm)	64
Type of actuator	MFC 8528P1 ×2
Actuator dimensions (mm)	103 ×35
Actuator active area (mm)	85 ×28
Actuator for adhering	CFRP-0.1mm thickness
Adhesion bond	Epoxy 3M-DP460
Weight (g)	14.1

Based on this new prototype obtained from integrative optimization, the bending mode frequencies in its swimming motion can be obtained. Table 5.7 presents the first three bending mode frequencies of the integrative optimized soft robotic fish in the fluid. The main bending propulsion mode occurs at the frequency about 2Hz, and the second and third bending modes generate at the frequency larger than 10Hz. Compared with the serial optimized soft robot, the mode frequencies of the integrative optimized soft robotic fish in the fluid is smaller.

Table 5.7 Bending Mode Frequencies of Prototype for Integrative Optimized Soft Robotic Fish in the Fluid

Item	Bending Mode Frequewncies (Hz)		
	1	***2***	***3***
Serial optimized robot	4	21	29
Integrative optimized robot	2	10	12

At different bending mode frequencies of the integrative optimized robot prototype in the fluid, the corresponding bending propulsion modes in the fluid are shown in Fig. 5.24 by high-speed camera (Casio Digital Camera EX-F1).

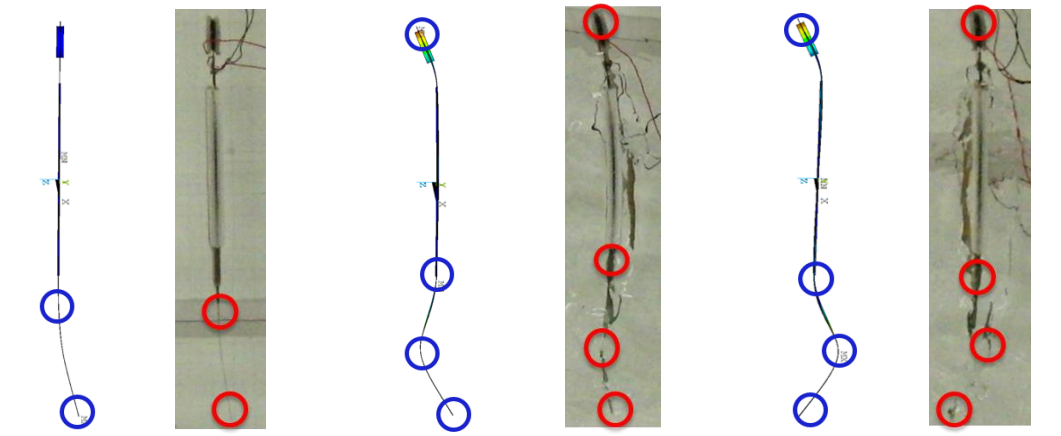

Fig. 5.24 Bending propulsion modes of prototype for integrative optimized soft robotic fish.

There are very similar bending deformation modes happen on the integrative optimized soft robotic fish at the corresponding bending mode frequencies between the simulation and experimental results. When the driving frequency is about 2Hz, the maximum displacement is obtained at the tail end. If the second and third bending modes occur at the frequency of about 10Hz and 12Hz, the different propulsion modes generate and the maximum deformation happens at different part of robot body. As a conclusion, the simulation results on bending propulsion modes about frequencies and mode shapes coincide with experimental results well and fish-like bending propulsion motion is also achieved on the prototype of the integrative optimized soft robotic fish.

The integrative optimized soft robotic fish also can realize the basic swimming motions in the fluid, such as forward motion. The swimming velocity of the integrative optimized soft robot is described in Fig. 5.25. Above mentioned serial optimized robot's velocity described in section 5.3 is also presented for comparison. At different driving frequencies, the swimming velocity of the integrative optimized soft robot is different. In the given frequency range, the maximum swimming velocity of the integrative optimized soft robot is smaller than that of serial optimized robot about 0.79m/s. However, the swimming velocity of the soft robot in the low frequency range is improved by this integrative optimized soft robot. The integrative optimized soft robot has the rela-

tively larger swimming velocity than the serial optimized robot at the low frequencies due to small stiffness and mass distribution causing the reduced mode frequencies.

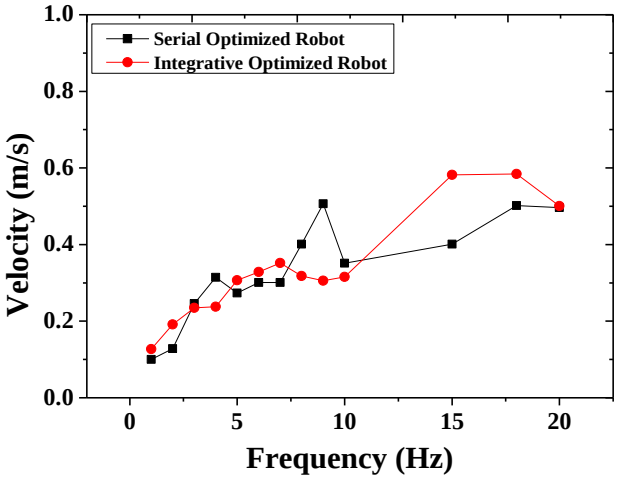

Fig. 5.25 Swimming velocity of integrative optimized soft robot at different frequencies.

To obtain the energy efficiency of the integrative optimized soft robot, its electrical energy at different frequencies is measured and shown in Fig. 5.26. The electrical energy of the soft robotic fish increases with the growth of the driving frequency. There is small difference on electrical energy between the serial optimized robot and integrative optimized robot, but the electrical energy of the integrative optimized soft robot is smaller.

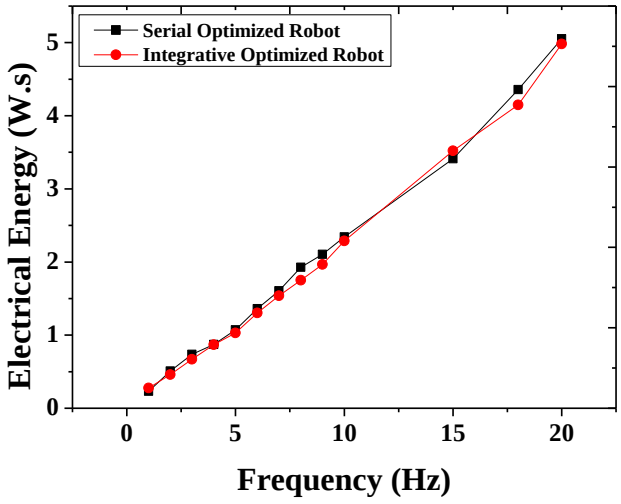

Fig. 5.26 Electrical energy of integrative optimized soft robotic fish at different frequencies.

According to the swimming velocity of the integrative optimized soft robotic fish presented in Fig. 5.25, its energy used per distance can be obtained by (5-13) and the results at different frequencies are described in Fig. 5.27 for comparison.

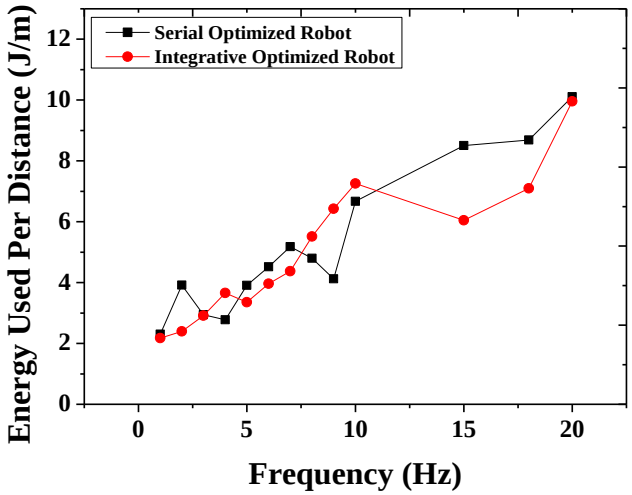

Fig. 5.27 Energy used per distance for integrative optimized soft robotic fish.

In Fig. 5.27, the energy used per distance is increasing with the growth of the driving frequency of the soft robotic fish in the given range. Based on different frequencies, the energy used per distance for the integrative optimized soft robot is different. Compared with the serial optimized robot, the energy used per distance for the integrative optimized soft robot is smaller at the frequencies where the first bending mode and larger swimming velocity happen. The energy used per distance is reduced by about 61% at 2Hz and 71% at 15Hz, where the first bending mode and larger swimming velocity of the integrative optimized soft robot occur, respectively, compared with the serial optimized soft robot. The minimum energy used per distance for the integrative optimized soft robotic fish is about 2.1J/m smaller than that of serial optimized soft robot about 2.3J/m. According to the maximum output work energy efficiency for the MFC actuator, the maximum energy used per distance for the integrative optimized soft robotic fish is and 0.34J/m, smaller than the that of the serial optimized soft robotic fish about 0.37J/m. As a conclusion, the energy used per distance for the integrative optimized soft robot at the frequency of first bending mode is smaller than the serial optimized soft robotic fish.

The energy efficiency of the integrative optimized soft robotic fish is higher at the first bending mode compared with the serial optimized robot. The integrative optimized soft robotic fish can use smaller electrical energy to obtain the larger swimming velocity in its propulsion motion. The integrative optimized soft robotic fish has the higher propulsion performance than the serial optimized soft robot.

Figure 5.28 presents the swimming number S_w of the integrative optimized soft robot at different frequencies.

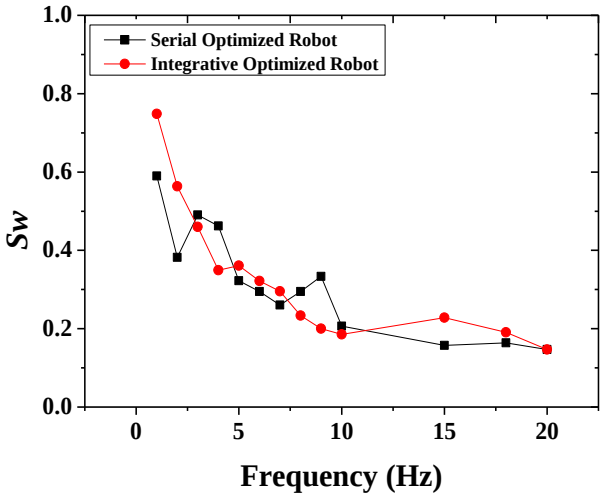

Fig. 5.28 S_w of integrative optimized soft robotic fish at different frequencies.

From the Fig. 5.28, the S_w of the integrative optimized soft robot is larger than the serial optimized robot described in Section 5.3.2 near the frequencies where the first, second and third bending propulsion modes occur, that is, the frequency near 2Hz and larger than 10Hz. Near the frequencies of first bending mode, the S_w of integrative optimized soft robot is increased by about 1.3 times compared with the serial optimized robot averagely. And the S_w of the integrative optimized soft robot is much close to the value of real fishes about 0.6 compared with the serial optimized robot. As a conclusion, although the maximum swimming speed of the integrative optimized soft robot is smaller than the serial optimized soft robot in the given range, the integrative optimized soft robot improves the swimming performance of the serial optimized soft robot at low frequency. At the frequency of main propulsion mode of the soft robotic fish, the inte-

grative optimized soft robot has the larger speed and better fish-like propulsion performance than the serial optimized soft robotic fish.

Table 5.8 presents the comparison results of swimming performances among some conventional soft robotic fish, such as maximum swimming speed and swimming number *Sw*. Compared with conventional soft robotic fish, the optimized soft robotic fish in this study have the better performances on maximum swimming speed by using body length per second (BL/s) and *Sw*. The maximum swimming speed of the soft robotic fish in this study is improved by more than one order of magnitude and swimming number is enhanced by at least 3 times. It can be considered than the serial and integrative optimized soft robotic fish in the study have the higher propulsion performance similar to those of real fishes than the conventional soft robotic fish.

Table 5.8 Comparison of Swimming Performance of Soft Robotic Fish

Soft Robotic Fish		**Soft Actuator**	**Maximum Speed (BL/s)**	**Maximum *Sw***
Kagawa University		ICPF	0.16	0.09
Polytechnic University of Madrid		SMA	0.1	0.2
Tokyo University		Electrostatic film	0.14	0.083
Michigan State University		IPMC	0.04848	0.044
This Study	Serial	PFC	4.6	0.6
	Integrative		3.5	0.75

Besides, based on the verified turning motion control of the soft robotic fish described in Chapter 3, the turning motion is also achieved on the optimized soft robotic fish. Figure 5.29 and 5.30 present turning motion of the optimized soft robot at its maximum swimming speed by using high-speed camera (Casio Digital Camera EX-F1). Here the soft robotic fish from integrative optimization is taken as an example for description. At 15Hz, the integrative optimized soft robotic fish achieves the turning left motion with about 53deg/s and turning right motion with about 51.6deg/s, larger than the old prototype whose maximum turning velocity is about 27deg/s. The optimized soft robotic fish has larger turning velocity than old robot. The propulsion performance on turning motion is improved by optimized soft robotic fish.

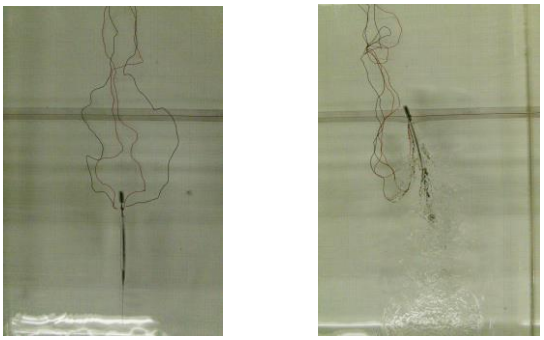

Fig. 5.29 Motion of turning left of prototype from integrative optimization at 15Hz.

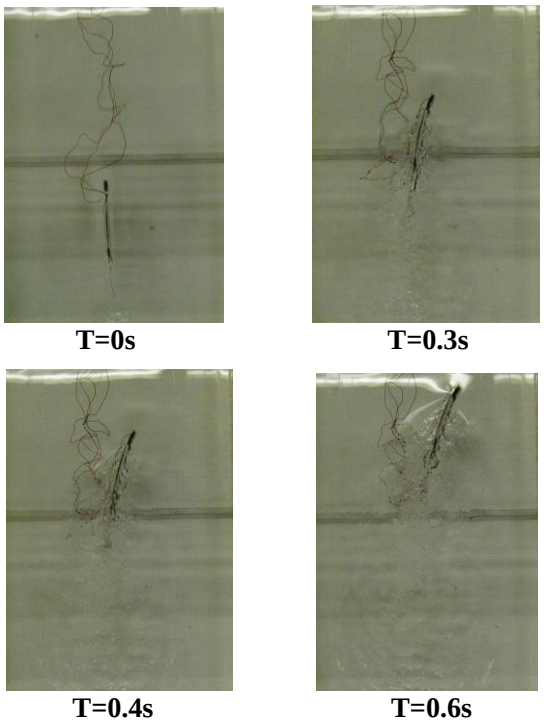

Fig. 5.30 Motion of turning right of prototype from integrative optimization at 15Hz.

5.5 Summary

In this chapter, new soft robotic fish is presented by optimization. The new soft robotic fish obtained from the serial optimization has the better propulsion performances similar to those of fishes than the old robot. And the larger displacement and higher swimming velocity generates on the new soft robotic fish compared with the old robot. The swimming velocity of the new soft robotic fish obtained from serial optimization can reach up to 0.79m/s at 25Hz, meets the desired purpose on performance improvement preliminarily. Based on integrative optimization, a new soft robot with better fish-like performance at the main propulsion mode is developed for further improvement, and turning velocity is improved by about two times by comparing the maximum turning velocity of the old robot. Based on these designed new soft robotic fish obtained by serial and integrative optimization, it is confirmed that the higher swimming speed and swimming performance similar to real fish are realized. It can be said that the new soft robotic fish has been developed successfully for improvement.

References for Chapter 5

[1] A. Azuma, Encyclopaedia of Creature's Motion, Asakura Publishing, 1997.

[2] H. Kagemoto, D. K. P. Yue and M. S. Triantafyllou, "Why do fish have the 'fish-like geometry'?," Proceedings of Annual Meeting, Japan Society of Fluid Mechanics, Vol. 29, pp. 395-396, 2010.

[3] Http://www.casio.com/products/archive/Digital_Cameras/High-Speed/EX-F1/. Ex-ilim EX-F1.

[4] Http://www.smart-material.com/media/Datasheet/MFC_V2.1-web-2014.pdf

[5] I. Tanaka and M. Nagai, "Hydrodynamic of resistance and propulsion-learn from the fast swimming ability of aquatic animals," Ship & Ocean Foundation, pp. 14-19, 1996.

Chapter 6. Conclusion

With the rapid development of industrial technologies and human society, the demand of the biomimetic underwater robots with good flexibility and mobility has been largely increased in many fields such as engineering, medical, military, gym, and so on. Due to the complicated underwater environment, biomimetic underwater robots with good efficiency are needed for some special underwork tasks. The fishes swimming in the marine have good flexibility, efficiency, adaptability and manoeuvrability. Based on requirement of underwater tasks and impressive swimming abilities of fishes, many researchers pay more attention on development of biomimetic robotic fish by mimicking the real fish. The conventional biomimetic robotic fish uses the motor to design the propulsion mechanism. The high rigidity body and complicated control system easily occur on robot structure using motor mechanism. The fish-like propulsion performance is not realized from these kinds of robots using motors for propulsion. In order to solve these problems and mimicking the fish's soft propulsion mechanism for robot design, the new actuation method based on soft structure is turning up and focused by many researchers. And many biomimetic soft robotic fishes considering soft behaviours of real fishes have been developed based on soft materials and compliant parts. Among these soft robotic fish, many robots using flexible actuators with smart material for robot propulsion, such as SMA or IPMC. By using flexible actuators, the biomimetic soft robotic fish with small volume and relatively simple control system can be developed easily, and relatively good propulsion performances similar to those of real fish can be obtained.

In the present research, the PFC is utilized as soft actuator to develop the biomimetic soft robotic fish. The surrounding fluid and interaction between flexible robot structure

and fluid are considered to solve the coupling problems of soft robotic fish for investigating its propulsion performances. To develop a biomimetic soft robotic fish with high performance, the numerical simulation method is adopted to design the optimal model for overcoming the previous problems of difficult design and high cost in the research. And in the simulation some problems should be solved. For example, what is dynamic response of the designed model of the soft robotic fish? Before manufacture, the dynamic response of the soft robot should be predicted at first to ensure the soft robot can realize the basic propulsion motion and displacement response. Then, what about propulsion characteristics such as displacement or propulsive force of the soft robotic fish? Does the designed model have the positive propulsion for swimming motion? If these characteristics can be identified from the designed model, the designed soft robot can be adopted as the suitable robot model for making the corresponding prototype. Otherwise, the manufacture of the robot prototype will cause high cost on time and money for achieving the relatively reasonable model of the soft robotic fish with desired performance.

In order to meet the requirements of designing and developing the optimal soft robot model, the design approach and numerical simulation system of soft robotic fish are presented firstly in this dissertation. In the design and numerical analysis of soft robotic fish, the surrounding fluid and interaction between soft robot structure and fluid are considered. According to the design method and numerical simulation system, the basic design procedure is proposed and the coupling methods are introduced for numerical simulation analysis of the soft robotic fish. It’s useful to develop the biomimetic soft fish robot with high performance effectively by optimization based on this design method and simulation system. The design method and numerical simulation system lay the foundations for the organization of the thesis.

Then, based on the proposed design method and numerical simulation system of biomimetic soft robotic fish, the modelling of soft robotic fish including driving structure and surrounding fluid is carried out based on FEM. In the modelling, the relationship between input voltage and generated stress of driving structure using flexible PFC actu-

ator is derived and the driving model of soft robotic fish using flexible PFC actuator is established by the experiment of beam model. Based on established driving model, the propulsion characteristics of the soft robotic fish in the fluid are investigated through two kinds of numerical simulation methods. Firstly, the coupling analysis considering surrounding fluid as acoustic fluid is performed. The propulsion mode and amplitude of the propulsion motion of soft robotic fish directly related to the propulsion mechanism and motion performance of the soft robotic fish in the fluid are investigated. Secondly, the FSI analysis of soft robotic fish is carried out, in which the interaction between soft robot structure and surrounding fluid including the dissipation due to fluid viscosity is taken into account. From FSI analysis, the hydrodynamic force and displacement of the soft robotic fish at different driving frequencies can be calculated, and vortex distribution in the wake of the soft robotic fish is identified for the case of fixing robot head. Besides, the motion control analysis is carried out based on propulsion mode of the soft robotic fish in the propulsion motion. When the input voltage amplitudes on both soft actuators are in asymmetrical distribution, the turning motion of the soft robotic fish is achieved by asymmetrical propulsion on both actuators. Based on investigation on design and control of the soft robotic fish by using these numerical coupling simulations, it is possible to optimize the soft robot model and improve the motion performance of the soft robotic fish in the fluid effectively.

In order to validate the feasibility of modelling and numerical simulation analysis on design and control of biomimetic soft robotic fish, the experiment evaluation is performed by using the actual robot prototype. The propulsion mode, amplitude of the propulsion motion and propulsive force of the soft robotic fish in the fluid are measured in the experiment. By comparing with the experimental results, the effectiveness of the numerical simulation analysis is verified. The modelling method and numerical analysis are useful to evaluate the propulsion characteristics of the soft robotic fish in the fluid for performance improvement.

Finally, the improvement of the soft robotic fish is performed to develop the soft robotic fish with high performance based on verified modelling and numerical analysis

using acoustic fluid. The new soft robot model is proposed by optimization and corresponding experiment evaluation on new soft robot prototype is carried out. The new soft robot prototype with higher swimming performance is confirmed by the experiment.

From the view of global perspectives, the following primary conclusions can be obtained from this research.

First, this research not only presents the feasibility of utilizing flexible PFC actuators in achieving the fish-like swimming motion, but also enhances the propulsion performance of the soft robotic fish in the fluid by considering the interaction between flexible robot structure and fluid. It overcomes the shortcomings from previous work in which the propulsion characteristics such as propulsion mode and interaction with surrounding fluid are not focused.

Second, different from many previous researches only focusing on hydrodynamics of robot body (that is, the robot is regarded as rigid body and no oscillating or undulating motion occurs on robot), the hydrodynamic performance of oscillating soft robotic fish is investigated in this research. In the numerical analysis, the robotic fish's flexible deflection, propulsion motion with large amplitude, and vortex distribution in the wake of the soft robotic fish are considered for improvement of propulsion performance. It provides multiple angles to develop the soft robotic fish with high performance in depth, and enhances the design flexibility of the soft robotic fish.

Third, the biomimetic soft robotic fish with higher swimming speed is developed successfully in the research. Compared with conventional soft robotic fish using IPMC, SMA or electrostatic film, the soft robotic fish in this research not only has simple structure with easy fabrication process, but also has larger swimming speed in the propulsion. The maximum swimming speed of the soft robotic fish is improved by more than one order of magnitude compared with those of conventional soft robotic fishes.

Fourth, the developed soft robotic fish in the research has better swimming performance similar to those of real fishes. The swimming number representing the fish swimming performance is enhanced by at least three times from the developed soft robot in the research by comparing with conventional soft robotic fish using flexible

actuators. It is conformed that the developed soft robotic fish in the research has higher swimming performance similar to those of real fishes than the conventional soft robotic fish. The similarity of fish swimming performance is greatly improved by the developed soft robot in the research.

The more specific lists of the main valuable conclusions in the research are shown as follows.

First, the proposed modelling method and coupling simulation platform have been established specifically by the experiment on actual robot prototype. It's useful to obtain the FSI solution of the soft robotic fish coupled with surrounding fluid for improvement based on verified numerical analysis.

Second, the fish-like swimming mode of the soft robotic fish in the fluid is identified by the verified coupling analysis using acoustic fluid. The propulsion mode about mode frequency and mode shape and amplitude of the propulsion motion of the soft robotic fish in the fluid are determined well based on coupling simulation. It is suitable to identify the fish-like propulsion motion of the soft robotic fish in the fluid by coupling analysis and it can use different propulsion modes to design different propulsion mechanisms in the fluid for improvement.

Third, the hydrodynamic force and displacement of the soft robotic fish are evaluated successfully by the effective FSI analysis for the case of fixing robot head. At different driving frequencies, the similar propulsive force curve and displacement curve occur in the simulation and experiment. The displacement is decreasing with the increased driving frequencies of the soft robotic fish in a certain range. The FSI analysis is useful to describe the hydrodynamic performance of the soft robotic fish and evaluate its propulsion characteristics in the fluid for improvement.

Fourth, vortex created by the tail motion of the soft robotic fish is identified by the verified FSI analysis using LES method for the case of fixing robot head. Based on FSI analysis using LES method, the vortex generates in the wake of the soft robotic fish at the frequency of 10Hz. It can be used to identify the vortex distribution around the soft

robotic fish. It provides the basic flow conditions for further improvement of propulsion performance of the soft robotic fish.

Fifth, new soft robots with higher swimming performance are proposed by optimization. Based on performance evaluation on new robot prototype, the new soft robot obtained by serial optimization has better propulsion performances similar to those of real fishes than the old robot. And larger displacement and higher swimming velocity are obtained on the new soft robot from serial optimization compared with the old robot. The swimming velocity of the new soft robotic fish from serial optimization can reach up to 0.79m/s (4.6BL/s). Besides, through integrative optimization, another new soft robot with better fish-like performance at main propulsion mode is developed for further improvement. The maximum swimming numbers of the soft robots from serial and integrative optimization are all near 0.6 similar to those of real fishes, greater than those of conventional soft robotic fish which are less than 0.2. Based on performance evaluation of the developed new soft robots obtained by serial and integrative optimization, it is confirmed that higher swimming speed and higher fish-like swimming performance are achieved. It can be said that the new soft robotic fish with higher performance has been developed successfully for improvement.

Sixth, the turning motion of the soft robotic fish is achieved by the useful motion control based on input voltage and propulsion mode. Through controlling the input voltage on both actuators for achieving the larger voltage amplitude on left actuator than that on right actuator, the motion of turning right is obtained. Otherwise, the motion of turning left is realized. Besides, compared with the old prototype, the larger turning velocity is achieved by the new developed soft robotic fish based on same controllability of input voltage. The turning velocity of the new soft robotic fish is improved by about two times compared with the old robot.

In a word, the design and control method based on numerical simulation analysis is useful and can be applied to evaluate the propulsion performance of the soft robotic fish in the fluid for further high-performance robot development and improvement. The bi-

omimetic soft robotic fish with high swimming speed and higher fish-like performance is achieved successfully based on verified numerical analysis.

In this research, some further work needed to be considered in the investigation of propulsion characteristics and hydrodynamic performance of the soft robotic fish. The in-depth investigation will be conducted in further research by the following aspects.

First, the propulsion motion of the soft robotic fish without fixed loads will be focused by the FSI analysis for investigating the propulsion performance of the soft robotic fish in the fluid. The forward motion, backward motion, turning motion, motion with uniform speed, and accelerated swimming motion of the soft robotic fish will be considered in the numerical simulation. Through the numerical modelling, the hydrodynamic characteristics of the soft robotic fish in different swimming motions will be investigated by using FSI analysis for improvement.

Second, the vortex distributions in the wake of the soft robotic fish in different swimming motions will be investigated by the FSI analysis for improvement. The quantitative analysis on vortex shedding and vortex structure in the wake of the soft robotic fish will be carried out by FSI analysis to establish the relationship between vortex shedding and robotic fish's propulsion motion.

Third, the FSI analysis of the soft robotic fish with flowing fluid will be performed for further soft robot design and development. The propulsion characteristics and vortex distribution of the soft robotic fish in the flowing fluid will be investigated for performance improvement. Through investigation of the hydrodynamic performance of the soft robotic fish in the flowing fluid based on FSI analysis, the relationship between fluid velocity and propulsive force of the soft robotic fish will be determined and corresponding design and control method of the soft robotic fish in the flowing fluid will be established for further improvement.

Fourth, based on effective modelling and control method using FSI analysis, the development of new biomimetic soft robot with advanced propulsion performance will be done. And corresponding hydrodynamic performance evaluation will also be considered in future work for improvement.

Appendix

Shear-Stress-Transport (SST) Model

This part outlines the theoretical details of the used SST model in the study.

In turbulence modelling, one of the main problems is the accurate prediction of flow separation from a smooth surface. Standard two-equation turbulence models usually fail to predict the onset and amount of flow separation under adverse pressure gradient conditions. This is an important phenomenon in many technical applications both for internal and external flows, particularly for airplane aerodynamics and swimming fish, in which the flow separation characterizes their fluid flow characteristics. Turbulence models based on ε-equation predict the onset and amount of separation too late. To solve these problems in this area, the most prominent two-equation models are k-ω based models. The k-ω based Shear-Stress-Transport (SST) model is designed to give a highly accurate predictions of flow separation under adverse pressure gradients by considering the transport of turbulent shear stress in calculation of eddy viscosity. Based on this model, the flow separation predictions are largely improved and it is recommended for high accuracy boundary layer calculations.

The k-ω based SST model is similar to the k-ω model. It solves two transport equations described as follows, one is turbulent kinetic energy k, and the other is turbulent frequency ω.

$$\frac{\partial(\rho k)}{\partial t}+\frac{\partial(\rho U_j k)}{\partial x_j}=\frac{\partial}{\partial x_j}((\mu+\frac{\mu_t}{\sigma_k})\frac{\partial k}{\partial x_j})+P_k-Y_k+P_{kb} \quad \textbf{(1)}$$

$$\frac{\partial(\rho \omega)}{\partial t}+\frac{\partial(\rho U_j \omega)}{\partial x_j}=\frac{\partial}{\partial x_j}((\mu+\frac{\mu_t}{\sigma_\omega})\frac{\partial \omega}{\partial x_j})+P_\omega-Y_\omega+P_{\omega b}+D_\omega \quad \textbf{(2)}$$

$$Y_k=\beta'\rho k\omega \qquad Y_\omega=\beta\rho\omega^2 \quad \textbf{(3)}$$

$$P_k = \min(\mu_t S^2, 10\beta'\rho\,\omega\,k) \qquad P_\omega = \alpha\frac{\omega}{k}P_k \tag{4}$$

$$D_\omega = 2\rho(1-F_1)\frac{1}{1.168\,\omega}\frac{\partial k}{\partial x_j}\frac{\partial \omega}{\partial x_j} \tag{5}$$

where ρ is density, U is velocity vector, μ is dynamic viscosity, μ_t is turbulence viscosity, σ_k is turbulence model constant for the k-equation, σ_ω is turbulence model constant for the ω-equation, β', β and α are coefficients in the k-equation and ω-equation. At high Reynolds number, the coefficient β' can be defined as 0.09. For the incompressible fluid, coefficients β and α meet the underlying model described by (6). P_k and P_ω are the turbulence production rates. P_{kb} and $P_{\omega b}$ are additional buoyancy production terms in the k-equation and ω-equation and they represents the influence of the buoyancy forces. Y_k and Y_ω are turbulent kinetic energy dissipation and turbulent frequency dissipation.

$$\begin{aligned} &\beta = F_1\beta_1 + (1-F_1)\beta_2 \qquad \alpha = F_1\alpha_1 + (1-F_1)\alpha_2 \\ &\alpha_1 = \frac{\beta_1}{\beta'} - \frac{\kappa^2}{2(\beta')^{0.5}} \qquad \alpha_2 = \frac{\beta_2}{\beta'} - \frac{\kappa^2}{1.168\ (\beta')^{0.5}} \end{aligned} \tag{6}$$

where β_1, β_2 and κ are constant, defined as 0.075, 0.0828 and 0.41, respectively. F_1 is blending function shown by (7) and equal to one near the surface and decreases to a value of zero outside the boundary layer (that is, a function of the wall distance).

$$\begin{aligned} F_1 &= \tanh(\arg_1{}^4) \\ \arg_1 &= \min(\max(\frac{\sqrt{k}}{0.09\omega y}, \frac{500\,\nu}{y^2\omega}), \frac{4\rho k}{1.168 CD_{kw} y^2}) \end{aligned} \tag{7}$$

$$CD_{kw} = \max(2\rho\frac{1}{1.168\omega}\frac{\partial k}{\partial x_j}\frac{\partial \omega}{\partial x_j},\ \ 1.0\times10^{-10}) \tag{8}$$

where y is the distance to the nearest wall and ν is the kinematic viscosity.

In this model, the turbulence viscosity can be expressed by (7), where S denoting the magnitude of the strain rate is an invariant measure of the strain rate and F_2 is a blending function restricting the limiter to the wall boundary layer. The very high levels of the shear strain rate S in stagnation regions are responsible for the excessive levels of the turbulence kinetic energy. Since the deformation near a stagnation point is nearly irrotational (vorticity rate is very small), the vorticity rate is proposed for replacement of strain rate for production term. In a simple shear flow, the strain rate and vorticity rate are equal.

$$\mu_t = \frac{a_1 k \rho}{\max(a_1 \omega, SF_2)} \qquad a_1 = 0.31 \tag{9}$$

$$S = \sqrt{2 S_{ij} S_{ij}} \qquad S_{ij} = 0.5\left(\frac{\partial U_i}{\partial x_j} + \frac{\partial U_j}{\partial x_i}\right) \tag{10}$$

$$F_2 = \tanh(\arg_2{}^2) \qquad \arg_2 = \max\left(\frac{2\sqrt{k}}{0.09\omega y}, \frac{500\nu}{y^2 \omega}\right) \tag{11}$$

Large Eddy Simulation (LES) Model

This part outlines the theoretical details of the LES model adopted in the study.

The governing equations for LES model are obtained by filter the time-dependent Navier-Stokes equations in the physical space. Filtering Navier-Stokes equations leads to additional unknown quantities. The filtered incompressible momentum equation can be described as follows,

$$\frac{\partial(\overline{U}_i)}{\partial t} + \frac{\partial(\overline{U}_i \overline{U}_j)}{\partial x_j} = -\frac{1}{\rho}\frac{\partial \overline{p}}{\partial x_i} + \frac{\partial}{\partial x_j}\left(\nu\left(\frac{\partial \overline{U}_i}{\partial x_j} + \frac{\partial \overline{U}_j}{\partial x_i}\right)\right) - \frac{\partial \tau_{ij}}{\partial x_j} \tag{12}$$

$$\tau_{ij} = \overline{U_i U_j} - \overline{U}_i \overline{U}_j \tag{13}$$

where τ_{ij} denotes the subgrid-scale stress, includes the effect of the small scales and is defined by (13).

The large scale turbulent flow is solved directly and the influence of the small scales is considered by appropriate subgrid-scale models. Among subgrid-scale models, the standard Smagorinsky model is widely adopted for LES simulation in application. An eddy viscosity approach is used which relates the τ_{ij} to the large-scale strain rate tensor $\overline{S}_{ij}$ by (14), where the subgrid-scale viscosity v_{sgs} only represents the small scales. It should be noted that the isotropic part of τ_{kk} is not modelled, but added to the filtered static pressure.

$$-\tau_{ij}+\frac{\delta_{ij}}{3}\tau_{kk}=2v_{sgs}\overline{S}_{ij} \qquad \overline{S}_{ij}=0.5(\frac{\partial\overline{U}_i}{\partial x_j}+\frac{\partial\overline{U}_j}{\partial x_i}) \tag{14}$$

In Smagorinsky model, the subgrid-scale viscosity is defined as follows,

$$v_{sgs}=(C_s\Delta)^2(2\overline{S}_{ij}\overline{S}_{ij})^{0.5} \tag{15}$$

where C_s is the Smagorinsky constant and Δ is filtering scale. The value of C_s for isotropic turbulence with inertial range spectrum is determined by (16). As for practical calculations, the value of C_s is changed based on the fluid flow type and mesh resolution. It is found to vary between 0.065 (channel flows) and 0.25. The value of 0.1 is generally used and found to yield the best results for a wide range of flows. This is the default value for C_s.

$$C_s=\frac{1}{\pi}(\frac{2}{3C_k})^{3/4} \tag{16}$$

Acknowledgements

First of all, I would like to extend my sincerest thanks to my advisor, Prof. Aiguo Ming, who not only gives me the opportunity to join in his laboratory, but also provides much support throughout my graduate studies. He is always tireless and spending much time to discuss with me. He encourages me to overcome that hard ones and guides me towards the research's essence. He is very tolerant for my slow process. His encouragement and excellent guidance provides me much motivation to solve the problems encountered in the study or life. He has been a great mentor. It's my great honor and privilege to study from him under his supervision in his laboratory. Without his guidance and kind support, I cannot finish this study. I would also like to thank Prof. Makoto Shimojo for his valuable advices and kindness.

I would like to acknowledge Prof. Hiroshi Maekawa and Dr. Yohei Inoue for their valuable guidance and discussions about this study. I learn a lot of knowledge about hydrodynamics from them. Their encouragement and enthusiasm are very motivating.

I would like to express my gratitude to other committee members of this dissertation: Prof. Hisayuki Aoyama and Prof. Kazuo Tanaka for their valuable comments and suggestions on how to improve my dissertation.

I would like to thank Dr. Jinlong Liu for his kind help and valuable discussions. I would like to thank Mr. Fei Meng, Mr. Jun Shintake, Mr. Kazunori Hashimoto, Mr. Toui Nishimura, Mr. Sato Keigo, and the members in the Shimojo and Ming Lab for their kind supports and helpful discussions. It is a great experience to study with you. Hope you everything is well in your life.

I would like to thank the financial support for my dissertation work from the Japanese Government (MEXT) Scholarship.

Finally, I am endlessly grateful to my parents and friends for their love and support. Without their support, I would not be able to overcome the challenge and complete it.

Publications

Journal Papers

1. Wenjing Zhao, Aiguo Ming, Makoto Shimojo, Yohei Inoue, and Hiroshi Maekawa, "Fluid-Structure Interaction Analysis of A Soft Robotic Fish Using Piezoelectric Fiber Composite," Journal of Robotics and Mechatronics, Vol. 26, No. 5, pp. 638-648, 2014. (related to Chap. 2, Chap. 3, Chap. 4 and Chap. 5)

International Conference Papers

2. Wenjing Zhao, Aiguo Ming, Makoto Shimojo, "Dynamic Analysis and Optimization of Soft Robotic Fish Using Fluid-Structural Coupling Method," Proceedings of the IEEE International Conference on Robotics and Automation (ICRA), pp. 1474-1479, 2014. (related to Chap. 2, Chap. 3, Chap. 4 and Chap. 5)
3. Wenjing Zhao, Jun Shintake, Aiguo Ming, Makoto Shimojo, "Structural Design and Dynamic Analysis of Robotic Fish with Piezoelectric Fiber Composite," 9th France-Japan & 7th Europe-Asia Congress on Mechatronics (MECATRONICS)/13th Int'l Workshop on Research and Education in Mechatronics (REM), pp. 161-168, 2012. (related to Chap. 2 and Chap. 3)
4. Aiguo Ming, Kazunori Hashimoto, Wenjing Zhao, Makoto Shimojo, "Fundamental Analysis for Design and Control of Soft Fish Robots using Piezoelectric Fiber Composite," Proceedings of the IEEE International Conference on Mechatronics and Automation (ICMA), pp. 219-224, 2013. (related to Chap. 2, Chap. 3 and Chap. 4)